Characterisation of particle-particle interactions using the atomic force microscope

Young, Paul Michael

Award date:
2002

Awarding institution:
University of Bath

CHARACTERISATION OF PARTICLE-PARTICLE INTERACTIONS USING THE ATOMIC FORCE MICROSCOPE

Submitted by:

Paul Michael Young

for the degree of Doctor of Philosophy
of the University of Bath
November 2002

ACKNOWLEDGEMENTS

I would like to thank my academic supervisors Dr. Robert Price, Dr. Michael J Tobyn and Prof. Anthony Smith for their continued support. I would also like to thank my industrial supervisors Dr. Mark Buttrum and Dr. Fiona Dey for their encouragement and input.

I would like to give specific thanks to members of the Bath Pharmaceutical Technology Research Group – Robert Price (for his passion of pharmaceutics) Fraser Steele (for his friendship, and grasp of statistics) and Stephen Edge (for his attention to detail). I would also like to thank previous members of the group and staff at the Virginia Commonwealth University including Mo Aydin, Martyn Clarke and Joanne Peart.
Also, a special thanks to Valerie Diart, Garrick Etherington and other researchers in the analytical/material science departments at Aventis Pharma, for their technical expertise and time. Thanks also, to other members of the Pharmaceutical Technology Research Group and Departmental Support Staff.

Finally, I would like to thank my parents and my partner Daniela for their love and continued support.

To Daniela Traini

TABLE OF COMMONLY USED ABBREVIATIONS

ω	-	angular velocity
ρ	-	gas density
υ	-	gas viscosity
$\hbar\varpi$	-	Lifshitz coefficient
π	-	Pi
γ	-	liquid surface tension
ε_0	-	permitivity constant
γ_s^d	-	dispersive surface energy component of a solid
γ_s^{sp}	-	polar surface energy component of a solid
a	-	projected gas probe surface area
AFM	-	atomic force microscope
AN	-	Lewis acid-base acceptor number
C	-	B.E.T. constant
CFC	-	chloro-fluorocarbons
CI	-	confidence interval
CPD	-	centrifugal particle detachment
d	-	separation distance
d_x	-	particle diameter (where x donates percentage undersize)
D_c	-	cantilever deflection
DN	-	Lewis acid-base donor number
d_p	-	pore diameter
DPI	-	dry powder inhaler
DSC	-	differential scanning calorimetry
DSCG	-	disodium cromoglycate
DVS	-	dynamic vapour sorption
e_{sep}	-	separation energy
F	-	force
FPF	-	fine particle fraction
FPF_{LD}	-	fine particle fraction of loaded dose
g	-	acceleration due to gravity
GSD	-	geometric standard deviation

h_c - channel diameter for Reynolds flow through a duct
HFA - hydro-fluorocarbons
HPLC - high performance liquid chromatography
IGC - inverse gas chromatography
k - spring constant
K_a - acidic component contribution to surface energy
K_D - basic component contribution to surface energy
LTSEM - low temperature (cryogenic) scanning electron microscopy
m - mass
N - Avogardro's constant
P - partial pressure
pMDI - pressurised metered dose inhaler
q - charge
r - particle radius
r_{cent} - radius of angular momentum
R - gas constant
RH - relative humidity
r_k - Kelvin radius
R_{rms} - root mean square roughness
RSD - relative standard deviation
SEM - scanning electron microscopy
t - statistical thickness
T - temperature
TAA - triamcinolone acetonide
TGA - thermogravametric analysis
TSI - twin stage impinger
V_a - volume of gas at adsorbed at a specific partial pressure
V_m - volume of adsorbed gas for monolayer coverage
v - molar volume of condensed vapour
V_N - net volume of carrier gas
XRPD - X-ray powder diffraction
RCF - relative centrifugal force

ABSTRACT

An investigation has been conducted into factors affecting the inter-particulate cohesion profile of three micronised drugs, as a function of humidity. An atomic force microscope (AFM) colloid probe technique was correlated with physico-chemical properties and in-vitro performance.

Briefly, micronised drug particles of salbutamol sulphate, triamcinolone acetonide (TAA) and disodium cromoglycate (DSCG) were mounted onto V-shaped tipless cantilevers using a developed micromanipulation technique. Interactions between the AFM 'drug probes' and a series of model drug surfaces were conducted at a 15,30, 45, 60 and 75% relative humidity using a custom built perfusion apparatus connected to the AFM.

As expected, separation energy distributions for drug probe interactions were dependent on the surface rugosity of the drug model surfaces. Separation energy measurements conducted between drug probes and individual micronised drug particles (mounted in polymer resin) suggested large variations in separation energy. Further analysis of such data suggested a lognormal separation energy distribution, however, limitations in individual particle measurements (finite particle measurements per experiment) allowed restricted statistical analysis.

Construction of large planar model drug surfaces (>100μm) allowed the collection of large data sets (~4096) over relatively large areas (~10μm), thus allowing a more complete distribution analysis. Drug probe separation energy interactions with compacted drug surfaces, indicated a lognormal distribution, most likely attributed to the variation in particle surface contact geometry. Conducting separation energy measurements between drug probes and 'atomically smooth' crystals, prepared via controlled crystallisation, further substantiated such observations, as normal separation energy distributions were observed (relating to low variation in particle crystal contact geometry).

Relative humidity had a statistically significant influence on the separation energy (cohesion) of all three micronised drugs. The separation energy for salbutamol sulphate and DSCG increased as humidity was raised, while the separation energy for TAA decreased. Variations in the humidity-cohesion profile for the three drugs were attributed to the chemical and physical properties of each specific drug.

To corroborate such observations, a series of bulk analysis techniques and in-vitro particle aerosolisation studies were conducted. The AFM separation energy cohesion profile correlated well with both the bulk moisture sorption and the fine particle fraction of aerosolised drug particles.

The AFM colloid probe technique has successfully been developed to allow the measurement of micronised particle interactions specific to inhalation technology. Furthermore such correlation between bulk and in-vitro behaviour, as a function of environmental conditions, may allow rapid screening of drugs during the formulation process.

1 INTRODUCTION.

1.1 DELIVERY OF DRUGS TO THE RESPIRATORY TRACT.

The delivery of pharmaceutical agents to the respiratory tract via the inhalation route has become an integral part of drug therapy. The advantages of pulmonary delivery are well recognised. Smaller therapeutic doses are required, the surface area of the lung is large (around 100 m^2, Patton 1996), and the delivery system allows rapid molecule transfer across cell membranes while avoiding first pass gastric metabolism (Timsina et al 1994).

In simple terms, the structure of the lung consists of a series of branching airways (Figure 1.1.1) starting at the trachea and decreasing in size through more than 17 bifurcations to terminate in the alveolar sacks (Patton 1996). Transfer of oxygen, carbon dioxide and macromolecules occur mainly through the alveolar, whose structure comprises of an endothelial capillary system surrounded by epithelial cells (which are coated with a surface fluid and surfactant layer). The whole structure is bound by intracellular fibres and is able to expand and contract during inhalation.

When delivered efficiently, a dose targeting at least twenty times less than that required for oral administration can be easily achieved with equivalent results and reduced side effects (Ganderton and Kassem 1992). However, the delivery of pharmaceutical agents via the inhalation route is restricted by the natural defence mechanism that is the upper airways. Impaction and sedimentation act as major forms of particulate entrapment, preventing ingress of natural airborne hazards (including pharmaceutical compounds) into sensitive regions of the lung. To circumvent such an effective defence mechanism, drug particulates need to possess minimal ballistic effect (to limit impaction), while maintaining a high velocity (to limit residence time and subsequent sedimentation) in the inhalation air stream.

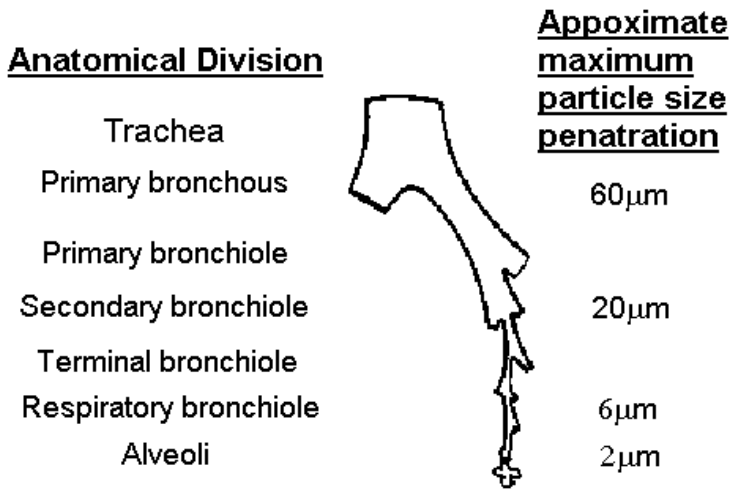

Figure 1.1.1 Diagrammatic representation of the human tracheal system (modified from Florence and Attwood, 1998).

The minimisation of impaction and sedimentation in the respiratory tract is not a complicated procedure. Simply put, a reduction in mass or density of the entrained particles will cause a reduction in the imparted forces. Such a reduction would clearly cause both a decreases in inertia (allowing particles to remain entrained through narrower bifurcations) and limit gravity-assisted sedimentation (Hinds 1999). For crystalline particles of typical density (ca. 1 $g.cm^{-3}$), a particle size of 5 μm or less is generally agreed to be sufficient to penetrate the smallest airways (Prichard 2001, Ganderton and Kassem 1992). For simplicity we can classify such particles as having a respirable size range.

The method of producing respirable particles for inhalation varies greatly, and is dependent upon a number of factors including delivery device and active agent. However, the delivery of pharmaceutical products via inhalation can usually be classified into three main delivery systems; the nebuliser, the pressurised metered dose inhaler (pMDI) and the dry powder inhaler (DPI). Both the nebuliser and pMDI aerosolise a solution or suspension of the required formulation. In the case of the nebuliser a constant flow of aerosolised droplets is supplied over a required time (either by fine jet,

centrifugation or vibration). The nebulised aerosol is generally passed into a facemask and delivered to the lung by natural tidal breathing. In comparison, pMDI formulations are contained within a pressurised liquid propellant (commonly chloro-fluorocarbons (CFC) or hydro-fluorocarbons (HFA)). In simple terms, the pMDI device aerosolises a metered quantity of drug through a rapid vaporisation process. Patients are taught to co-ordinate the depression of the metering valve with their inhalation to insure efficient delivery.

Dry powder inhalers harness the energy supplied by the patient's inhalation to aerosolise the drug as a powder. Single dose and metered dose devices are available with the formulation stored in capsule, reservoir or blister pack form. However, all devices work on the same principle by generating a turbulent airflow (via propeller, decreasing air channels etc.) to disperse the powder formulation.

The dry powder inhaler has many advantages over the pMDI and nebuliser. High doses are possible (pMDI is limited to 1mg) and device design may be less cumbersome. In addition, co-ordination problems are not encountered, as patient inhalation is the driving force for particle aerosolisation. Furthermore with the advent of the Montreal protocol, banning the use of CFC propellants, in combination with recent concerns over environmental issues with HFA propellants, a strong move to dry powder formulation has been observed.

The production, handling and aerosolisation of dry powder particles (of respirable size), come with a series of unique formulation problems. For example, particulates need to be of a suitable size range. Techniques for producing such particles include the use of spray drying (Broadhead et al 1992), supercritical fluids (Shekunov and York 2000) and electrodynamic spraying (Gomez et al 1998).

However, the most common route for manufacture of micron-sized particulates (<5 μm) is by reducing the particle size of the 'mother' crystal material. This is achieved by comminution or high-energy milling techniques (Staniforth 2000). The subsequent particulates can be classified as having a respirable particle size, and the technique of size reduction referred to as micronisation.

A consequence of producing particles with a respirable size range is the substantial increase in potential adhesive nature. Micronised powders will have a high surface-area to mass ratio, since the volume and surface area of a sphere are related to the cube and square of the radius. Consequently, the force imparted to overcome small particle adhesion will tend to be small with respect to the actual adhesion force (Hinds 1999). Thus, the adhesive and cohesive forces present in a dry powder inhalation formulation will play a dominant role on the storage, handling and eventual aerosolisation efficiency. Subsequently, it has become the focus of many DPI investigations and can be found in abundance in the literature (Booth and Newton 1987, Kulvanich and Stewart 1988, Lord 1993, Safatov et al 1998, Podczeck et al 1997(a, b), Podczeck 1998(a), Clarke et al 2002).

Fundamental measurement of such forces would be of great advantage when undertaking a formulation program, and have subsequently become the focus of this investigation. A brief overview of such particle interaction mechanisms is given in Chapter 1.2.

1.2 ADHESION AND COHESION MECHANISMS IN DRY POWDER INHALERS.

The development of a dry powder formulation requires knowledge of the forces interacting between the individual components in the system. Interactions between active drug, carrier, ternary agents and device materials will therefore have a net contribution on device performance and efficiency. Current strategies for device formulation include, agglomeration (Ikegami et al 2000), blending with large and/or fine inert carrier material (ordered mixing) (Hersey 1975) and the use of low surface energy materials (Staniforth 1997). These systems are not only subjected to inter-particulate forces but also rely on them for their operation.

Generally, there are three major attractive forces involved during the interaction of particulates in a dry powder system. These are categorised as van der Waals, electrostatic and capillary forces. The contribution of each force to the total inter-particulate interaction will depend on both the environmental conditions and material properties. For example, the roughness of two contiguous materials will directly influence the adhesion due to factors such as: variation in contact area and degree of vapour condensation. On a chemical level each material will have its own intrinsic interactive properties based on the molecular structure of the material and the way it is ordered as a mass (i.e. crystal structure). Similarly, the affinity of a material towards water will directly influence the degree of sorbed water, and thus capillary forces. In summary, the forces between one material and another will therefore related to the combination of these properties.

A summary of van der Waals, electrostatic and capillary forces (and the influence of environmental and physical parameters on them), is given in Chapter 1.2.1, 1.2.2 and 1.2.3, respectively.

1.2.1 van der Waals Forces.

van der Waals forces represent long-range interactions between atoms. These forces can be further categorised as Debye-Induction force, Keesom-orientation forces and dispersion forces.

Debye-induction forces occur when one molecule containing a dipole induces an electrical dipole in a neighbouring apolar molecule resulting in an attractive force. Keesom-orientation forces occur when two molecules with dipole moments orientate themselves so that the positive pole of one will be in contact with the negative pole of the other.

However, the most ubiquitous of the van der Waals forces will be dispersive or London forces. Dispersive forces are finite between all atoms and therefore all particulate systems. At any instantaneous moment in time, the position of electrons with relation to their nuclear protons will induce a dipole. This in turn will induce a polar response in neighbouring atoms resulting in a finite attractive mechanism between all atoms (Visser 1989). Haymaker developed this theory to calculate the van der Waals forces acting between two large semi-infinite bodies by assuming additive molecular forces throughout the material (Visser 1989). However, this was further developed by Lifshitz when he eliminated the total additive molecular force in favour of a screening affect caused by the atoms present on the surface of the two contiguous bodies (Visser 1989, Langbein 1969).

The van der Waals theory can thus be applied to homogeneous macroscopic systems with forces acting over a separation distance of 1-100nm (Zimmon 1982, Podczeck 1998b). The force of interaction between a sphere and a planar surface (F_{vdw}) can be described by Equation 1.1.1

$$F_{vdw} = \frac{\hbar\varpi}{8\pi d^2} r$$ *Equation 1.1.1 van der Waals force of attraction.*

Where d is the distance between a perfect sphere and planar surface, r the sphere radius and hϖ the Lifshitz coefficient (an extension of the Haymaker coefficient relating the molecular properties to individual materials).

Since the van der Waals forces act over short distances and the subsequent adhesion is related to instantaneous dipole poison of the local molecules, it stands to reason that, they will be dominated by the contact geometry of the contiguous surfaces. For example, the presence of nano-scale asperities on the surface of two contiguous bodies would only serve to decrease the van der Waals forces acting between them (Biggs and Spinks 1998, Hinds 1999).

1.2.2 Electrostatic Interactions.

Electrostatic forces in dry powder particulate systems can be attributed to contact electrification. Upon contact, electrons will flow from one material to the other in order to equal the workfunction of each. Particle separation will result in an equal and opposite charge (or contact potential) on the two materials; this gives rise to the electrostatic component observed dry powder systems (Peart et al 1995, Byron et al 1997). Since pharmaceutical powders are mostly insulating organic crystals the electrical relaxation of the material (particle resistivity) can be minutes to hours, potentially causing unpredictable processing and aerosolisation behaviour.

The electrostatic force (F_{elec}) acting between a charged spherical particle and a surface can be expressed by Equation 1.2.2.

$$F = \frac{q^2}{16\varepsilon_o d^2}$$ *Equation 1.2.2 Electrostatic force calculation.*

Where q is the charge, ε_o is the permitivity constant and d is the distance between the two surfaces. Again such theoretical calculations assume perfectly spherical and planar surfaces. However, in almost all circumstances pharmaceutical powders do not conform to such assumptions, and thus can result in experimental force values of up to 50 times greater than theoretical (Eklund 1995).

The process of contact electrification is generally attributed to both quantum mechanics and the surface chemical properties of a material. On a quantum level close proximity of atoms in a solid structure causes the individual electron levels present in each atom to become less defined energy bands in the macroscopic structure. For a metal, the outer electrons are present in valance bands with excitation energy levels being classified as conduction bands. The highest filled energy band is labelled the Fermi band with the energy required to remove one electron from the surface to infinity being the workfunction.

For an insulating material, a region known as a 'forbidden energy band' separates the valance and conduction bands almost eliminating the possibility of electron transition. The transfer of charge between insulators is therefore not as well understood as for metals. Charge transfer between such materials is likely to take place due to a multitude of material factors. Crystal impurities and localised dislocations across a lattice will broaden energy bands further; this enables the possible transfer of electrons between localised energy bands resulting in a electrostatic behaviour. Gady et al (1998) have shown that contact electrification between a polystyrene sphere and different conducting materials is only favourable if the difference between the electron acceptor sites of the polystyrene overlaps the Fermi level of the conductor. Subsequently, such factors could have a direct impact on DPI formulation, for example where the choice of mixing vessel material influences the final powder content uniformity (Lord 1993).

Permanent immobile electrostatic charge due to molecular characteristics can also exist in insulating materials due to chemical states and/or contamination present on the surface (Bailey 1984). The presence of polar groups (electron donors or acceptors) on a surface may result in a permanent electrostatic characteristic. Furthermore, ionised surfaces can be present on a crystal face even thought the overall charge is neutral. For example the (III) face of sodium chloride can have a positive or negative charge dependent on the last layer of ions forming the crystal surface (Führer 1996). Finally, stochiometric excess during production can also lead to surfaces containing residual ion tensids (Führer 1996).

By applying a workfunction to insulators it is possible to construct an electrostatic series. However, it must be stressed that unlike a metal, the most energetic electrons will not have a single value; therefore making such a series qualitative at best. During mixing or aerosolisation, frequent collisions between individual particles will result in interfacial charge transfer over the surface. Eliminating frictional forces, this charging will continue until a saturation point is reached (Figure 1.2.1) (Bailey 1984).

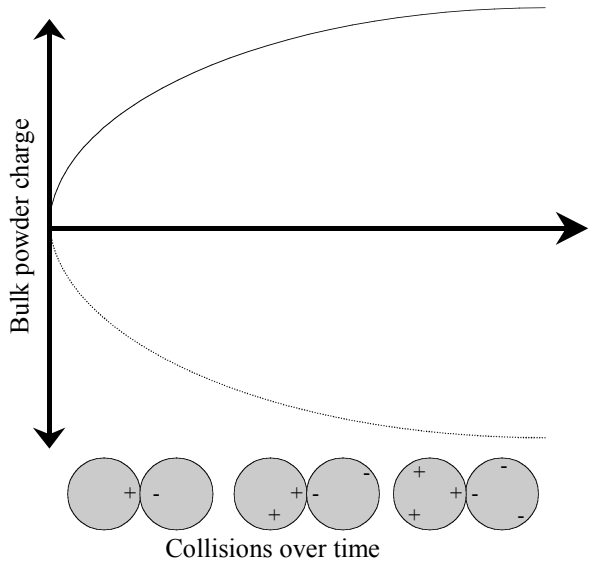

Figure 1.2.1 Relationship between interfacial charging and charge saturation.

When considering the electrostatic behaviour observed in a bulk powder system, interactions other than the simple contact model should be considered. Particle friction due to slip or roll may affect the charging profile of two materials (Bailey 1984). Electrostatic behaviour observed in powder handling has therefore been generalised under the title 'triboelectrification'. Triboelectrification during powder handling will be influenced by atmospheric, mechanical and physical characteristics.

For example, it has been observed that as the dielectric constant and/or the particle size increases, the minimum work required to remove an electron from a particle surface to infinity decreases. This makes the transfer of charge from large to smaller particles more favourable (Bailey 1984). Such observations may also be linked to bipolar charging of pharmaceutical powders as reported by Byron et al (1997).

Depending on the resistivity of a material the charge can become redistributed over the surface of a particulate. Amorphous spherical particles will tend to redistribute charge evenly across the surface, while crystalline material will localise the charge at corners or asperities (Führer 1996) thus forming iso-energetic regions on a surface (Hersey 1975, Staniforth 1996). Where water is present on a particulate surface the redistribution will become easier (Führer 1996). It is therefore logical to conclude that at higher humidity, electrostatic forces will be less dominant.

Previously, it has been suggested that a specific humidity will exist for charge dissipation. At this critical humidity, triboelectrification can no longer take place due to the lack of resistivity in the medium (Kulvanich and Stewart 1988). Furthermore, it has been reported that at higher humidities (~50 to 80% RH) capillary forces can be considered to dominant particle interactions (Kulvanich and Stewart 1988). However, it is important to note that such assumptions will be material specific.

1.2.3 Capillary Forces.

Capillary forces exist due to the condensation of water vapour on the surface of two contiguous bodies. At a critical point liquid bridges will be formed between them, which will become stable when the vapour pressure of the liquid bridge equals the partial pressure of the water vapour in the surrounding atmosphere (Schubert 1984). The extent of capillary forces can be directly related to relative humidity, gap geometry (between the two substrates) and the material properties. The chemical affinity of a material for water will greatly affect this interaction (Kontny 1988), with capillary forces more likely to occur between hydrophilic systems.

Such capillary forces will be substantially reduced in the case of auto-adhesion, as the meniscus radius will not reach the full particle radius (Podczeck 1998b). However, as powders used in inhalation therapy are not perfectly spherical or planar systems, the presence of surface asperities, surface pores and particle size will affect the contact geometry and thus capillary force contribution. Depending on the physico-mechanical and chemical properties of the interacting substrates, capillary forces have been reported to become apparent at relative humidities of 50% and dominant between 65 and 75% (Zimmon 1982). However, it has been shown that humidity can have little influence on the adhesion of some materials (Kulvanich and Stewart 1988).

1.3 HISTORICAL METHODS USED TO DETERMINE PARTICLE-PARTICLE INTERACTIONS.

The direct measurement of inter-particulate and particulate-substrate adhesion forces enables the collection of data that can be directly applicable to powder handling, stability and aerosolisation efficiency in a DPI formulation.

Historically, many techniques have been developed to enable the measurement of detachment forces for a range of particle sizes. These include, centrifugal detachment, aerodynamic methods and ultrasonics. The most relative of these techniques are described in more detail here.

1.3.1 Centrifugal Particle Detachment (CPD).

The use of an ultracentrifuge to measure the separation force of powdered particulates to various substrates dates back to 1962 (Böhme et al), and has been easily adapted for the measurement of pharmaceutical powders. Assuming that the substrate and particle are at 90° to the angular velocity, the force of separation (F_{sep}) can be calculated from Equation 1.3.1

$$F_{sep} = m\omega^2 r_{cent}$$ *Equation 1.3.1 Force for separation (F_{sep}) by centrifuge*

Where m is the particle mass, ω is the angular velocity ($rad.s^{-1}$) and r the radius from the particle to the rotation axis. In addition, deviation from a 90° angular velocity allows measurement of both frictional and adhesion forces.

Examples of the centrifugal detachment technique include studies into substrate variation (Booth and Newton 1987, Clarke et al 2002), carrier based formulation (Staniforth 1980, Lord 1993, Kulvanich and Stewart 1988, Podczeck 1998) and the influence of humidity (Podczeck et al 1996, Podczeck et al 1997a,b) on the adhesion properties of pharmaceutical powder systems.

1.3.2 Aerodynamic Particle Re-entrainment.

In simple terms, it is possible to assess the adhesion forces acting on particles by removal in a controlled airstream. Such aerodynamic determination of adhesion force can be classed under the term re-entrainment. The re-entrainment of a powder particulate into an airstream is dependent on both the adhesion and frictional forces between the powder and substrate. This is due to the airstream being at an angle other than 90° below the plane of the surface. Re-entrainment takes place parallel to or above the substrate. Therefore, the force can be related to the detachment angle and coefficient of friction. A commonly used method for aerodynamic adhesion studies of pharmaceutical powders is the re-entrainment tube. The re-entrainment tube is essentially a long duct containing a sample platform mounted down stream from the airflow. Particulate samples are mounted on the platform and their removal is assessed as a function of flow rate, pressure drop or turbulence through the duct.

Using the re-entrainment tube, Corn and Stein (1965) reported increased detachment velocities were required as the particle size and/or surface roughness decreased. Further work by Akiyama and Tanijiri (1989) showed increased adhesion with increased relative humidity, while Lord (1993) and Staniforth (1995) demonstrated how the re-entrainment tube could be applied in the measurement of pharmaceutical powders, (showing that an increased flow rate and pressure drop is required to entrain finer particulates). Although re-entrainment studies do not directly measure adhesion energies, Akiyama and Tanijiri (1989) and Lord (1993) have demonstrated good correlation with in-vitro and bulk powder analysis techniques.

1.3.3 Miscellaneous Measurement of Detachment Force.

In addition to the two most commonly used approaches (centrifuge and re-entrainment) a series of other approaches has been employed to measure detachment forces between particulates and substrates. These include gravimetric, vibrational and impact methods. Zimmon (1982) and Podczeck

(1998b) give comprehensive reviews of available methods; a brief overview of only the most widely used is given here.

1.3.3(a) Separation due to gravity.

The separation force is determined at the point a particulate detaches from a surface due to its own mass under gravity. This is generally achieved by mounting the sample on a pendulum and increasing its angle consecutively until the powder is removed (Zimmon 1982). As most pharmaceutical powders are less than 100 μm, gravitational forces are not strong enough to overcome the van der Waals forces. Consequently this technique is of little use.

1.3.3(b) Separation by impaction.

A hammer is impacted on a fixed substrate back at a known velocity. The particulates separate from the substrate, as a function of their mass in relation to the conservation of momentum. Again the limiting factor of this method is the force required to remove fine particulates. A realistic limit of 5μm can be removed using the impact technique and therefore is not particularly appropriate for measurements on powders designed for inhalation.

1.3.3(c) Separation by vibration.

The separation force is measured as a function of the vibrational energy applied to the surface the particles are adhered to. By using ultrasonic vibrators with MHz frequencies it is possible to remove micron-sized particles. However, there is a high possibility of sample damage due to the high frequencies utilised. Subsequently, this method is not generally adopted.

1.4 FUNDAMENTAL CONSIDERATIONS AND LIMITATION OF HISTORICAL FORCE MEASUREMENT TECHNIQUES.

Although potentially useful, the direct measurement of particle interactions using the techniques described in Chapter 1.3 produce data of limited use, as they are bulk powder techniques. Furthermore, fundamental restrictions apply, related to the maximum forces that can be imparted on particles of respirable size.

For simplicity, such restrictions can be explained by calculating the theoretical force required to remove a 'perfect' sphere (of given diameter), from a planar surface, when subjected to acceleration forces imparted from each technique. An empirical formula (Equation 1.4.1), describing the adhesion (F_{adh}) of a solid sphere to a planar surface, was chosen to represent the force of adhesion (Corn 1961, Hinds 1999), while Equation 1.3.1 was used for CPD calculation. In addition, the equation F = ma was used to estimate both the gravitational and re-entrainment forces.

$F_{adh} = 0.063\ 2r[1+0.009(\%RH)]$ *Equation 1.4.1 Empirical adhesion force*

Where *d* is the particle diameter. By plotting the forces (required to remove particles along with the various forces acting on the particles) against particle size, the minimum particle size that can be removed using a particular technique can be assessed (Figure 1.4.1).

Using the empirical formula for adhesion (Equation 1.4.1), the gravitation forces alone would not be effective for removal of particles below approximately 0.002 m in diameter. Likewise, under linear acceleration of 133 $m.s^{-1}$ (excluding frictional and turbulence considerations) this critical diameter would only reduce to around 1mm. Clearly, such forces would not be suitable for the measurement of respirable sized material. As expected, the centrifugal forces acting on respirable sized particles would be far greater than the both gravity and re-entrainment methods. However, using optimum

centrifuge settings of 40,000 rev.min^{-1} at a radius 0.0674 m, (as described by Clarke et al 2002) the minimum theoretical particle size detached would be around 10 μm.

Essentially, such theoretical calculations (Figure 1.4.1) highlight the limitations of current force measurement methodology.

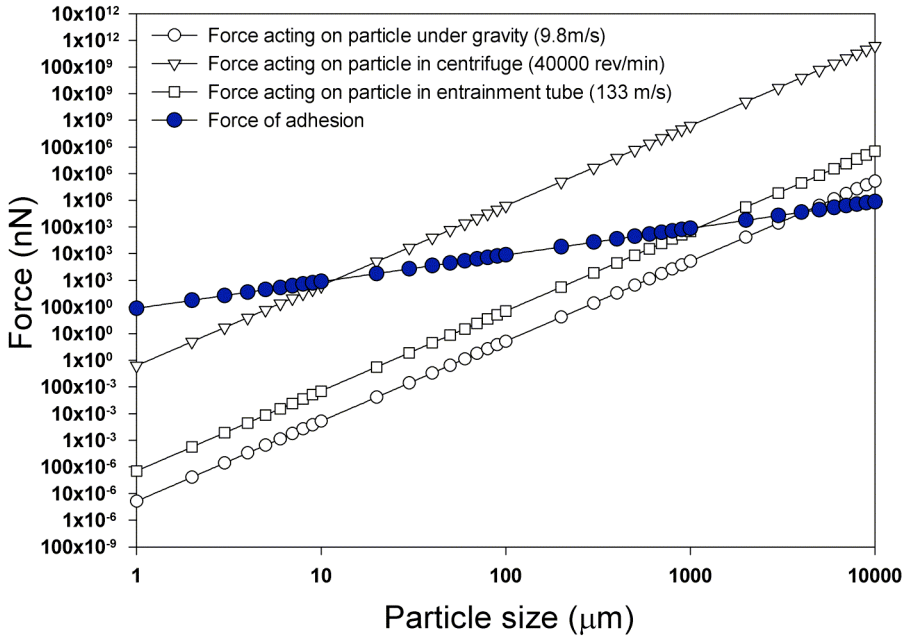

Figure 1.4.1 Theoretical Force required to removal a hydrophobic sphere (of specific diameters) from a planar surface plotted alongside theoretical forces acting on it due to gravity, and linear accelerations.

However, It is important to note, that such calculations are based on both empirical and theoretical equations which assume uniform hydrophobic spheres with standardised density (1000 Kg.m^{-3}) at 45% RH. In comparison, micronised particles, will to some extent, have irregular surface morphology, and will be far from perfect spheres. Subsequently, the forces acting on the particles may vary greatly from the theoretical and empirical calculations, due to variations in contact geometry. To further satisfy the null-hypothesis that particles could be removed using CPD or re-entrainment a preliminary investigation was undertaken to examine the detachment force of micronised particles from planar surfaces.

A detailed overview of the CPD and re-entrainment studies is given in Appendix A 1.1 and A 1.2, respectively. Micronised salbutamol sulphate (albuterol sulphate) was used as the model particulates and aluminium or glass stubs chosen as the adhering substrate. Briefly the CPD followed the methodology described by Clarke et al (2002) while a custom-built experimental set-up was used for re-entrainment investigation.

Essentially, both techniques indicated individual particles to remain on the substrate surface using both maximum centrifugal acceleration and re-entrainment flow rates (133 $m.s^{-1}$). Such observations were confirmed visually and are shown in Figure 1.4.2 and 1.4.3 for CPD and re-entrainment studies, respectively.

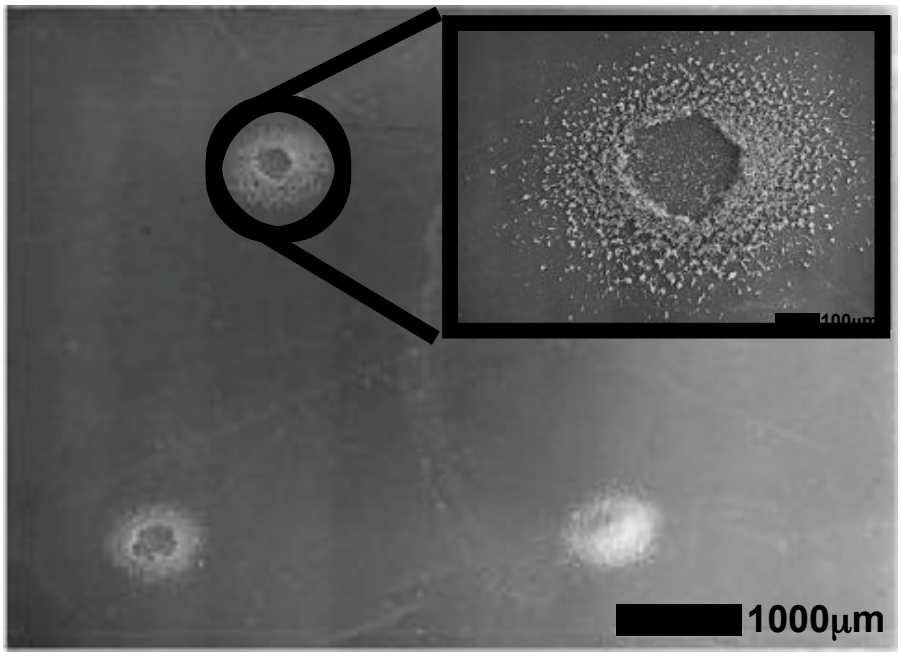

Figure 1.4.2 CPD particle distributions on aluminium stubs, post centrifugation (adapted from Clarke et al *2002).*

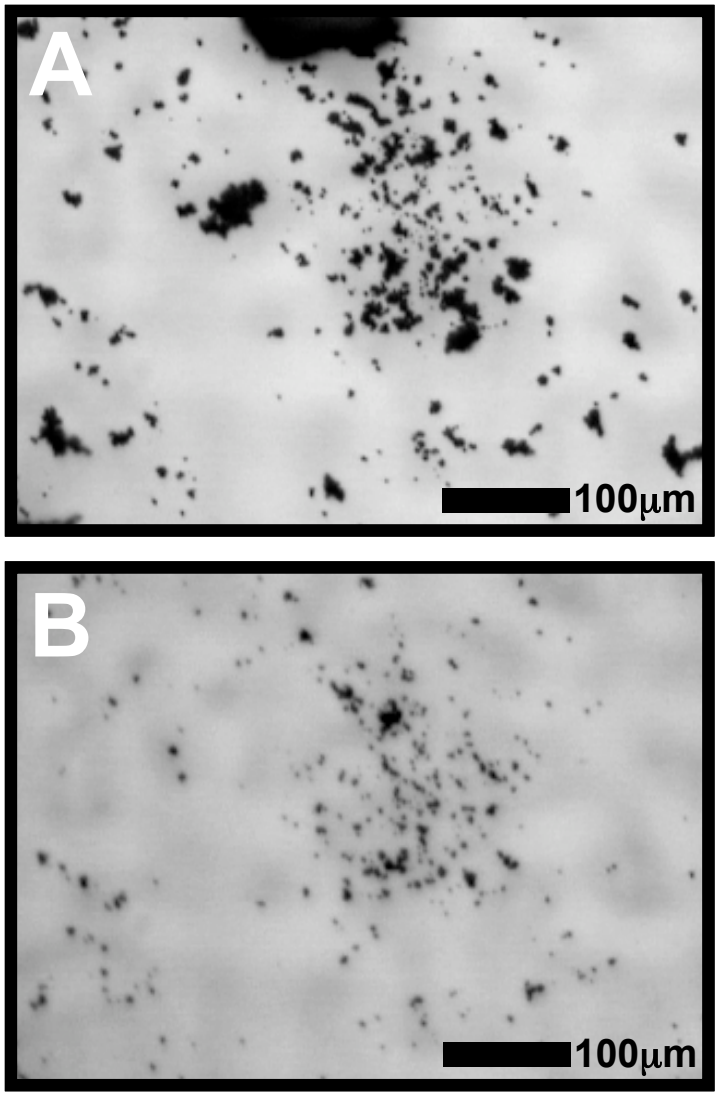

Figure 1.4.3 Entrainment tube particle depositions (a) prior to and (b) post acceleration velocities of 133 m.s^{-1}.

Although previous studies using CDP and re-entrainment have suggested the removal of micronised particles possible (using current methodology), the most likely explanation for such results would be due to detachment of agglomerated material.

Simply put, the majority of micronised particles, when handled, will almost certainly form loose agglomerates due to large contact areas and consequent cohesive forces. Subsequently, the removal of agglomerated particles, deposited on planar surfaces, would be more likely than their individual counterparts (due to an increased mass to surface area ratio). Such

experimental errors would ultimately lead to underestimation of micronised particle force values by many orders of magnitude. This can be seen, for instance, when considering the CPD or re-entrainment studies; where although large percentages of drug particles were removed (agglomerates) the individual particles remained.

Although the likelyhood of individual particle detachment does become unlikely at the respirable size range, it is important to remember that particle substrate adhesion will also be dependent on the physico-mechanical properties of the two contiguous surfaces. For example, when using a low surface energy substrate (such as PTFE) or material with a nano-scale roughness, the adhesion will be significantly decreased, thus increasing the potential for removal (Packham 1996, Podczeck 1998b).

However, in most situations this will not be the case. In general, many materials used in a DPI will not readily facilitate particle removal. Hence, the primary forces influencing aerosolisation efficiency within DPI systems will be cohesion forces between the agglomerated micronised particles. Subsequently, the measurement of inter-particulate cohesion would provide a means of assessing the aerosolisation efficiency of drug particles entrained in airstreams during patient delivery.

The potential for using the aforementioned methods to determine such interactions would be limited, as it would not allow differentiation between agglomerate and particle-particle interactions. Furthermore, both chemical or optical determination of detachment forces would produce potential problems, as the substrate would be constructed from the same material as the particles under observation. The atomic force microscope (AFM) may provide a means of overcoming such limitations.

1.5 POTENTIAL OF ATOMIC FORCE MICROSCOPY IN DETERMINING INTERPARTICULATE INTERACTIONS.

The atomic force microscope (AFM) was developed in 1986 by Binnig et al and to date presents itself as the only means of determining the force of interaction between a particulate upon approach and retraction from a substrate. Force measurements of this type are achieved by attaching a sample particulate to a micro-fabricated cantilever probe. Measurements of the forces are determined as a function of the cantilever deflection with respect to cantilever/substrate separation. Furthermore, the technique allows real time in-situ investigation with little or no sample preparation, without the need for chemical or visual analysis.

Although the AFM was proposed as a tool for such colloidal measurements in 1991 (Ducker et al), literature relating the AFM to pharmaceutical powder adhesion is very limited. Indeed, the majority of such reports have been published during the course of this investigation (Ibrahim et al 2000, Sindel and Zimmermann 2001, Louey et al 2001, Eve et al 2002 ,Berard et al 2002). A more comprehensive review of the AFM apparatus is given in Chapter 4.

1.6 AIMS OF THE STUDY

The process of micronisation results in the formation of particulates with a high surface area and therefore high surface free energy. Subsequently this may lead to an unstable cohesive system that would readily agglomerate or adhere to surfaces (in order to lower the net free energy). It is believed that the cohesive and adhesive forces differ between particulate systems, thus leading to large variations in mixing, stability and DPI performance. It is proposed that such variations are due to a combination of particulate morphology and intrinsic surface energy, with the interactions between these systems being dependent upon the environmental conditions in which they are processed, stored and delivered.

The primary aim of the study was to characterise the physico-mechanical properties of three micronised powders, believed to have significantly different surface free energies and physical properties. Three micronised drugs, of comparable particle sizes, were chosen for investigation; salbutamol sulphate, whose formulation is generally regarded as relatively straightforward, disodium cromoglycate (DSCG), a hygroscopic powder, and triamcinolone acetonide (TAA), a material recognised for its electrostatic charging during handling and processing.

Of particular interest, was the influence of humidity on the interactive properties of the three materials, as such environmental factors would potentially have different influences on particle-particle cohesion. In order to obtain such goals, the materials were first characterised using a series of general micromeritic, thermal and imaging techniques. Furthermore, the influence of humidity on the water sorption, surface energy and crystal structure were analysed under controlled environmental conditions.

The primary technique used for particle characterisation was atomic force microscopy. A micromanipulation technique was developed to enable the attachment of 5 μm particles to AFM cantilevers, while a custom-built perfusion apparatus was constructed to allow environmental control. Separation energy measurements between individual micronised particles and model drug substrates could then be conducted at a range of humidities and analysed to produce specific cohesion profiles for each micronised drug.

Finally, for correlation purposes, a series of in-vitro aerosolisation investigations for each micronised drug were conducted while contained within an environmental humidity test chamber.

2 GENERAL MATERIALS, METHODS AND CHARACTERISATION.

In order to understand the complexity of such particle-particle interactions the micronised drugs were first characterised in terms of particle size, surface area, density, solubility, chemical composition, thermal response and sample morphology.

2.1 MATERIALS.

Micronised salbutamol sulphate (batch no. 300317), micronised triamcinolone acetonide (TAA) (batch no. 85BPR) and disodium cromoglycate (DSCG) (batch no. F60267) were supplied by Aventis Pharma (Holmes Chapel, Cheshire, UK). All solvents used throughout the study were supplied by BDH (Poole, Dorset, UK) and were of at least analytical grade. Dry nitrogen and helium was supplied by BOC gases (Guilford, UK). Water was prepared by reverse osmosis (MiiliQ, Molsheim, France).

The chemical structures for salbutamol sulphate, TAA and DSCG are shown in Figure 2.1.1 (a, b and c, respectively) In general, both the chemical and macroscopic crystal structure for salbutamol sulphate and TAA are straight forward. Salbutamol sulphate contains two salbutamol groups to each sulphate group and thus forms a relatively neutral monoclinic crystal system.

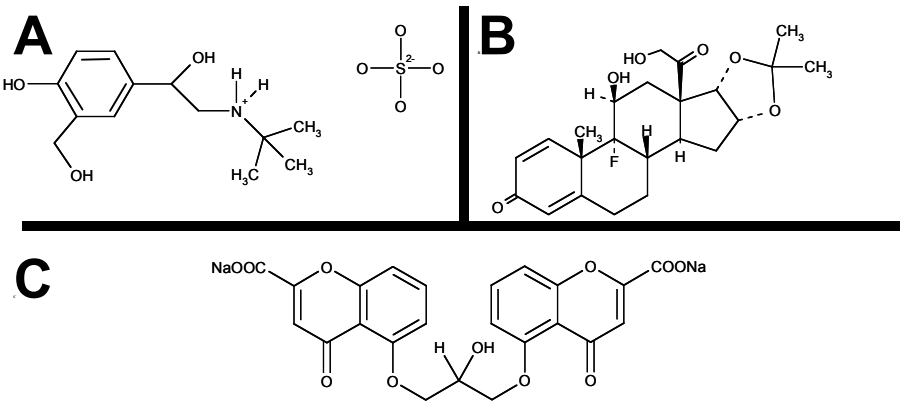

Figure 2.1.1 Chemical structures for (a) salbutamol sulphate, (b) TAA and (c) DSCG.

Likewise the structure for TAA is generally considered relatively normal and can be compared to other commonly used steroids such as beclometasone dipropionate and budesonide (Florey 1972). However, it is important to note, little can be found in the literature regarding the crystal structure of TAA.

In comparison, DSCG can be classed as a nematic, chromonic liquid crystal that below 93% RH forms a solid solution (Hartshorne and Woodard 1973, Cox et al 1971, Chen et al 1999) In simple terms, the crystal structure can be considered as a interstitial solid of 'stacked' cromoglycate groups (molecular rods) held together by water molecules (Hartshorne and Woodard 1973, Cox et al 1971) Effectively, disodium cromoglyate will adsorb water into the crystal structure and reach a dynamic equilibrium at any specific humidity (Hartshorne and Woodard 1973, Cox et al 1971). The adsorption of water into the crystal lattice is accompanied by a modification of the cromoglycate molecular torsional angles. Such modification will consequently cause minor alterations to the crystal structure (Chen et al 1999).

2.2 PARTICLE SIZE.

The particle size distribution of the three micronised drugs was determined by laser light scattering. In simple terms, such measurements are achieved by measuring the intensity and pattern of scattered light from a laser passing through a particulate sample (BSI 1999). In addition, the application of Mie theory, taking into account the optical properties of the material, allows measurement of particles with a diameter of less than 10μm. Particle size distributions are calculated by matching experimental and theoretical diffractograms (BSI 1999).

2.2.1 Materials and Methods.

Particle size analysis was determined by laser light scattering (Mastersizer 2000, Malvern Instruments, Worcs, UK) using a large volume circulating sample dispersion cell. Approximately 100 mg of powder was suspended in a 0.1% w/w lecithin cyclohexane solution and ultrasonicated for 5 minutes at 25°C prior to analysis (experimentally determined to be sufficient to fully de-agglomerate each powder (Appendix 2.1)). Cumulative undersize particle diameters were calculated and corrected for refractive index using best-fit algorithm software. All samples were prepared and analysed in triplicate.

2.2.2 Results and Discussion.

The median particle diameter ($d_{0.5}$), 10^{th} percentile and 90^{th} percentile undersize values for the three micronised drugs were calculated from the particle size distribution and are summarised in Table 2.2.1. In addition, graphical representation of the size distributions is detailed in Appendix 2.2.

Drug	$d_{0.1}$ (μm)	$d_{0.5}$ (μm)	$d_{0.9}$ (μm)
Salbutamol sulphate	0.60	4.79	10.53
TAA	2.57	4.39	7.48
DSCG	2.71	5.44	11.12

Table 2.2.1. Particle diameter distributions for the micronised drugs.

Median $d_{0.5}$ particle diameters for salbutamol sulphate, TAA and DSCG were calculated as 4.79 μm, 4.39 μm and 5.44 μm, respectively, using refractive indices of 1.29, 1.32 and 1.30, suggesting all three micronised drugs were of similar size and were suitable for inhalation applications (Pritchard 2001). In addition, the presence of two discrete peaks for salbutamol sulphate (between approximately 0.1 and 1 μm and 1 and 11 μm) suggested a bimodal particle size distribution with the majority of particles between 1 and 11 μm.

2.3 SURFACE AREA.

Specific surface areas of the three micronised drugs were determined by nitrogen adsorption. Briefly, the principle involves measuring the difference in pressure between a sample and reference blank, under isothermal conditions, after addition of finite quantities of adsorption gas. By applying the B.E.T equation, describing monolayer-multilayer surface adsorption it is possible to calculate the point of monolayer coverage and thus surface area (Webb and Orr 1997). The linear form of the BET equation is given in Equation 2.3.1

$$\frac{P}{V_a(P_0 - P)} = \frac{1}{V_m C} + \frac{(C-1)}{V_m C}\frac{P}{P_0} \qquad \textit{Equation 2.3.1} \qquad \textit{BET equation.}$$

Where *P* is the partial pressure of adsorbate, V_a is the volume of gas adsorbed at the specific pressure, V_m *is the volume of adsorbed gas in a monolayer,* P_o is the saturation point of the adsorbate and *C* is the BET constant. Subsequently, by plotting the transform $\frac{P}{V_a(P_0 - P)}$ vs. $\frac{P}{P_0}$ the monolayer coverage can be calculated from the slope and intercept.

2.3.1 Materials and Methods.

Specific surface area was measured by 5-point BET nitrogen adsorption (Gemini 2360, Micromeritics, Dunstable, UK) at 77 K in triplicate. Samples were accurately weighed into standard glass bulbs and dried under nitrogen at 40°C for 24 hours prior to analysis (FlowPrep 060 Micromeritics, Dunstable, UK).

2.3.2 Results and Discussion.

Specific surface areas for salbutamol sulphate, TAA and DSCG were 3.76(0.03), 5.14(0.19) and 8.85(0.09) $m^2.g^{-1}$, respectively (n=3).

2.4 POROSIMETRY.

Porosimetry determination works on a similar principle to that of surface area calculations (Chapter 2, 2.3). As with surface area determination, in which calculations are based on the monolayer-multilayer relationship described by the BET theory, condensation of gas in the multilayer region can be investigated by incrementing the vapour pressure until saturation (typically 0.995 P/P_o). By calculating the vapour sorption as a function of P/P_o, specific values for pore diameters can be calculated. Calculations are based on the BJH method (Webb and Orr 1997), which adopts the Kelvin equation (Equation 2.4.1)

$$\ln\left(\frac{P^*}{P_0}\right) = -\left(\frac{2\gamma\nu\cos\theta}{RTr_m}\right)$$

Equation 2.4.1 Kelvin equation.

Where P^* is the critical pressure, γ is the liquid surface tension, ν is the molar volume of condensed vapour, θ is the contact angle between the solid and condensed phase and r_m is the radius of curvature of the meniscus.

In simple terms, the BJH theory assumes a stepwise sorption/desorption of adsorbate into surface pores in relation to pore saturation (set arbitrarily at around 0.995 P/P_o). The relative adsorbate sorption/desorption at each step can thus be used to theoretically calculate the volume of pores filled at each step.

The thickness (t) of adsorbate remaining on the pore walls is calculated from Equation 2.4.2

$$t = \left[\frac{13.99}{0.034 - \log_{10}\left[\frac{P}{P_0}\right]}\right]^{\frac{1}{2}}$$

Equation 2.4.2 Adsorbed layer thickness.

Thus by combining statistical thickness (*t*) and Kelvin radius (r_K), the pore diameter (d_p) may be calculated (Equation 2.4.3).

$$d_p = 2 * (t + r_k) \qquad \textit{Equation 2.4.3} \qquad \textit{Pore diameter calculation.}$$

2.4.1 Materials and Methods.

Porosimetry of the three micronised drugs were investigated using a Micromeritics Tristar 3000 (Micromeritics Dunstable, UK). Samples of each micronised drug were dried using the same conditions and experimental procedure as described in Chapter 2.3. Approximately 0.5 g of each dried sample was weighed into standard sample vials and exposed to a pressure cycle of 0.005 to 0.995 (P/P_0) at 77 K.

2.4.2 Results and Discussion.

A summary of the relative pore volumes for salbutamol sulphate, TAA and DSCG are given in Table 2.4.1 and Figure 2.4.1

Pore Volume type.	Salbutamol - sulphate ($cm^3.g^{-1}$)	TAA ($cm^3.g^{-1}$)	DSCG ($cm^3.g^{-1}$)
Single point desorption total pore volume. (<0.8514 nm at P/Po 0.005)	0.000408	0.000859	0.001309
BJH adsorption cumulative pore volume. (1.7-300 nm pore diameter)	0.008242	0.011106	0.02327
BJH desorption cumulative pore volume. (1.7-300 nm pore diameter)	0.008169	0.01102	0.023246

Table 2.4.1 Pore volumes (<300 nm) for the three micronised drugs.

The cumulative pore volumes for all three micronised drugs were relatively low. However, this was to be expected, as the materials were essentially crystalline and would therefore not contain a large amount of pores.

It would be envisaged, that the majority of 'pores' present on the surface would be due to a combination of factors, including cracks and crevices (induced during the milling process), variation in particle size (i.e. small crystallites (<100 nm) throughout the powder) and intrinsic crystal surface defects (produced during the crystallisation process).

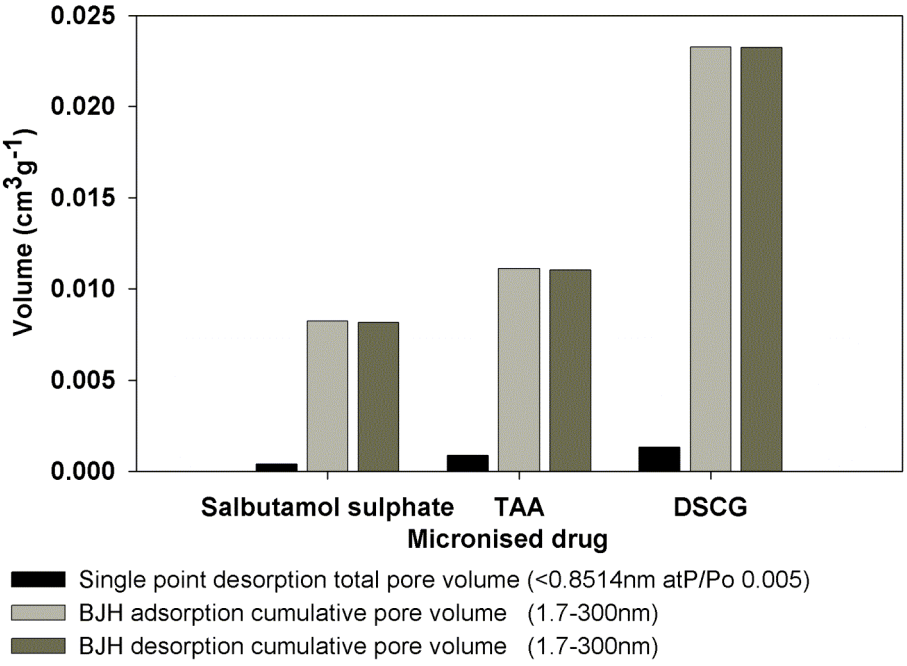

Figure 2.4.1 Pore volumes (<300 nm) for the three micronised drugs.

The cumulative pore volumes for DSCG were approximately twice that of salbutamol sulphate or TAA. Although this may be related to the presence of mechanically induced surface damage, one possibility is the influence of crystal structure. In simple terms, the crystal structure of DSCG can be classified as a series of DSCG molecules stacked to form 'rods', which are held together by interstitial water molecules in the form of channels. It therefore stands to reason, that in a 'dry' state, a similarly sized molecule such as nitrogen could easily fill the channels.

2.5 TRUE DENSITY.

True density measurements were determined by helium pycnometry. Measurements are preformed by measuring the pressure change of helium in a calibrated volume in relation to a known mass with unknown volume (Webb an Orr 1997).

2.5.1 Materials and Methods.

True density measurements were determined using helium pycnometry (Accupyc 1330 Gas Pycnometer, Micromeritics, Norcross, GA). Samples were prepared by drying in open pans at 40°C for 24 hours prior to analysis. The temperature was maintained at 27°C during out-gassing and analysis. Each sample was run ten times.

2.5.2 Results and Discussion.

True density measurements for salbutamol sulphate, TAA and DSCG were determined as 1.309 ± 0.003 $g.cm^{-3}$, 1.318 ± 0.004 $g.cm^{-3}$ and 1.57 ± 0.001 $g.cm^{-3}$, respectively.

2.6 SOLUBILITY.

Accurate solubility values for the three micronised drugs were determined in order to understand the affinity and interactions of the drugs with water.

2.6.1 Materials and Methods.

A supersaturated solution of drug in water was prepared by continued addition of drug to approximately 20 ml water (reverse osmosis, Millipore, Watford, UK). Samples were agitated in a gyratory water bath shaker (G76, New Brunswick Scientific, New Jersey, USA) at 25° C for 48 hours prior to analysis. Each sample was filtered (under vacuum) through a 0.4 μm cellulose acetate filter. The collected solution was then re-filtered through a 0.1 μm PTFE single use syringe filter (Whatman, Madison, UK). The recovered solution was weighed and dried in an oven at 50°C. The recovered, dry mass was reweighed and solubility calculated. Samples were analysed in triplicate.

2.6.2 Results and Discussion.

Solubility for the three micronised drugs in water is given in Table 2.6.1. As expected, the sulphate of salbutamol was freely soluble in water, while the TAA can be classified as practically insoluble. In addition, the solubility for DSCG could not be accurately recorded as it formed a lyotropic, chromonic liquid crystal. (Cox et al 1971, Hartshorne and Woodard 1973). This observation was confirmed by observation of DSCG under a microscope using a crossed polarised filter.

Salbutamol sulphate	42.1 ± 0.3% $^{w}/_{w}$
TAA	0.0097± 0.0001% $^{w}/_{w}$
DSCG	N/A*

Table 2.6.1. Solubility values for salbutamol sulphate, TAA and DSCG in water at 25°C. N/A DSCG formed a lyotropic chromonic liquid crystal.*

2.7 DIFFERENTIAL SCANNING CALORIMETRY.

The influence of heating on the thermal properties of the micronised drugs was investigated using differential scanning calorimetery (DSC). In principle, DSC operates by measuring the heat flow associated with chemical changes in a material (i.e. crystallisation or melting) in relation to change in temperature. This is achieved by measuring the current required to maintain an equal heat flow to both a sample and reference during heating or cooling (Charsley and Warrington 1992).

2.7.1 Materials and Methods.

Thermal properties of the micronised drugs were investigated using a differential scanning calorimeter (DSC 2920, TA instruments, Surrey, UK). Approximately 5-10 mg of micronised drug was accurately weighed into a DSC sample pan and crimped with a lid to form a hermetic seal. The sample and reference (empty hermetically sealed pan) were heated using a 10 $^{\circ}C.min^{-1}$ ramp rate. Calibration of the DSC was checked by measurement of an indium standard (melting point, 156.6°C).

2.7.2 Results and Discussion.

Representative thermograms of salbutamol sulphate, TAA and DSCG are shown in Figure 2.7.1 (a, b and c, respectively).

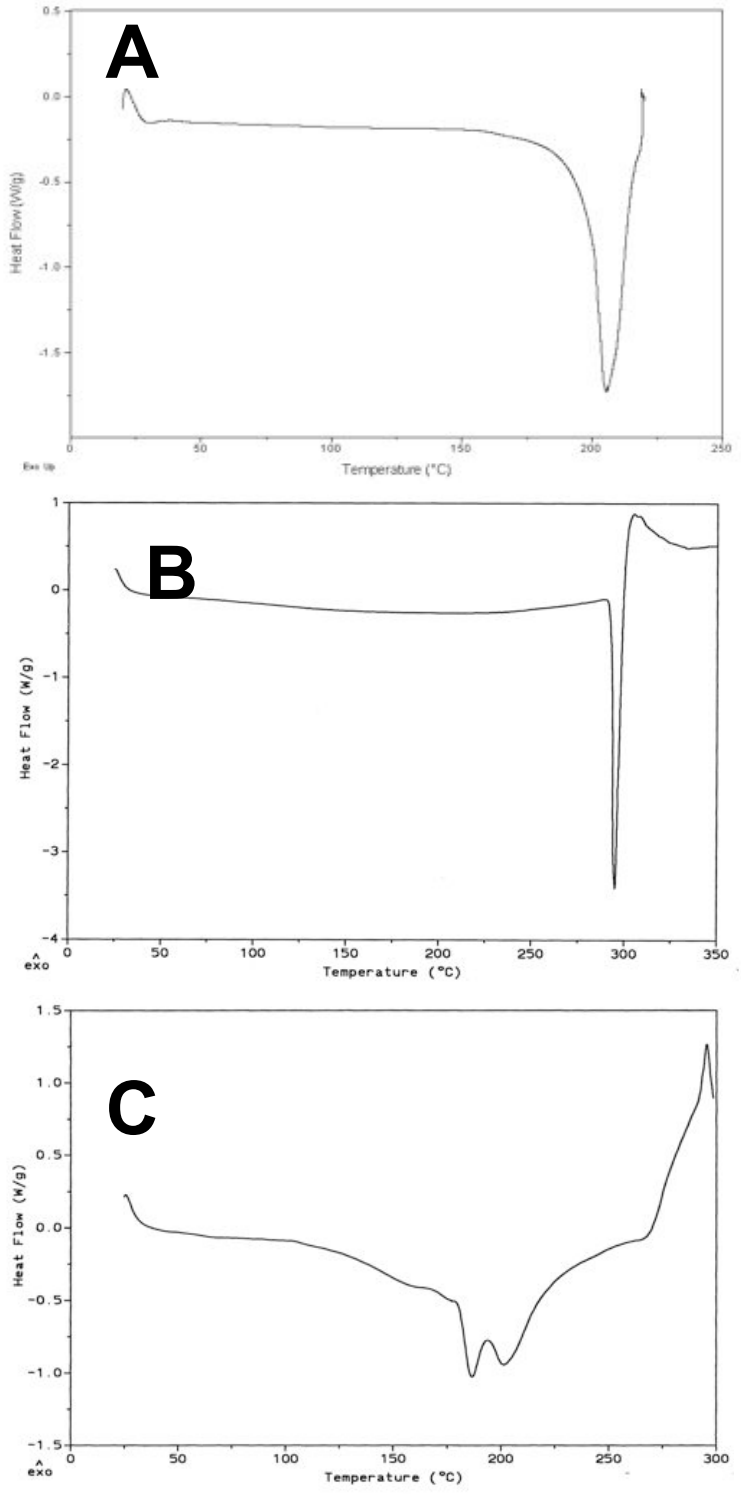

Figure 2.7.1 Differential scanning calorimeter thermographs of (a)salbutamol sulphate, (b) TAA and (c) DSCG.

The DSC thermograph for salbutamol sulphate (Figure 2.7.1a) suggested an isothermal response with respect to heat flow until an endothermic response was observed with a peak at approximately 205°C (suggesting a melt with decomposition). In general, such observations were in good correlation with previously published data (Ward and Schultz 1995).

Analysis of the DSC thermographs for TAA suggested a relatively stable isothermal behaviour (with respect to temperature), until a large endothermic-exothermic response was observed at approximately 294°C. Such observations suggested a melting with subsequent degradation (Figure 2.7.1b), and are in good agreement with previously reported studies (Florey, K 1972).

In contrast, the thermal response for DSCG (Figure 2.7.1c) produced a wide endothermic response from approximately 100°C to 250°C, indicative of water loss and melting of a hydrated organic material (Charsley and Warrington 1992). Again, such observations are in good agreement with previously published work (Cox et al 1971), which demonstrated DSCG to undergo a complex phase transition when heated.

2.8 THERMOGRAVAMETRIC ANALYSIS.

The influence of heating on the mass change of the three micronised drugs was investigated using thermogravametric analysis. In simple terms the technique involves suspending a sample (typically 10-100 mg) from a microbalance, inside a cylindrical oven cell. Nitrogen is passed through the cell, and the oven is heated by a programmable temperature controller. Changes in mass can thus be recorded as a function of temperature and/or time. A more detailed description of this technique can be found elsewhere (Charsley and Warrington 1992).

2.8.1 Materials and Methods.

Approximately 50 mg of sample was weighed onto a tarred, open sample pan in the thermogravametric analyser. (TGA 1 Thermogravametric analyser, Perkin Elmer Instruments, Connecticut, USA). Samples were heated from 25°C to 250°C at a rate of 5°C.min^{-1}.

2.8.2 Results and Discussion.

Representative mass vs. temperature plots for salbutamol sulphate, TAA and DSCG are shown in Figures 2.8.1, 2.8.2 and 2.8.3, respectively. Mass vs. temperature plots for the three drugs are plotted on equivalent scales for comparative purposes. In addition, detailed (smaller scale) temperature axis plots for salbutamol sulphate (Figure 2.8.1b) and TAA (Figure 2.8.2b) are also included to allow closer examination of mass change.

The relative mass for salbutamol sulphate (represented as a percentage) decreased relatively little over the temperature range 25°C~175°C, with a ~0.1% w/w mass loss most likely being attributed to the removal of surface adsorbed moisture. In addition, a large drop in relative mass was observed at approximately 200°C, suggesting a melt and decomposition.

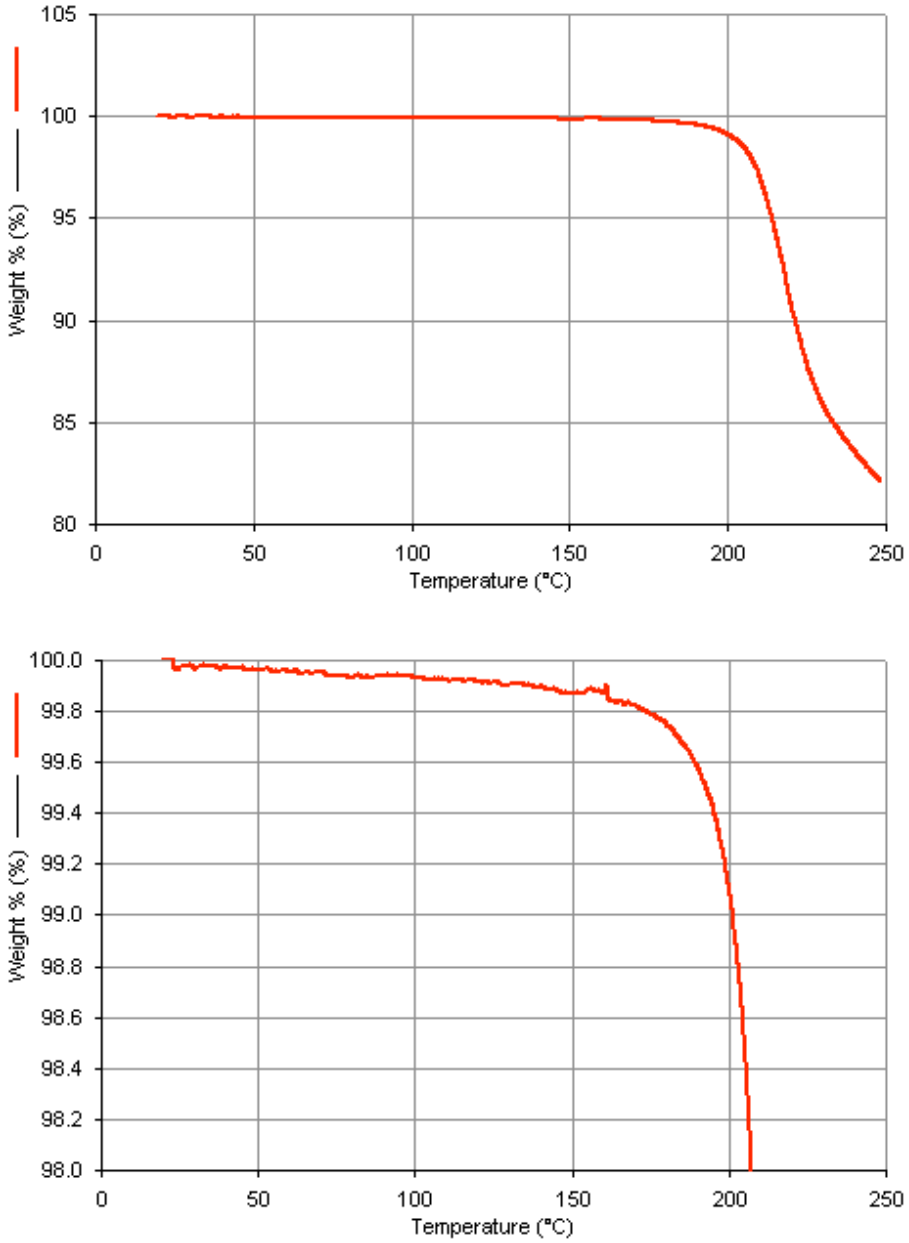

Figure 2.8.1 Thermogravametric response for Salbutamol sulphate. (25°C - 250°C at 5°C.s^{-1}). Data are presented as two separate scaled graphs for comparative reasons.

The relative mass for TAA decreased by approximately 1.2% w/w over the temperature range 25°C to 250°C, with the majority loss between 25°C and 100°C. Again, such observations are in good agreement the loss of adsorbed surface water.

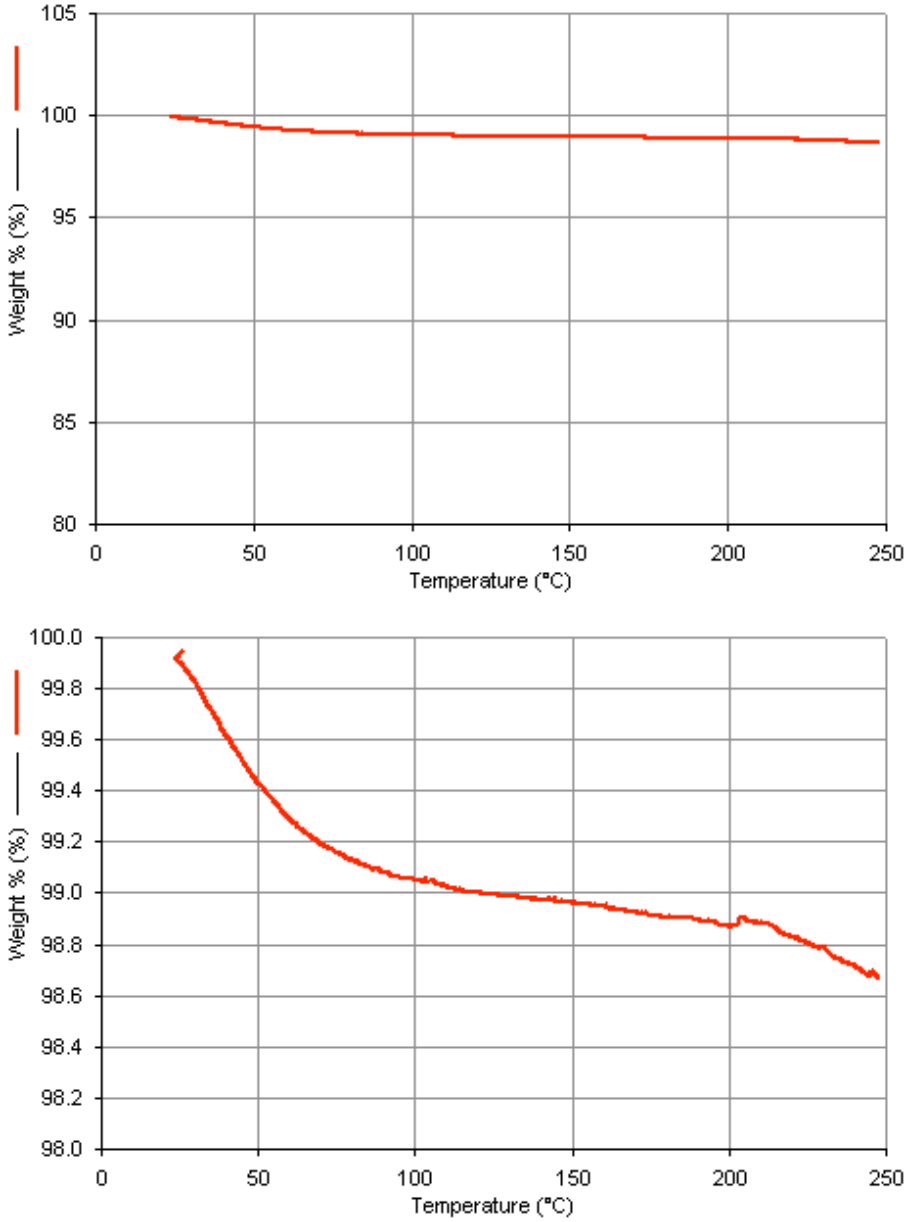

Figure 2.8.2 Thermogravametric response for TAA (25°C - 250°C at 5°C.s^{-1}). Data are presented as two separate scaled graphs for comparative reasons.

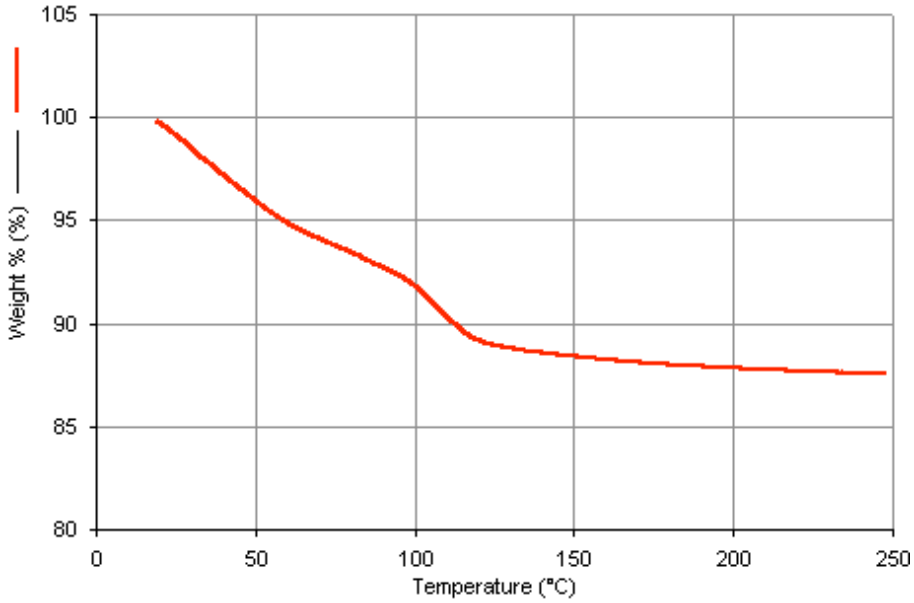

Figure 2.8.3 Thermogravametric response for DSCG – (25°C - 250°C at 5°C.s^{-1}).

In contrast, the mass loss for DSCG over the temperature range 25°C-250°C was far greater (~12%) than salbutamol sulphate and TAA. Such observations are expected, however, as DSCG is reported to contain up to nine water molecules per molecule of DSCG (Cox et al 1971). In addition, an inflection in the mass vs. temperature curve (~100°C) suggests a metastable region. Since the DSCG crystal requires water molecules to hold the structure together (Chen et al 1999), it stands to reason that a critical, stable region would exist, below which an amorphous collapse will occur.

2.9 SCANNING ELECTRON MICROSCOPY.

General morphology of the three micronised drugs was investigated by scanning electron microscopy (SEM). In simple terms, SEM generates high-resolution images of conducting samples, by collecting and analysing the secondary electrons (weekly bound conduction-band electrons) ejected as a result of high-energy electron beam collisions.

2.9.1 Materials and Methods.

Particle morphology of salbutamol sulphate, TAA and DSCG were investigated using cryogenic low temperature scanning electron microscopy (JEOL 6310, JEOL, Japan) at 10 KeV, using a method described elsewhere (Clarke et al 1998)[*].

2.9.2 Results and Discussion.

Low temperature scanning electron micrographs for the micronised salbutamol sulphate, TAA and DSCG samples are shown in Figure 2.9.1 (a, b and c, respectively). Representative photomicrographs of the 'as supplied' salbutamol sulphate and DSCG (Figure 2.9.1, a and b) suggest that the crystals have a columnar crystal shape. Photomicrographs of the 'as supplied' TAA (Figure 2.9.1c) suggest the crystal form to have an irregular plate-like crystal shape.
In addition, large variations in crystal size were observed for all three drugs. This observation correlates well with particle size data (Section 2.1) and can be attributed to the limitations of high-energy milling processes.

[*] Scanning electron micrographs taken elsewhere in the thesis used conventional SEM and not LTSEM. Samples were imaged on a Jeol 6310, (Jeol Japan) at 10 KeV. Samples were gold coated prior to analysis (Edwards Sputter Coater, UK).

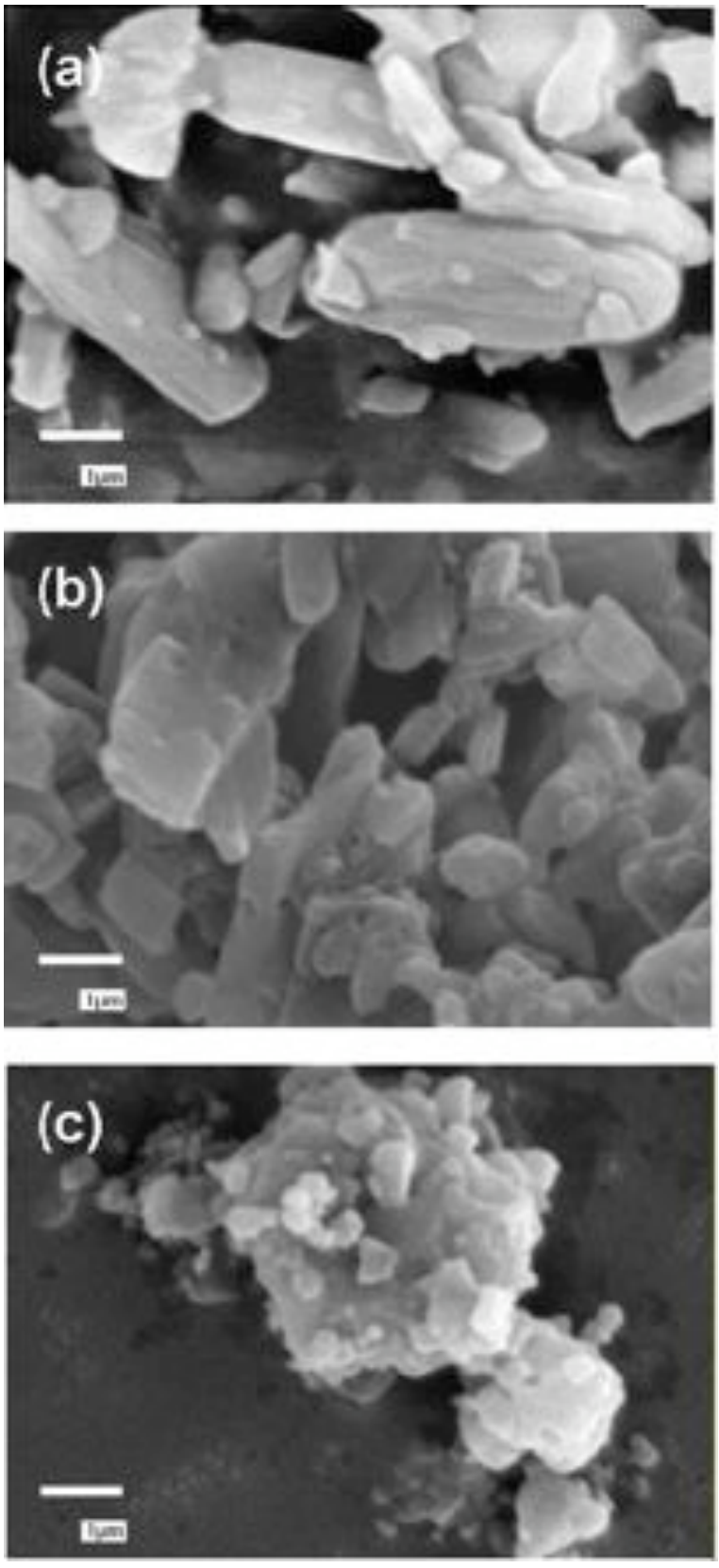

Figure 2.9.1. Low temperature scanning electron micrographs (magnification X 15,000) of (a) salbutamol sulphate, (b) DSCG and (c) TAA.

2.10 GENERAL DISCUSSION.

From preliminary investigations into the physical properties of the three micronised drugs, it becomes clear that large variations in (for example) particle size, morphology, thermal response and solubility exist. Such differences are to be expected however, as the three materials are chemically very different, and will subsequently have very specific physico-chemical and mechanical properties.

Such large variations in the physico-mechanical nature of the three micronised drugs may potentially influence all aspects of formulation, storage and delivery to the patient. For example characteristics such as density, surface area and morphology will directly influence inter-particulate adhesion forces (Hinds 1999). In addition, thermal analysis, solubility and pore size calculations indicate that the three materials to have varied degrees of water affinity (sorption and/or hydration). Such observations suggest potential variations in capillary condensation for the three micronised drugs, which would ultimately influence the degree of capillary interaction.

Consequently, a series of investigations were undertaken to determine the influence of relative humidity on the physico-mechanical properties of the three micronised drugs in an attempt to assess the impact of humidity on dry powder aerosolisation performance.

3 INFLUENCE OF HUMIDITY ON THE PHYSICAL PROPERTIES OF THE MICRONISED DRUG.

3.1 INTRODUCTION.

As previously discussed, the presence of adsorbed and/or absorbed water in pharmaceutical dry powder systems may directly influence the magnitude of the specific forces (i.e. Van der Waals, electrostatic and capillary forces) contributing to the total interaction mechanism. Consequently, a series of investigations were undertaken to determine the influence of relative humidity on the physico-mechanical properties of salbutamol sulphate, TAA and DSCG in an attempt to assess the impact of humidity on potential dry powder aerosolisation performance.

3.2 KARL FISCHER WATER DETERMINATION.

Equilibration water content of each of the micronised drugs was determined by coulometric Karl Fischer water titration. In simple terms, the reaction of water with iodine and sulphur dioxide in the presence of an alcohol and base can be measured as a function of remaining iodine present in solution.

Reaction 1: $SO_2 + CH_3OH + RN \Leftrightarrow CH_3SO_3^- + RNH^-$

Reaction 2: $CH_3SO_3^- + H_2O + I_2 + 2RN \Rightarrow CH_3SO_4 + 2RNH^+ + 2I^-$

In a coulometric Karl Fischer titration, the iodine is electrolytically generated from the anolyte and monitored by platinum electrode. As long as water is present in the reaction cell, a proportional current will be generated to produce the iodine. The reaction between one mole of water and iodine is equivalent to a charge of 10.72 *C.*mg^{-1}, therefore allowing total water content to be measured as a function of electrical input. A more detailed description of this technique is given elsewhere (Connors 1988).

3.2.1 Materials and Methods.

Equilibration water content of each of the micronised drugs was determined by storing small samples (<100 mg) of the micronised materials, in tightly sealed containers, together with different saturated salt solutions for 12 hours at a series of specific relative humidities (Appendix 3.1). Each powder was then accurately weighed (~100 mg for salbutamol sulphate and ~20 mg for TAA and DSCG), and placed directly into the titration cell before being analysed for total water content (n=3) by coulometric Karl Fischer Titration (MKC-510E, Kyoto Electronics, Tokyo).

3.2.2 Results and Discussion.

Equilibrium moisture content values for salbutamol sulphate, TAA and DSCG are given in Appendix 3.2. Moisture sorption profiles, shown graphically in Figure 3.2.1 suggested a significant (ANOVA $p<0.05$), positive increase in water content, for all three micronised drugs, as the storage humidity is increased. The water content of salbutamol sulphate was the least affected by storage humidity, increasing from 0.11 ± 0.01% w/w at 0% RH to 0.19 ± 0.03% w/w water content after storage at 84% RH. The TAA water content increased from 0.63 ± 0.06% w/w at 0% RH to 1.97 ± 0.03% w/w after storage at 84% RH. In comparison the DSCG water content increased from 3.17 ± 0.55 at 0% RH to 17.17 ± 0.31% w/w on storage at 84% RH.

In order to compare the significance of these variations a Fisher pairwise analysis ($p<0.05$) was performed on each of the three drugs at paired humidities. Although significantly different across the humidity range (ANOVA $p<0.05$), pairwise analysis indicated the influence of humidity on salbutamol sulphate to be significant between 11 and 29% RH only. Furthermore, analysis of the unpaired humidities suggested no significant variance above 29% RH. Fisher pair wise analysis for both TAA and DSCG water content after storage at varied specific humidities suggested all paired and unpaired humidities to statistically affect water sorption.

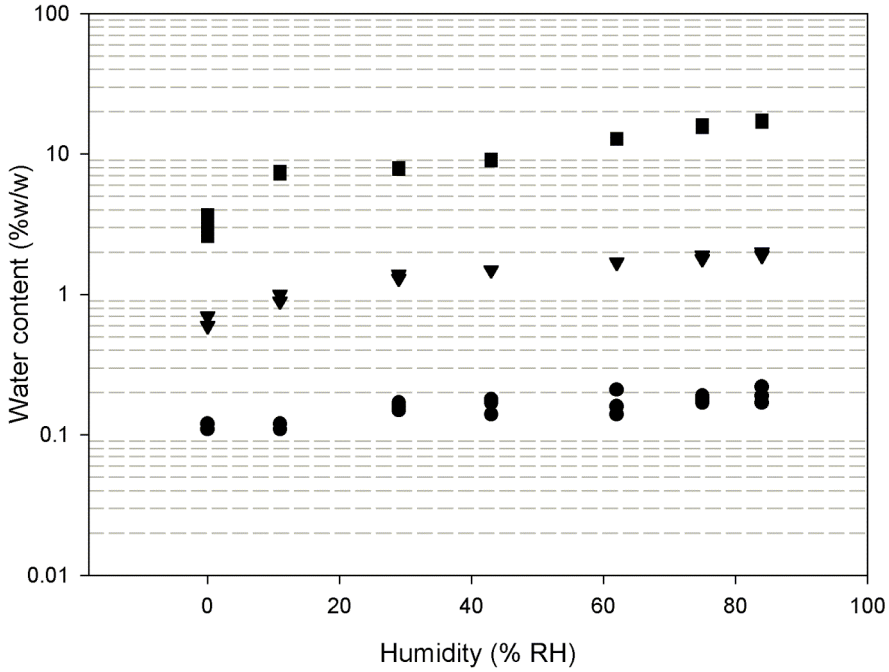

Figure 3.2.1 Moisture sorption profiles, obtained by Karl Fischer water titration, for ● salbutamol sulphate, ▼ TAA and ■ DSCG (n=3).

However, it is important to note that mean water content after storage in a humidity free environment was 0.11, 0.63 and 3.17% w/w for salbutamol sulphate, TAA and DSCG, respectively. This observation suggested either incomplete de-sorption of water or the possibility of molecularly bound water in the crystal structure. However, the most likely explanation is experimental error. Although the utmost care was taken in determining specific water content, the kinetics of water sorption after storage at 0% RH would be very rapid upon exposure to ambient conditions. In addition, the lack of statistical significance in water content for salbutamol sulphate may possibly be attributed to the lack of resolution when attempting to measure such small quantities of water. In order to further investigate these phenomena, dynamic vapour sorption of the three micronised drugs was undertaken.

3.3 DYNAMIC VAPOUR SORPTION.

The Influence of humidity on water sorption and de-sorption for salbutamol sulphate, TAA and DSCG was investigated gravimetrically, using dynamic vapour sorption (DVS). Briefly, the DVS, as shown graphically in Figure 3.3.1, consists of a 7 Figure Cahn microbalance housed inside a temperature-controlled cabinet. Relative humidity is controlled by mixing ratios of humidified and dry nitrogen together using two independent mass flow controllers, before passing over the balance reference and sample cell.

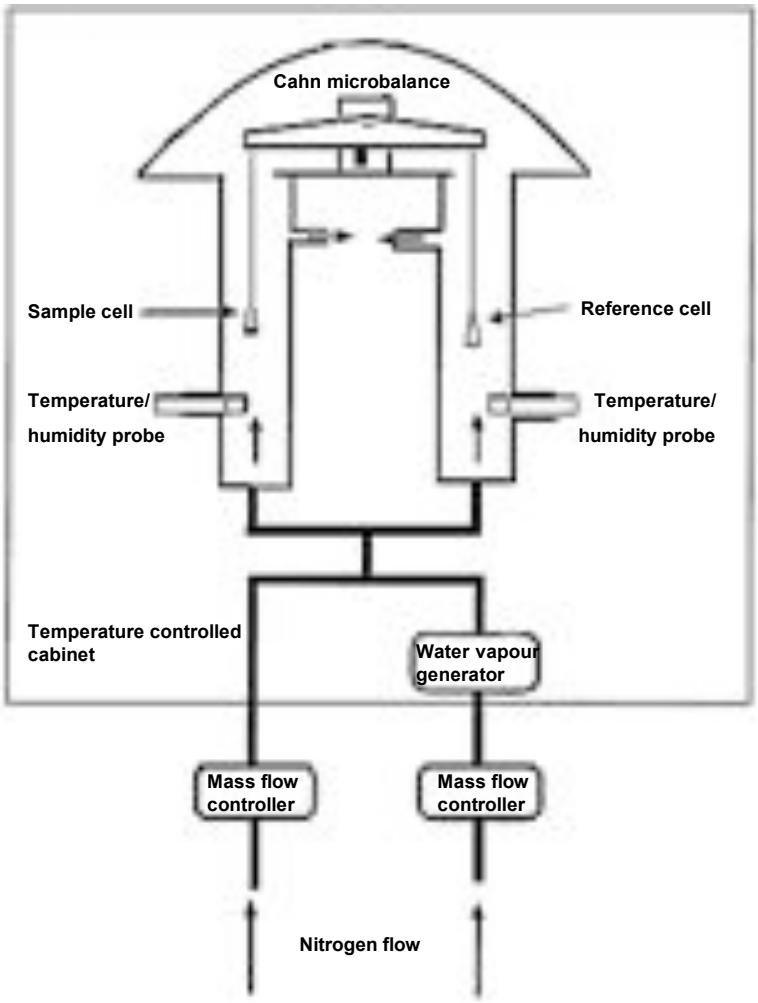

Figure 3.3.1 Schematic diagram of a DVS (Modified from DVS SMS application note Surface Measurement Systems Ltd, London, UK*).*

3.3.1 Materials and Methods.

Moisture sorption profiles for salbutamol sulphate, TAA and DSCG were determined by DVS (DVS-1, Surface Measurement Systems Ltd, London, UK). Approximately 10mg of sample was weighed into the sample cell and subjected to two 0-90% RH cycles, over 10% RH increments. Equilibration moisture content at each humidity was determined by a change in mass to time ratio of 0.002 dm/dt.

3.3.2 Results and Discussion.

Time vs. equilibrium moisture content for salbutamol sulphate, TAA and DSCG are shown graphically in Figures 3.3.2a, 3.3.3a and 3.3.4a, respectively. In addition, DVS moisture sorption isotherms, calculated as percentage dry mass, for salbutamol sulphate, TAA and DSCG are shown in Figures 3.3.2b, 3.3.3b and 3.3.4b, respectively.

The water sorption isotherms for salbutamol sulphate (shown in Figure 3.3.2b) follow a sigmoidal class L-3 curve (Giles et al 1960) suggesting multi-layer water sorption onto the crystal surfaces. Monolayer coverage of water can be calculated from the slope and intercept of the linear BET single point equation from data obtained around the first inflection (Chapter 2). Values (R^2 = 1) of 0.06% w/w water for monolayer coverage and 2.24 $m^2.g^{-1}$ for surface area were determined from the DVS data, using a projected water molecule surface area of 11.13 x 10^{-20} m^2 (Webster et al 1998). This correlated well with the surface area measurements obtained by nitrogen adsorption of 3.76 $m^2.g^{-1}$ with predicted water monolayer coverage of 0.06% w/w.

Regression analysis indicated monolayer coverage (0.06% w/w) to occur at 23% RH, suggesting that separation energy measurements conducted by AFM at 30, 45, 60 and 75% RH would be under increased multi-layer water coverage.

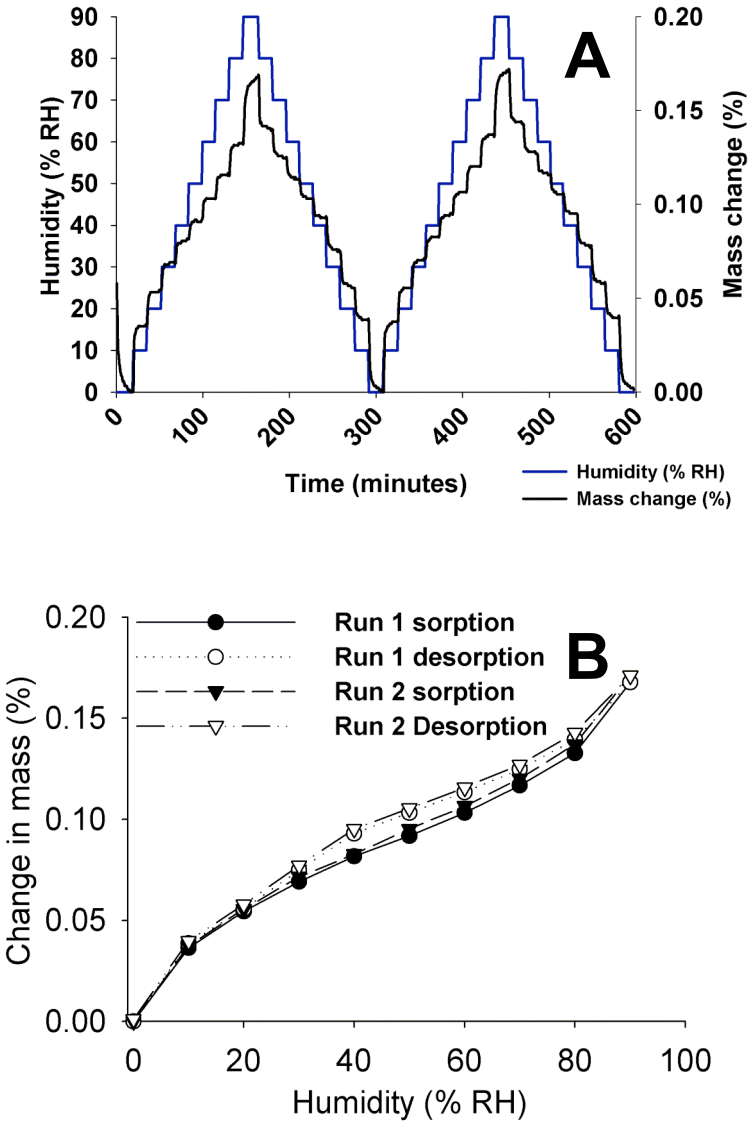

Figure 3.3.2 (a) Moisture sorption profile and (b) corresponding moisture sorption isotherms for salbutamol sulphate.

In comparison, analysis of the moisture sorption curves for TAA and DSCG suggests non-Langmuir type isotherms and thus would not allow such comparative BET calculation.

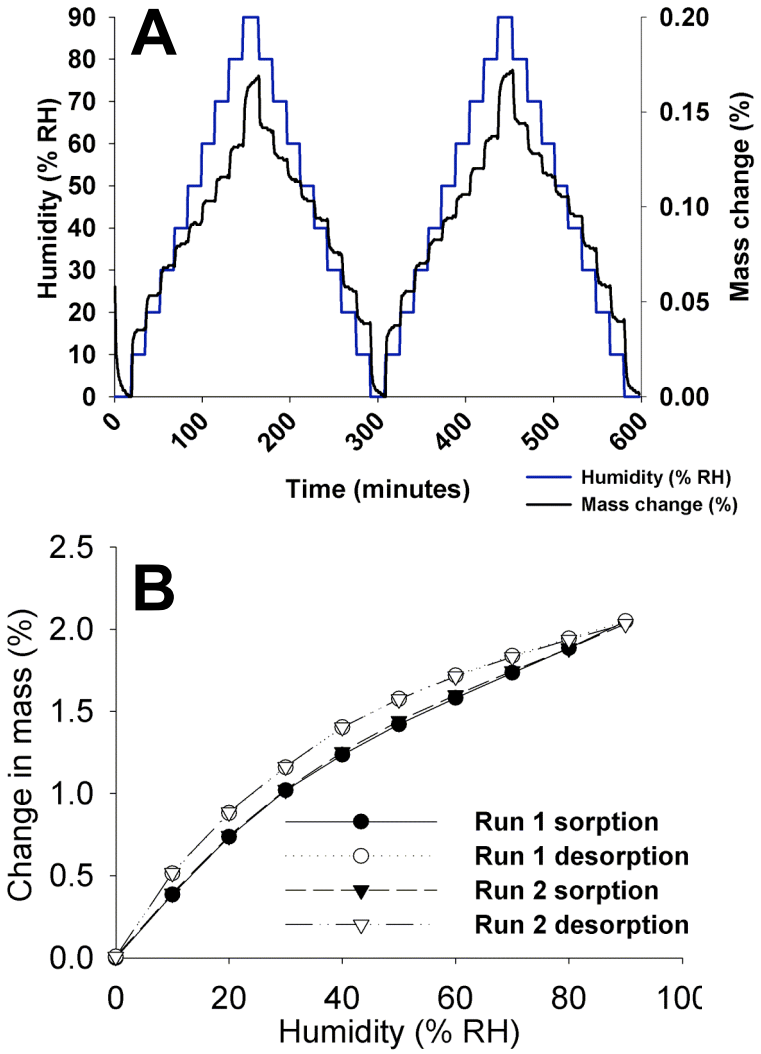

Figure 3.3.3 (a) Moisture sorption profile and (b) corresponding moisture sorption isotherms for TAA.

The relative percent moisture sorption for TAA was approximately one order of magnitude greater than that of salbutamol sulphate. Since the surface areas were of similar order (3.76 and 5.14 $m^2.g^{-1}$ for salbutamol sulphate and TAA, respectively) this suggests TAA has a higher affinity for water. Thus, it is proposed that the moisture sorption curve for TAA may be a class H curve (Giles et al 1960). Class H curves are essentially a 'high affinity' form of the L type curve in which the adsorbate may be chemisorbed.

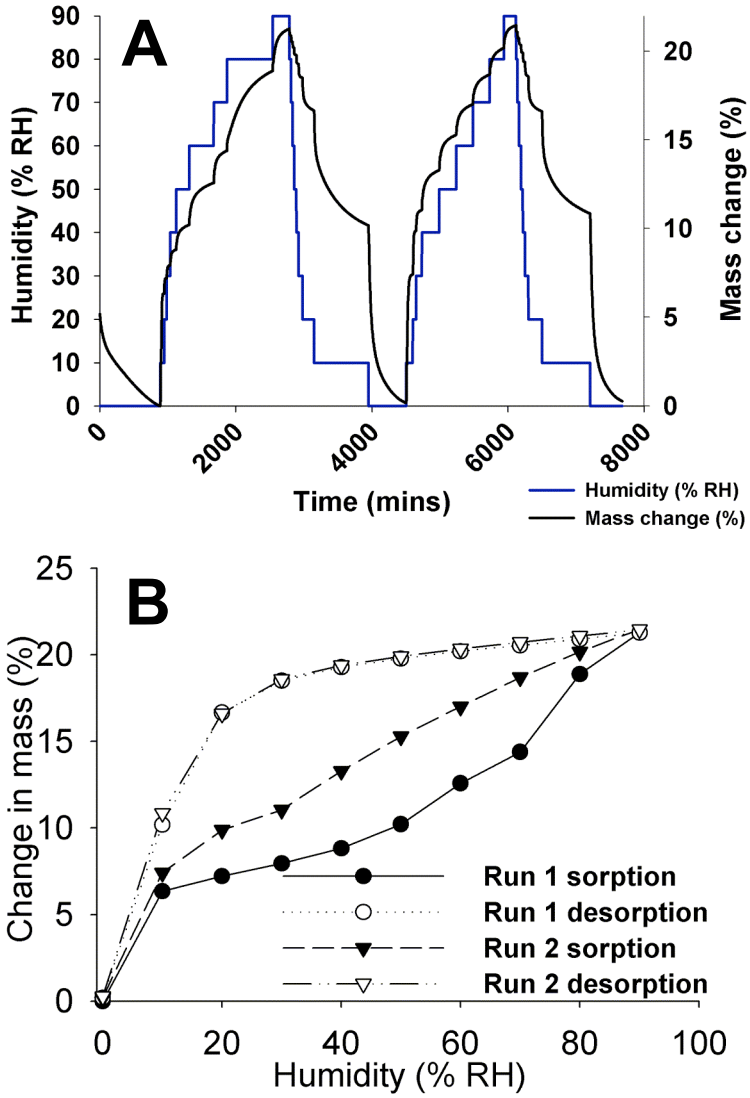

Figure 3.3.4 (a) Moisture sorption profile and (b) corresponding moisture sorption isotherms for DSCG.

Moisture sorption isotherms for DSCG (Figure 3.3.4b) suggest a class C sorption curve (Giles et al 1960). Class C curves are indicative of porous materials, with a high affinity for the adsorbate, and suggest absorption into the crystal structure. This is to be expected however, as DSCG is essentially a solid solution, whose crystal structure contains channels that allow the up to nine molecules of water per molecule of DSCG (depending on the relative humidity), before collapsing into a series of liquid crystal mesomorphs (Hartshorne and Woodard 1973).

In, addition a plot of the moisture sorption and desorption (two cycles) rate kinetics for the three micronised drugs are shown in Figure 3.3.5. Data were based upon a nominal 10mg sample and assumed equilibrium moisture content at a dm/dt of 0.002.

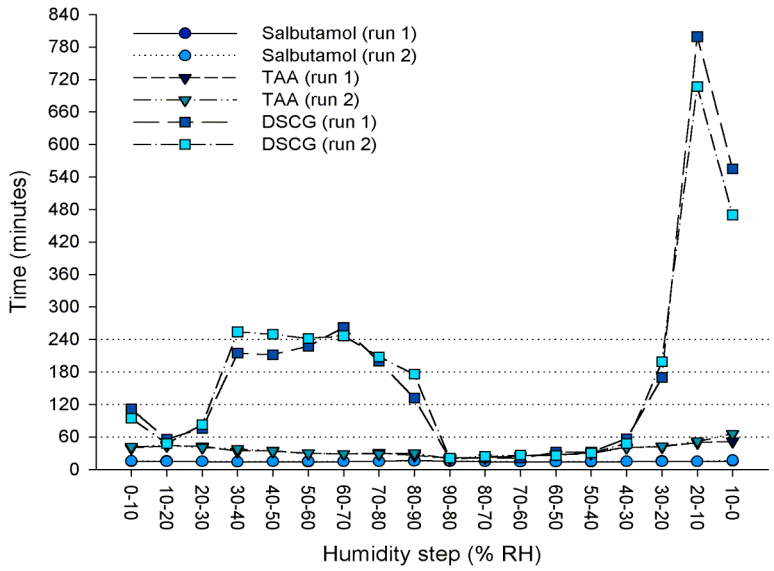

Figure 3.3.5 Influence of humidity on the rate kinetics of the micronised drugs exposed to two humidity ramp cycles (approximately 10mg)

The rate of moisture sorption and desorption for both salbutamol sulphate and TAA was relatively rapid with equilibrium being reached in less than 60 minutes at each humidity step. In comparison, the moisture kinetics for DSCG was significantly slower, with equilibrium times of up to 4 hours at some steps. This is mostly likely due to the rate at which water can penetrate into the crystal structure (Hartshorne and Woodard 1973, Chen et al 1999). Essentially, such observations indicate that DSCG should be stored for a minimum of four hours when equilibrating at a specific humidity. However, it is important to note, the data was not normalised for mass, and larger masses will inevitably require longer equilibration times. Subsequently storage times of ≥12 hours were instigated for equilibration storage of all micronised powders used in the in-vitro studies (Chapter 5), while a minimum of 60 minutes (for salbutamol sulphate and TAA) and 4 hours (for DSCG) were chosen for the AFM studies (Chapter 4).

3.4 X-RAY POWDER DIFFRACTION.

X-ray powder diffraction works on the same principle to that of conventional X-ray crystal analysis. Just as light is diffracted through a grating, a monochromatic X-ray will be diffracted by the atomic spacing that exist between the atoms in an ordered crystalline material. By rotating the crystal in relation to the X-ray beam, the three-dimensional structure can be calculated from the diffracted X-rays that pass between the crystal planes. For crystalline powder samples, the orientation of the crystalline material will be random, and thus the monochromatic X-ray will produce a diffraction cone of semi apex angle 2θ. Although this does not allow finite structural determination, it does provide a unique diffraction pattern that is particular to the material under investigation. A detailed account of the theory is given elsewhere (Guinier 1994).

3.4.1 Materials and Methods.

X-ray diffraction spectra of salbutamol sulphate, TAA and DSCG at varied humidity were obtained using an X-ray powder diffraction system with perfusion unit add-on (D5000, Bruker AXS, Cheshire, UK). Settings were as follows; Fast scan, 2 to 39.960 2-Theta, step size 0.036 2-Theta, step time 0.5 seconds Temp 25°C. X-ray powder diffractographs were taken at 15, 45 and 75% RH (±5% RH).

3.4.2 Results and Discussion.

X-ray powder diffraction patterns of salbutamol sulphate, TAA and DSCG presented in Figure 3.4.1, 3.4.2 and 3.4.3, respectively, suggested good correlation with diffraction patterns found in the literature (Ward and Schultz 1995, Ahn et al 2002 and Chen et al 1999).

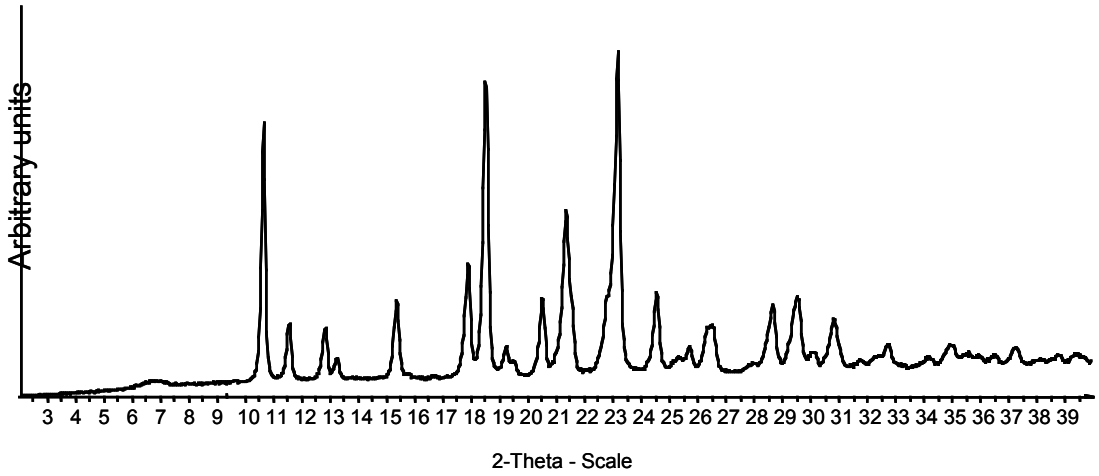

Figure 3.4.1 X-ray powder diffraction patterns of salbutamol sulphate, overlaid at 15, 45 and 75% RH.

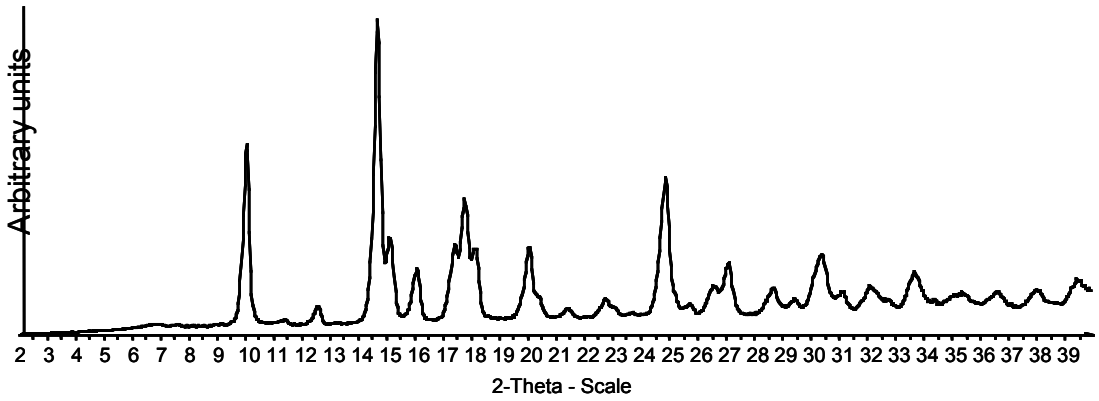

Figure 3.4.2 X-ray powder diffraction patterns of TAA, overlaid at 15, 45 and 75% RH.

Comparison of the XRPD patterns for salbutamol sulphate and TAA (overlaid in Figure 3.3.1 and 3.3.2, respectively) exhibited no change in diffraction patterns at 15, 45 and 75% RH, suggesting that the presence of water vapour had no influence on the crystal lattice. In contrast, the staggered diffraction patterns for DSCG taken at 15,30 and 75% RH (Figure 3.3.3), exhibited subtle differences in the relative peak intensities. Such observations have been reported previously and are most likely related to the sorption of water into the crystal lattice (Chen et al 1999).

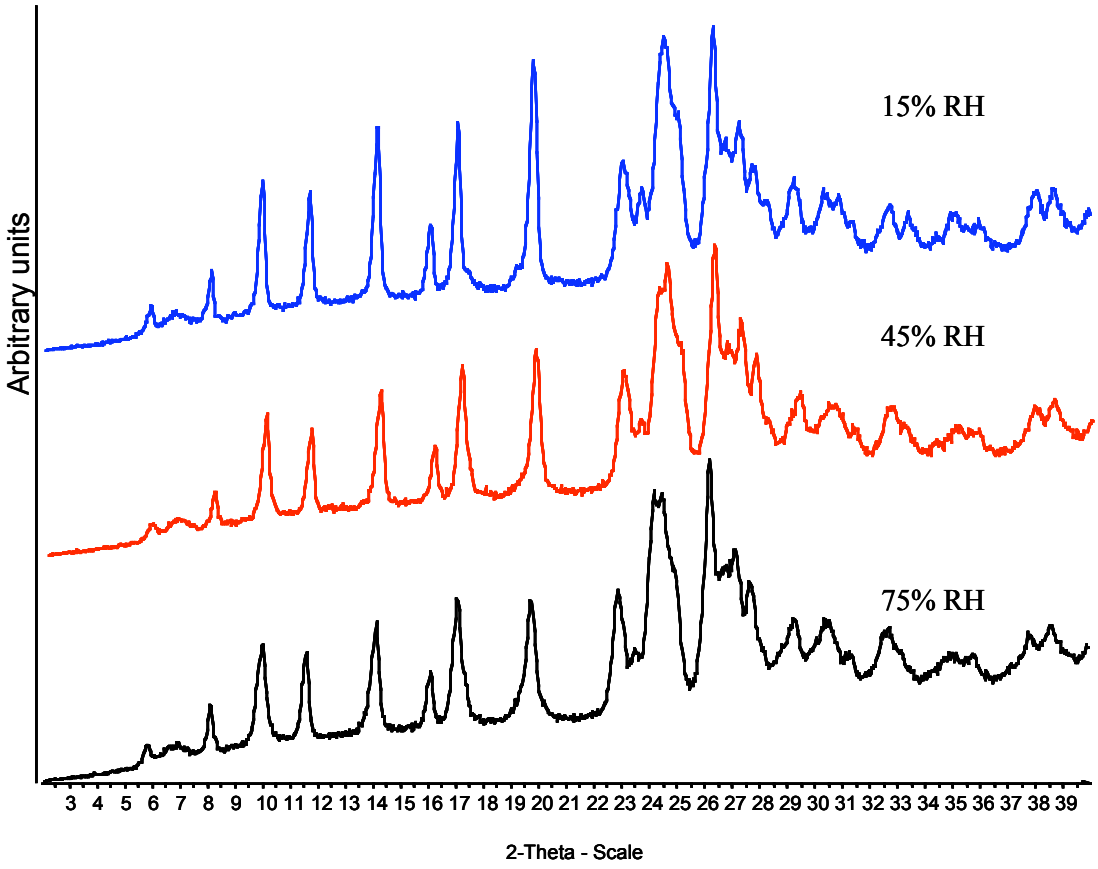

Figure 3.4.3 X-ray powder diffraction patterns of DSCG, staggered at 15, 45 and 75% RH.

3.5 INVERSE GAS CHROMATOGRAPHY.

As previously discussed, the adhesion/cohesion of two contiguous surfaces will be dependent on both the dispersive (γ_s^d) and polar (γ_s^{sp}) components of the surface free energy (Podczeck 1998b). Techniques, such as contact angle (Good 1992) and capillary intrusion (Desai et al 2002) have previously been used to determine surface free energy of pharmaceutical materials. However, for micronised materials, these techniques tend to be limited, due to unpredictable surface morphology (contact angle issues) and mass of sample required (capillary intrusion). The use of inverse gas chromatography (IGC) may provide a means of determining both dispersive and polar components of surface free energy for micronised drugs without such limitations (Ticehurst et al 1994).

Inverse gas chromatography is essentially a modification of normal phase gas chromatography. In normal phase gas chromatography, columns are packed with a known stationary phase, and the analyte separated or quantified by the relative retention time from the mobile gas phase. In comparison, IGC columns are packed with the analyte (in this case, micronised powder) and the retention times of known sample probes are measured from the mobile gas phase.

Since apolar liquids (e.g. n-alkanes) will interact by dispersive forces only, it stands to reason that a direct relationship between molecular mass and retention time will exist. Such a response can be expressed using Equation 3.5.1 as described by:

$$RT \ln V_N = 2N(\gamma_s^d)^{0.5} a(\gamma_l^d)^{0.5} + C \qquad \textit{Equation 3.5.1}$$

Where R is the gas constant, T the temperature, N Avogadro's number, *a* is the projected surface area of the sample probe, γ_l^d the dispersive component of the probe and V_N the net volume of carrier gas required to elute the probe molecules from the column (corrected for column dead time and compression

factors). Hence by plotting $RT\ln V_N$ against $a(\gamma_l^d)^{0.5}$ for a series of n-alkanes, the dispersive component (γ_s^d) of the analyte can be calculated from the slope.

In addition, by using a series of polar probes, the acidic-basic component of the analyte can be investigated. By plotting the polar probe retention volume ($RT\ln V_N$) against $a(\gamma_l^d)^{0.5}$, the specific polar interaction can be calculated by measuring the vertical distance between the polar probe and n-alkane linear fit line (ΔG_{sp}). Furthermore, by a assigning specific donor numbers (DN) and corrected acceptor numbers (AN), based on the Lewis acid-base concept (Gutmann 1978), the specific acid-base components can be calculated from Equation 3.5.2.

$$\frac{\Delta G_{sp}}{AN'} = \left(\frac{DN}{AN'}\right)K_a + K_D \qquad \textit{Equation 3.5.2} \qquad \textit{Acid-base calculation.}$$

Where K_a and K_D can be obtained from the slope and intercept.

Furthermore, by passing the carrier gas through a perfusion system, it becomes possible to investigate the influence of humidity on the surface energetics of a specific powder sample.

3.5.1 Materials and Methods.

The surface free energy components of micronised salbutamol sulphate, TAA and DSCG were determined using a commercially available IGC (SMS IGC 2000, Surface Measurement Systems Ltd, London, UK). A schematic of the apparatus is given in Figure 3.5.1.

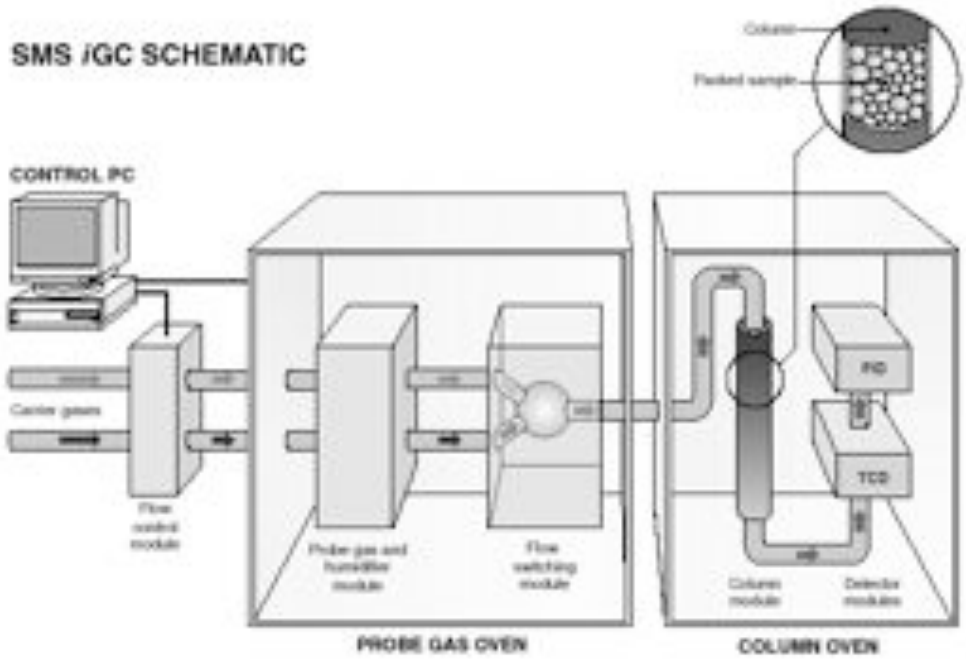

Figure 3.5.1. Schematic diagram of the IGC apparatus. (modified from SMS IGC pharmaceutical application note, Surface Measurement Systems Ltd, London, UK).

Powder was weighed into standard glass IGC columns and plugged with glass wool. Each column was tapped for five minutes, using the minimum setting on a jolting voltumeter (Surface Measurement Systems Ltd, London, UK) to a produce 'uniform' powder bed. Each column was equilibrated in the IGC at 0% RH, at 318.05 K, under dry nitrogen for 12 hours prior to analysis. The retention time of a series of n-alkanes (hexane to decane) and polar probes (ethanol, ethyl acetate and acetone) were analysed at infinite dilution by flame emission detector. Column settings and run times for all three drugs were optimised at 318.05 K. Approximately 0.5 g of salbutamol sulphate and TAA were used for each column while 0.25 g of DSCG was used (due to increased retention times). For each column, one run was conducted at three relative humidities (0% RH then 15% RH then 75% RH), with a six hour equilibration time being instigated after humidity was altered.

3.5.2 Results and Discussion.

Micronised salbutamol sulphate, TAA and DSCG samples were analysed by IGC at 0, 15 and 75% RH using both apolar and polar probes. An example of the apolar linear response and polar probe retention times for a salbutamol sulphate column at 0% RH is shown in Figure 3.5.2.

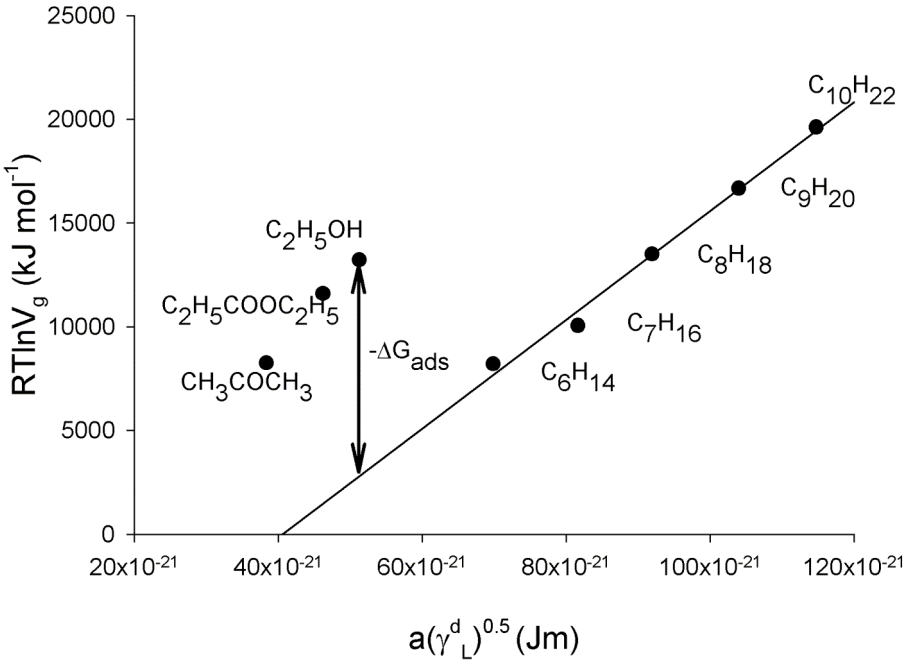

Figure 3.5.2 Plot of RTlnV$_g$ against a(γ^d_L)$^{0.5}$ for salbutamol sulphate at 0% RH.

The specific surface free energy components (calculated from the probe retention time) are shown in Table 3.5.1. Corrected donor DN' numbers (Gutmann 1978) and acceptor numbers AN' (Riddle and Fowkes 1990), used for the estimation of the acidic and basic components of the surface free energy, were as follows (AN':DN') Acetone 42.5:8.7, Ethyl acetate 42.8:5.3 and ethanol 50:35.9.

Analysis of the IGC data indicated both salbutamol sulphate and TAA had similar dispersive surface energies (TAA was slightly higher than that of salbutamol sulphate).

	Humidity (% RH)	Dispersive surface energy ($mJ.m^{-2}$)	K_a acidic	K_b (basic)
Salbutamol - Sulphate	0	44.6	0.0047	0.0740
	15	38.3	0.0049	0.0739
	75	40.5	0.0036	0.1420
TAA	0	47.4	0.0041	0.1620
	15	46.6	0.0043	0.1786
	75	49.9	0.0036	0.3095
DSCG	0	80.7	0.0043	0.4776
	15	65.5	0.0038	0.3497
	75	63.7	0.0024	0.3257

Table 3.5.1 Surface energy components) of three micronised drugs at controlled humidity.

Relative humidity had little influence on the dispersive component of salbutamol sulphate or TAA. In comparison, DSCG had a much higher dispersive energy than salbutamol sulphate and TAA. At 0% RH the dispersive energy for DSCG (~80 $mJ.m^{-2}$) was almost double that of salbutamol sulphate and TAA. As humidity was increased, the dispersive energy decreased to around 60 $mJ.m^{-2}$. However, this was still around 20 $mJ.m^{-2}$ higher than salbutamol sulphate and TAA. One possible explanation for such observations may be due to the molecular channels existing through the DSCG crystal structure (Hartshorne and Woodard 1973). Essentially, at 0% RH, DSCG will have a significantly reduced quantity of water molecules present in the interstitial crystal structure and thus, have a higher affinity for adsorbates.

Analysis of the acidic (K_a) and basic (K_b) polar contributions to the surface free energies indicated all three micronised drugs to have similar acidic contributions (around 0.004). In comparison the basic component indicated a trend salbutamol sulphate < TAA < DSCG. The reason for such variation will be both chemical and physical (i.e. functional groups dominating crystal planes and the chemical structure of the active molecule), and will be discussed later (Chapter 6).

3.6 GENERAL DISCUSSION.

Investigation into the influence of humidity on the physical properties of salbutamol sulphate, TAA and DSCG has shown each micronised drug to have very different moisture sorption profiles, crystal structure and surface free energy.

Consequently, it would be envisaged that cohesive interactions between each micronised drug may vary with respect to humidity. Since globalisation and mass travel could potentially expose commonly used prescription medicines (such as the micronised drugs used here) to large variations in climate (for example; 0% RH in North Africa to 100% RH in S.E. Asia (Anon. 2002)), the degree to which humidity influences cohesion could potentially be crucial.

To investigate further, the influence of humidity on drug cohesion, the AFM colloid drug probe technique was utilised (Chapter 4).

4 INTERPARTICULATE INTERACTIONS MEASURED BY AFM.

4.1 INTRODUCTION.

The atomic force microscope colloid probe technique was used to quantitatively measure the influence of humidity on the cohesive interactions of micronised salbutamol sulphate, TAA and DSCG at specific humidities.

The atomic force microscope was developed in 1986 and is commonly used for the high-resolution (sub-angstrom) topographical imaging of surfaces (Binnig et al 1986). However, the technique was further developed to allow the measurement of forces acting between a tip and substrate under specific media (Ducker et al 1991)

In simple terms, the AFM consists of a micro-fabricated cantilever whose deflection is recorded (usually by laser reflection) as it interacts with a moving substrate. Direct measurement of force can be determined by ramping the tip vertically (Z axis), towards, and away from a sample. The relative deflection of the cantilever as the tip approaches, makes contact with, and is removed from a surface produces a force-distance curve. Hysteresis in the approach and retraction cycles of the force distance curve can be related to the magnitude and type of forces acting between the two surfaces (Heinz and Hoh 1999). By applying Hookes law (Equation 4.1.1) relating the extension of a spring under applied load, the forces acting between the cantilever tip and surface can be calculated.

$$F = kD_c$$ *Equation 4.1.1 Hookes law.*

Where D_c is the cantilever deflection, F the force acting on the cantilever (N) and k the cantilever spring constant ($N.m^{-1}$).

A schematic representation of an ideal force-distance curve is shown in Figure 4.1.1. Initially, as the tip is brought towards a surface there is no interaction and therefore no deflection of the cantilever (Figure 4.1.1a). This continues until the short-range van der Waals forces overcome the cantilever spring constant and pulls the tip onto the sample surface (Figure 4.1.1b). Continued vertical movement of the surface is met by a linear response in cantilever deflection (Figure 4.1.1c, d) as a predetermined cantilever load is applied and removed. This area is referred to as the region of constant compliance; lack of linearity within this region indicates tip and/or surface deformation.

Continued retraction from the surface results in an extended cantilever deflection related to the adhesion properties between the cantilever tip and surface (Figure 4.1.1e). The cantilever deflection due to the tip adhesion is overcome when the cantilever spring constant is greater than the adhesion forces between the two surfaces. The maximum deflection value relative to point of no deflection is equal to the adhesion force. Continued removal from the surface to the initial height above the surface produces no deflection (Figure 4.1.1f). Integration of the area within the adhesion portion of a force-piezo distance curve will be equal to the energy of separation. The main advantage of determining separation energy (e_{sep}) is that it takes into account variations in mechanical properties between the tip and substrate, thus including the influence of elastic/plastic response in the materials under investigation.

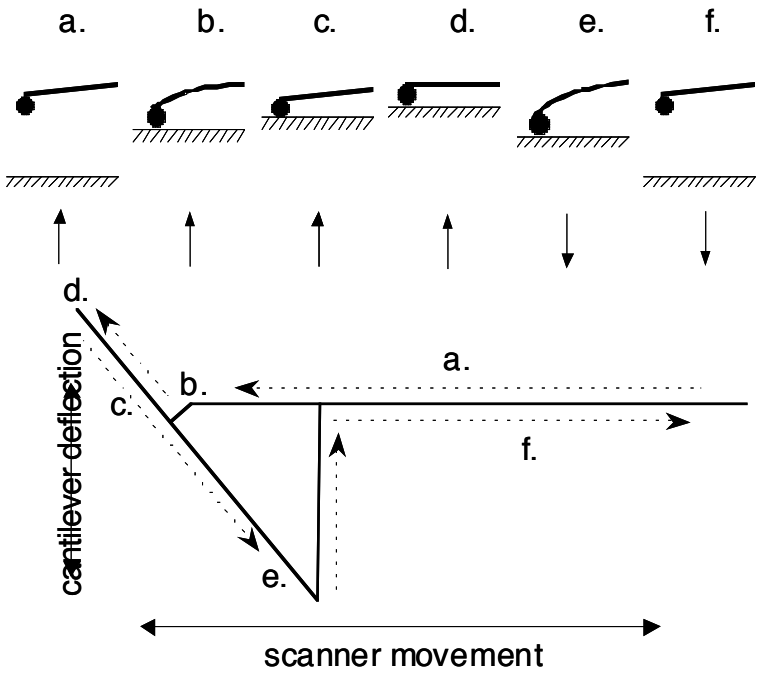

Figure 4.1.1 Schematic representation of an ideal force curve between an AFM cantilever drug probe and substrate, (a.) approach of probe with no cantilever deflection, (b.) jump to contact, (c) point of no applied force, (d) applied cantilever deflection equals applied deflection, (e) negative deflection due to probe adhesion, (f) retraction of probe with no cantilever deflection.

As previously discussed, the AFM force measurement approach can be further modified by incorporating a colloidal material onto the cantilever tip, allowing direct measurement of interactive forces between a particulate and substrate.

Previous investigations using cantilever mounted colloidal probes have mainly focused on the physical interactions between inorganic polymeric spheres and atomically flat substrates (Biggs and Spinks 1998, Yalamanchilli et al 1998). However, the technique has rapidly diversified into areas such as biotechnology (Heinz and Hoh 1999) and xerography (Mizes et al 2000). Recently, investigators have reported the AFM colloid probe technique as a useful tool in determining variations in adhesion between pharmaceutical systems (Ibrahim et al 2000, Louey et al 2001, Sindel and Zimmermann

2001). The use of AFM to determine interactions between lactose, a common pharmaceutical excipient, and gelatin capsules has shown capsule processing to influence particle-capsule interaction (Ibrahim et al 2000). Additionally, disparities in the adhesive forces between a silica sphere colloid probe and batches of lactose tablets have been reported (Louey et al 2001). Furthermore, recent studies have investigated lactose-lactose interaction using the colloid probe technique (Sindel and Zimmermann 2001).

The attachment of a micronised drug particulate to the apex of a tipless cantilever may be a route for the measurement of drug-drug interactions (cohesion) at specific humidities. Although previous studies, to investigate capillary interactions have been conducted using the AFM (Sedin and Rowden 2000, Berard et al 2002), these have generally concentrated on either tip-substrate interactions (Sedin and Rowden 2000) (probe/tip radius of curvature 20-40 nm), or larger pharmaceutical drug probe-substrate interactions (Berard et al 2002) (drug probe length >100 μm). The main focus of this investigation was to apply the colloid probe technique to micronised drug-drug interactions.

It is important to note, that there is only a limited amount of AFM literature directly applicable to particle-particle interactions for inhalation therapy. The most relative research using micronised drug probes was published by Eve et al (2002) during the course of this investigation. However this focused more on inhaler device components, and did not investigate the influence of humidity.

In order to quantify the behaviour of salbutamol sulphate, TAA and DSCG particulates in a DPI system, a study was undertaken to generate a cohesion profile for the micronised drugs at varied humidity using the AFM colloid probe technique. Because of the difficulty in conducting multiple force-distance measurements between two individual particulates of micron size (1-10 μm), three techniques were developed to produce model substrates of the drugs; polymer mounting, direct compression and controlled crystallisation.

Multiple force-distance curves between AFM cantilever mounted drug particulates and their corresponding model drug substrates were conducted across pre-specified areas using Force-Volume™ imaging, described in more detail elsewhere (Heinz and Hoh, 1999, DI *Application Note*).

Force-Volume imaging provided a large matrix (n = 4096) of separation energy values at each humidity allowing comparison and statistical analysis. In addition, Force-Volume data provided limited, low resolution, topographical height data (calculated as a function of the constant compliance region), which could be compared to higher resolution AFM images obtained separately using standard tips and imaging modes (e.g. Tapping Mode™).

4.2 MATERIALS AND METHODS.

4.2.1 Micromanipulation of Drug Particles Onto Tipless AFM Cantilevers.

A multi-stage micromanipulation technique for the attachment of micron sized drug particulates to tipless cantilevers was developed/adapted from the method described by Preuss and Butt (1998). Briefly, a small droplet of epoxy resin was transferred to a clean glass cover slip and mounted on a custom-built microscope slide holder (Figure 4.2.1).

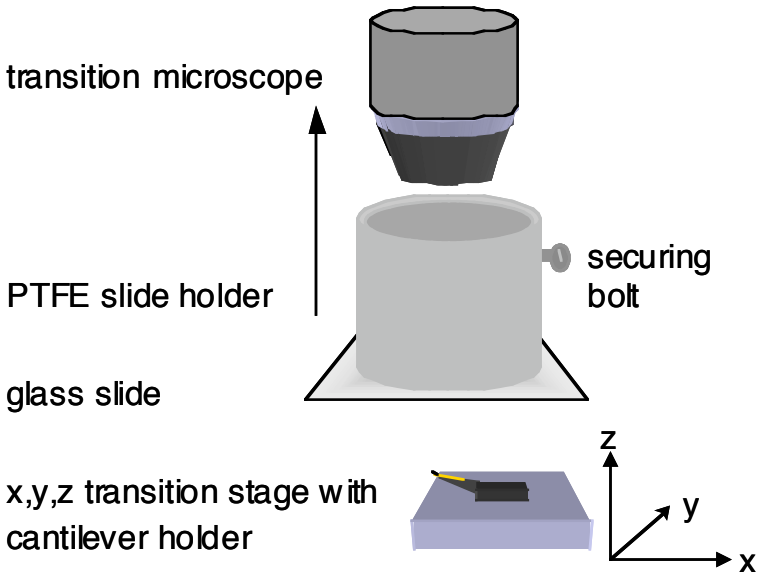

Figure 4.2.1 Schematic diagram of the micromanipulation PTFE slide holder assembly

The slide holder assembly was attached to a 160 X bifocal transmission microscope lens (Ziess, Germany) and adjusted to focus with a securing bolt. A tipped 'v-shaped' cantilever (NP20 Digital Instruments, Cambridge, UK) was mounted in a custom built tip holder and attached to a X,Y,Z transition stage. The tip was elevated into the glue and drawn along the X-axis to produce micron-sized protrusions. The tipped cantilever was removed and replaced with a, nominal 0.58 $N.m^{-1}$ spring constant, tipless cantilever (DNP-020 Digital Instruments, Cambridge, UK), and adjusted to remove a small

quantity of glue from a protrusion. The glass cover slip, containing glue, was removed from the slide holder and replaced with a clean cover slip containing a sample of the drug particulates. A representative micronised particle (approximately 2 to 5 μm) was then selected and attached to the cantilever. A CCD video, reflection microscope (Digital Instruments, Cambridge, UK) with a 500 X long working distance lens was used throughout the micromanipulation process to evaluate tip quality, quantity of glue, and tip particle integrity prior to and post curing. Prepared drug probe tips were stored in tightly sealed containers for 24 hours prior to use. The micromanipulation process is shown graphically in Figure 4.2.2.

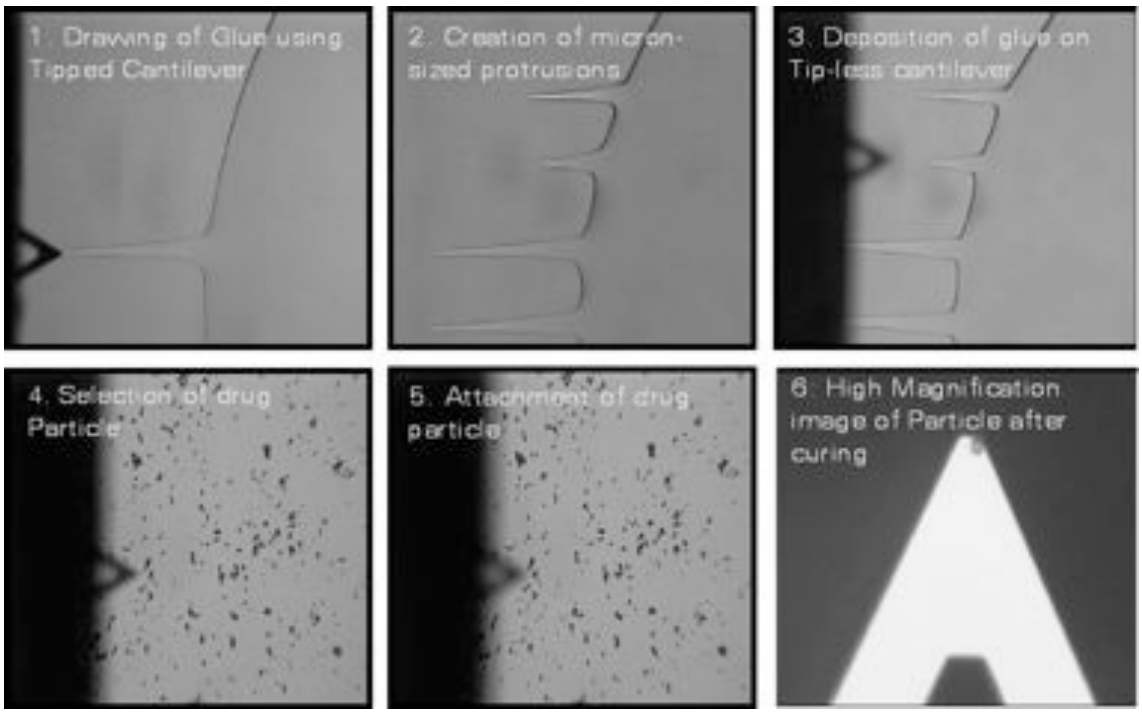

Figure 4.2.2 Photographs of the key stages of the micromanipulation process (cantilever length = 100μm)

In addition, where possible, the colloid probes were investigated using scanning electron microscopy (SEM) (Jeol 6310, Jeol, Japan) at 10 KeV. Sample probes were mounted on carbon sticky tabs and gold-coated (Edwards Sputter Coater, UK) prior to imaging. It must be noted, however, imaging of probes using this technique was conducted at the end of a probe's lifespan (i.e. on completion of the required measurements), due to the necessary gold coating process.

4.2.2 Control of Relative Humidity.

The influence of relative humidity on particle substrate separation energy was investigated using custom-built perfusion apparatus connected to the AFM. Filtered nitrogen gas was split at source and passed, independently, through a desiccator, containing silica gel and a bubble chamber, with moisture trap. Both the dry and 100% humidified nitrogen were passed through separate needle-valve flow controllers and fed into a sealed AFM scanning head containing a calibrated temperature-humidity monitor (Thermo-Hygro™ meter, Bioforce Nanosciences Inc. Ames, USA). Total flow into the AFM head was approximately 1cm^3 minute and was 25ºC ± 0.2ºC. Temperature of the humidified nitrogen was ≤ 25ºC to eliminate the possibility of condensation. A schematic representation of the perfusion apparatus is given in Figure 4.2.3.

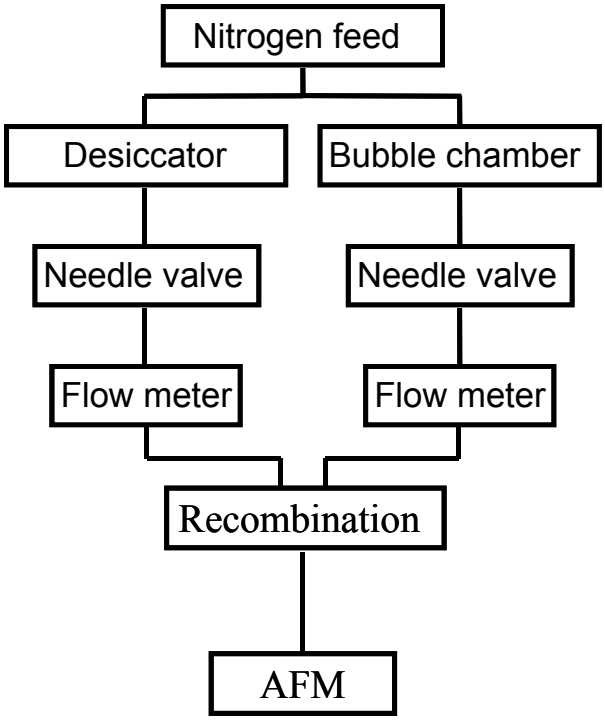

Figure 4.2.3 Schematic representation of the perfusion apparatus.

4.2.3 Preparation of Sample Substrates.

In order to investigate the influence of humidity on the cohesive properties of the micronised drugs using the colloid probe technique, the preparation of fixed drug substrates was required. Three immobilization techniques for such measurements were developed; (A), individual particle mounting in a heat sensitive polymer, (B) the use of model drug compacts formed by direct compression and (C) the preparation of larger (≥100 μm) 'atomically flat' crystalline drug substrates with uniform flat surfaces, by controlled crystallisation of the original micronised material.

4.2.3(a) Individual micronised particle immobilization.

Micronised particle samples were immobilised on steel AFM stubs using Tempfix (SPI Supplies, West Chester, USA) at 40°C using a custom built Peltier connected to a thermocouple temperature controller (SE5000, Marlow Industries, Dallas, Texas). Briefly, the steel AFM sample stub was mounted on the Peltier and heated to 120°C. A small quantity of Tempfix was melted onto the stub and cooled to 40°C at which point the resin becomes tacky or adhesive. A small quantity of the powder was lightly brushed through a 45 μm aperture stainless steel sieve (BS410/1986, Endecotts, London, UK) onto the AFM sample stub. The sieving procedure was found to remove large agglomerates. The AFM sample stubs, containing Tempfix-mounted particles, were left to cool to room temperature before removing loose material with a filtered nitrogen air stream. The polymer mounted drug samples were stored in tightly sealed containers for 24 hours prior to use. Utmost care was taken when handling the samples to avoid contamination.

4.2.3(b) Model drug compact preparation.

Model surfaces from the micronised material were prepared by direct compression (TA HDi Texture analyser, Stable Micro Systems, Surrey, UK). Approximately 250 mg of micronised material was weighed into a 10 mm stainless steel die and compacted at a compression rate of 0.5 $mm.s^{-1}$ (500 kg, dwell time 180 seconds). Compaction profiles for each model compact were recorded to assess repeatability. Prepared drug compact surfaces were stored in tightly sealed containers for 24 hours prior to use.

4.2.3(c) Atomically smooth crystalline drug substrates.

Large planar surfaces of the micronised material were produced by controlled crystallization techniques. The precise method of crystallisation was dependent on the solubility profile of the specific drug. Independent solubility profiles and crystallisation methods were developed for salbutamol sulphate and TAA while the method described by Cox et al (1971) was adapted for the crystallization of DSCG.

Solubility profiles of salbutamol sulphate and TAA in mixtures of ethanol and water were determined by saturating each drug in ethanol/water mixtures. Samples were shaken for 12 hours at 25°C (G76, Gyrotory water bath shaker, New Brunswick Scientific, Edison, USA) in sealed volumetric flasks. The saturated solutions were filtered and dried at 40°C before calculating solubility by mass.

Salbutamol sulphate was re-crystallised by primary nucleation. A 10% w/w saturated solution of salbutamol sulphate in 50/50 ethanol/water was filtered then stirred at 20°C in a sealed crystallisation vessel. Ethanol was added at a rate of 15 $ml.hour^{-1}$ (using a computer controlled syringe driver) until the solvent mass ratio was 80/20 ethanol/water. A diagrammatic representation of the crystallisation apparatus is shown in Figure 4.24. Recovered crystalline material was filtered and dried at 40°C.

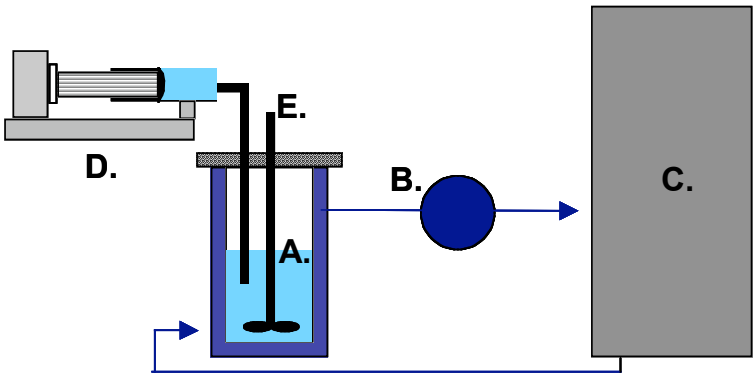

Figure 4.24 Schematic diagram of the crystallisation apparatus. Where A. crystallisation vessel containing water jacket, B. pump and tubing (arrows indicate water flow), C. temperature controlled water bath (K20, Haake, Karlsruhe Germany), D. Syringe and syringe driver (PHD 2000, Harvard Apparatus, Kent, UK), E. mechanical stirrer.

Similarly, TAA was re-crystallised by primary nucleation. Briefly, a 2% w/w saturated solution of TAA in ethanol was filtered and stirred at 25°C in the sealed crystallisation vessel. Water was added at a rate of 15 ml.hour^{-1} until the solvent mass ratio was 20/80 ethanol/water. Again the recovered crystalline material was filtered and dried at 40°C.

The method for crystallisation of DSCG was adapted from Cox et al (1971). Briefly, ethanol was added at a rate of 2 ml.hour^{-1} to an aqueous 10% w/w 'saturated' solution of DSCG, until a 4:7 v/v ethanol/water mix was achieved. In addition, a saturated ethanol atmosphere was produced by sealing the apparatus in a chamber containing excess ethanol. This allowed slow adsorption of ethanol vapour into the aqueous solution and thus precipitated DSCG crystals over a period of days (Cox et al 1971).

4.2.4 Atomic Force Microscopy.

Multiple force curves for the interactions between the AFM drug probes and corresponding drug substrates were conducted by AFM in force volume mode (Multimode SPM with Nanoscope III controller, Digital Instruments, UK). Individual force curves (n= 4096) were conducted over a 10 μm x 10 μm area with the following settings; approach-retraction cycle 2 μm, cycle rate 8.14 Hz and constant compliance region, 60 nm. The area under each curve was integrated using custom built batch conversion software and exported to produce a 64 x 64 block of separation energy values corresponding to the X an Y positions of the force distance curves. In addition, offline analysis of individual force curves was conducted, as curve shape can indicate many interactive physical properties (Heinz and Hoh 1999).

Validation of the technique and batch conversion software was undertaken by conducting individual drug-probe force curve measurements on an atomically flat mica surface (Grade V-1 Muscovite Mica, SPI Supplies, PA, USA) at a range of settings (i.e. cycle rate, constant compliance force).

A series of separation measurements, between the drug probes and their corresponding model surfaces were conducted at 15, 30, 45, 60 and 75% RH. A new drug probe / model drug substrate were used for each humidity experiment. Experimental matrix details are shown in Table 4.2.1

Substrate	Corresponding polymer mounted drug particulates	Corresponding model drug compact	Corresponding re-crystallised substrates
Experimental Humidity (% RH)	15 45 75	15 30 45 60 75	15 30 45 60 75
Salbutamol – sulphate	Drug probe n=1 Substrate n=5 (particles)	Drug probe n=5 Substrate n=5	Drug probe n=3 Substrate n=3
TAA	Drug probe n=1 Substrate n=5 (particles)	Drug probe n=5 Substrate n=5	Drug probe n=3 Substrate n=3
DSCG	Drug probe n=1 Substrate n=5 (particles)	Drug probe n=5 Substrate n=5	Drug probe n=3 Substrate n=3

Table 4.2.1 Matrix for AFM drug probe-drug substrate cohesion measurements.

4.3 RESULTS AND DISCUSSION.

4.3.1 Validation of the AFM Colloid Probe Technique.

A scanning electron photomicrograph of a typical salbutamol sulphate, TAA and DSCG AFM colloid drug probes, imaged after the AFM study, are shown in Figure 4.3.1 (a, b and c, respectively). All of the mounted drug particulates used in the AFM study exhibited an approximate size 2-5 μm and were clearly proud of the epoxy resin on the cantilever. Care was taken during drug probe preparation to limit the amount of drug glue contact. Where possible, these observations were confirmed by SEM post analysis.

However, high magnification optical microscopy (used to assess the quantity of glue and subsequent particle mounting process) enabled qualification of particle integrity, dimensions and cantilever/glue clearance (through the Z - axis depth of field). Initially, UV light curing glue was used for particle mounting, as this allowed a longer 'operator' time scale in which to conduct the micromanipulation process (this approach was subsequently adopted by Eve et al 2002). However, a quick setting epoxy resin was finally chosen as this reduced the possibility of low molecular weight polymer creep and also avoided exposure of the organic drug materials to potentially harmful UV radiation.

Spring constants used for the calculation of drug probe-substrate interactions were initially taken from the manufacturers nominal values. However, tolerance in AFM cantilever spring constants is a well-recognised problem as the spring constant is proportional to the cube of cantilever thickness (Hutter and Bechhoefer 1993). In general it is believed batch-to-batch variations in cantilever thickness to be as great as 0.4 μm to 0.7 μm (for a standard 0.6 μm tip). In order to reduce such batch-to-batch production variations, a wafer of cantilevers was purchased (containing > 500 tips).

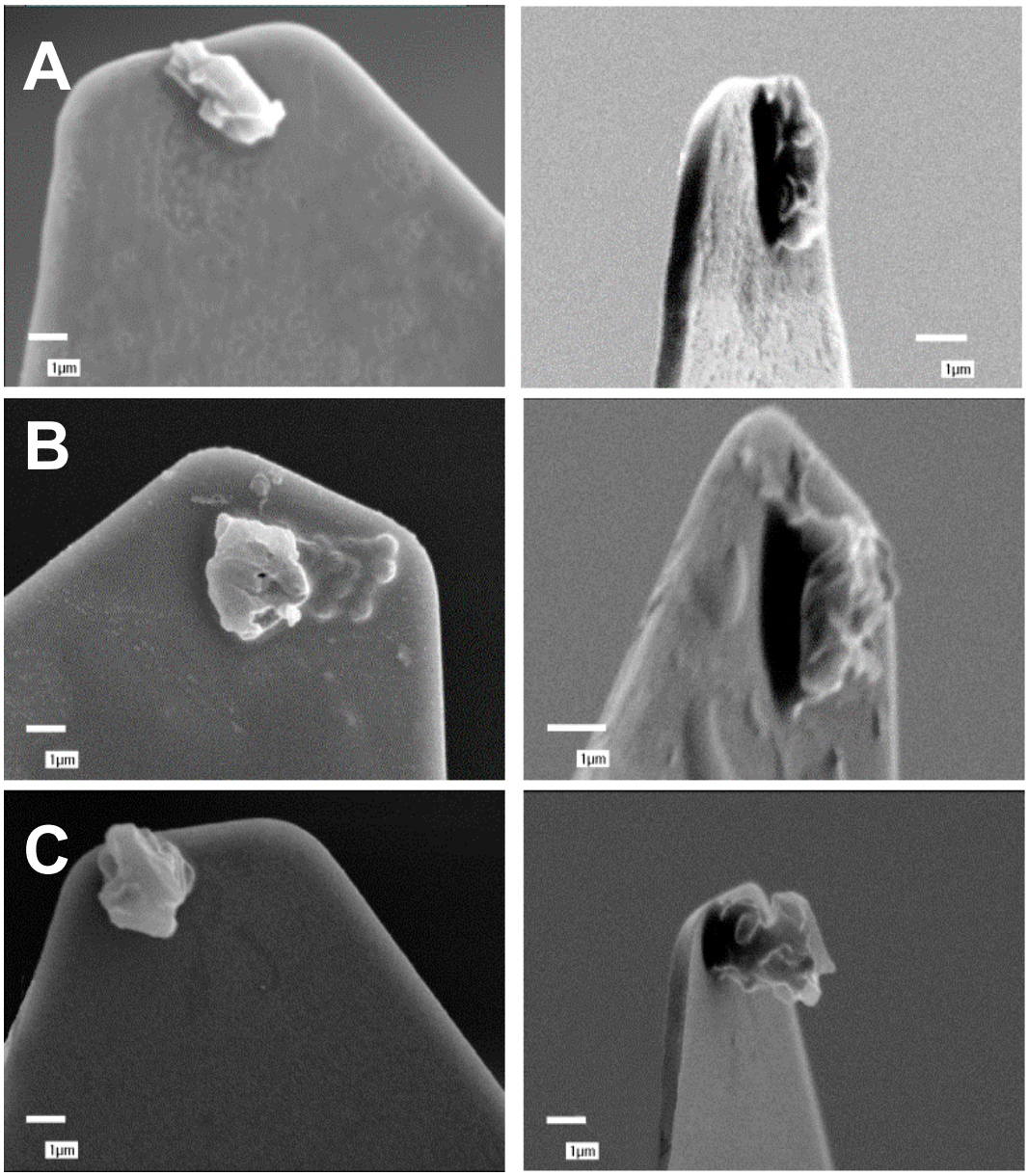

Figure 4.3.1 Scanning electron micrographs of (a) salbutamol sulphate, (b) TAA and (c) DSCG drug particulates mounted on the apex of pyramidal AFM cantilevers.

Personal correspondence with Digital Instruments (DI, Cambridge, UK) indicated that such large variations in spring constant were significantly reduced between cantilevers from the same wafer (~10-20% RSD). Randomly chosen tips (n=5) from across the wafer indicated less than a 14% variance from the nominal spring constant, using the thermal method (Hutter and Bechhoefer 1993).

Force-distance curves between a colloid drug probe and mica surface (Grade V-1 Muscovite Mica, SPI Supplies, PA, USA) were conducted at a range of settings (i.e. approach/retraction rate, Z-scan size and constant compliance region) to investigate the influence of controllable variables on separation force and energy. A mica substrate was chosen, as freshly cleaved surfaces were both atomically flat and free from environmental contamination. In addition, the planar surface of the mica eliminated variations in probe-substrate contact geometry.

Although previous studies have demonstrated specific sample rate and compressive force to influence force-distance curve measurements (Biggs and Spinks 1999), experimental validation of these settings indicated neither cycle time (0.1 Hz to 16 Hz for a 2 μm scan size) nor constant compliance loading (1 nm and 200 nm) to affect force curve measurement (Appendix 4.1.1 and 4.1.2, respectively). However, this was not particularly unexpected as the micronised drugs used throughout the investigation were relatively brittle, crystalline materials and would not appreciably deform under stress.

4.3.2 Physical Characterisation of the Model Drug Substrates.

In order to quantify the influence of humidity on drug cohesion, the drug substrates prepared using the three techniques described in section 4.2 were first characterized for morphology, reproducibility and stability at the experimental humidities.

4.3.2(a) Individual micronised particle immobilization.

Scanning electron photomicrographs of the salbutamol sulphate, TAA and DSCG, particles mounted in the Tempfix polymer are shown in Figure 4.3.2a, b and c, respectively).

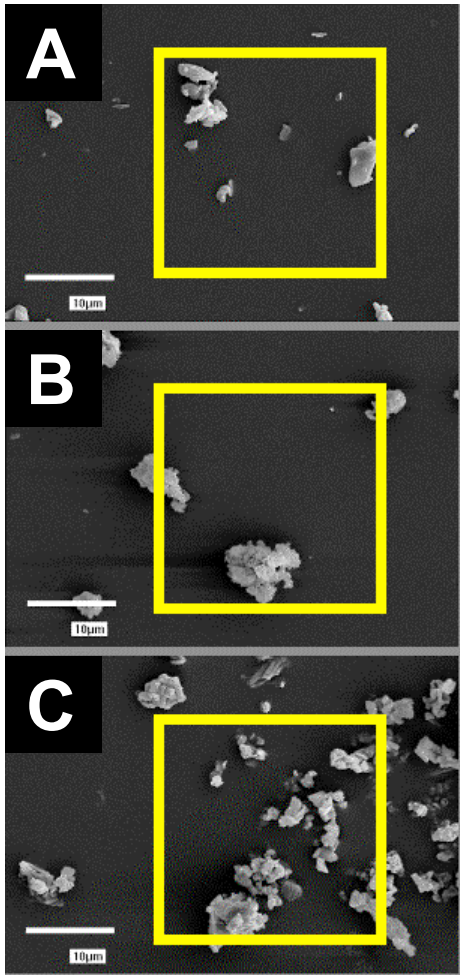

Figure 4.3.2 Scanning electron photomicrographs of (a) salbutamol sulphate, (b) TAA and (c) DSCG drug particles mounted in Tempfix polymer resin.

The drug particulates were clearly embedded in the Tempfix polymer and appeared proud of the surface.

A representative AFM Tapping Mode 'height' image of the salbutamol sulphate particles mounted in Tempfix resin is shown in Figure 4.3.3. The salbutamol sulphate drug particulates had an irregular morphology and were clearly proud of the Tempfix polymer surface. In addition, AFM Tapping Mode images on randomly chosen areas of a 'control' Tempfix surface (not shown here), prepared without drug particle mounting, showed no such exposed irregularities. Atomic force microscope 'height' images for TAA and DSCG mounted in Tempfix produced similar results.

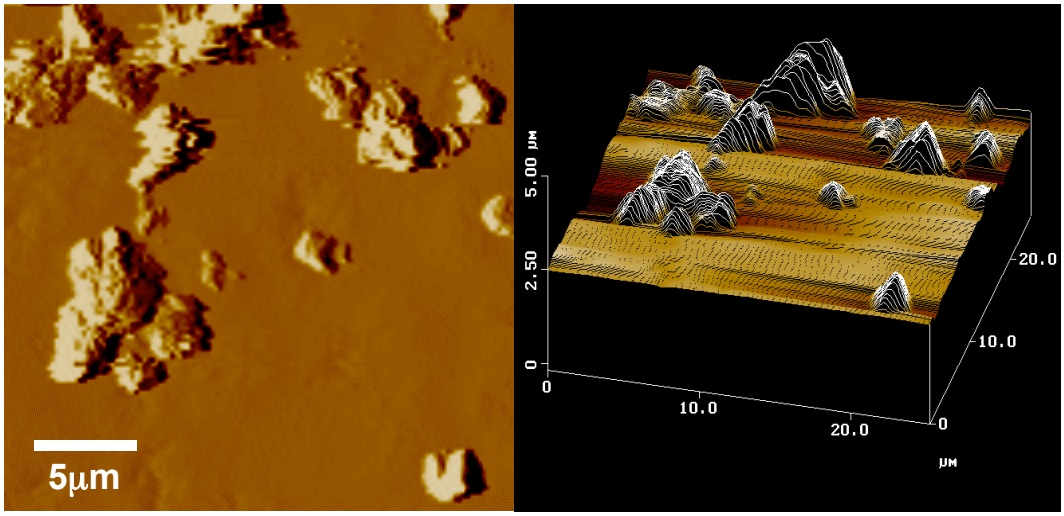

Figure 4.3.3 Tapping Mode height profile for salbutamol sulphate particles mounted in Tempfix polymer. (25 x 25 µm area).

Analysis of the Tempfix mounted drug particles indicated they were all within the particle size range as measured in Chapter 2.

Representative AFM 'amplitude response' images of salbutamol sulphate and TAA at 45% RH are shown in Figure 4.3.4 (a and b, respectively). It can be seen from Figure 4.3.4(a) that salbutamol sulphate exhibits a columnar shape while TAA (Figure 4.3.4(b)) appears to have a more flattened platelet morphology. Similar low magnification AFM images of DSCG suggested a columnar shape. In general, the low magnification AFM images agreed well

with studies of the micronised drugs using low temperature scanning electron microscopy (Chapter 2).

Both salbutamol sulphate and TAA showed no macroscopic changes in particle morphology over the humidity range 15-75% RH. In comparison, the morphology of DSCG clearly changed as humidity was increased from 15 to 75% RH suggesting sorbed moisture to integrally influence particle morphology. Representative high-resolution AFM images (amplitude response) of a DSCG particle after exposure to 15, 45 and 75% RH (for approximately 4 hours at each humidity) is shown in Figure 4.3.4c.

Variations in particle morphology of the micronised DSCG with respect to relative humidity were not unexpected however, and such observations correlated well with the large moisture sorption and variation in X-ray powder diffraction pattern across the humidity range (Chapter 2).

As previously discussed, DSCG is effectively a nematic choromonic liquid crystal that below 93% RH forms a solid solution (Cox et al 1971, Hartshorhe and Woodard 1973, Chen et al 1999). In essence, the planar cromoglycate molecules are ‘stacked’ to form long rods that in turn form an interstitial solid held together by water molecules. These water channels can subsequently contain up to approximately 9 molecules of water per unit cell before collapsing to form a liquid crystal mesophase (at 93% RH) (Cox et al 1971, Hartshorhe and Woodard 1973, Chen et al 1999).

Adsorption or de-sorption of water molecules into the crystal structure will subsequently cause changes in the torsional angles of the cromoglycate molecules (Cox et al 1971, Hartshorhe and Woodard 1973, Chen et al 1999), resulting in a variation in the unit cell dimensions. Consequently it is likely that such a change in crystal structure with respect to humidity would have a significant impact on the macroscopic particle morphology.

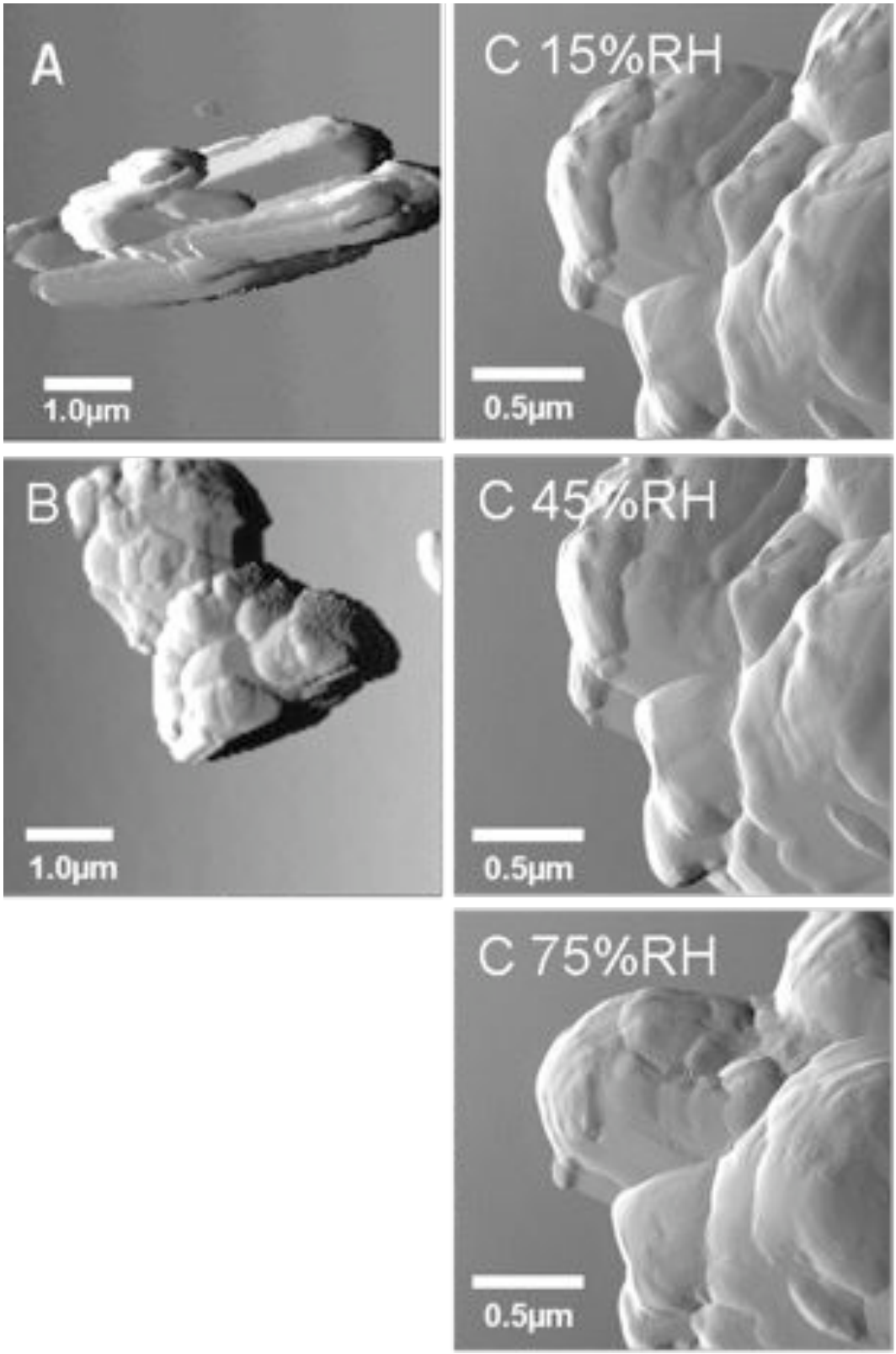

Figure 4.3.4 Atomic force microscope images of micronised drug particles mounted in Tempfix polymer: (a) salbutamol sulphate (45% RH), (b) TAA (45% RH) and (c) DSCG (taken at 15,45 and 75% RH).

4.3.2(b) Model drug compact preparation.

Compaction profiles for salbutamol sulphate, TAA and DSCG are shown in Figure 4.3.5 (a, b and c, respectively). All three micronised drugs showed similar compaction profiles, and produced relatively brittle model compacts with smooth planar surfaces present on the dye faces (observed under an optical microscope).

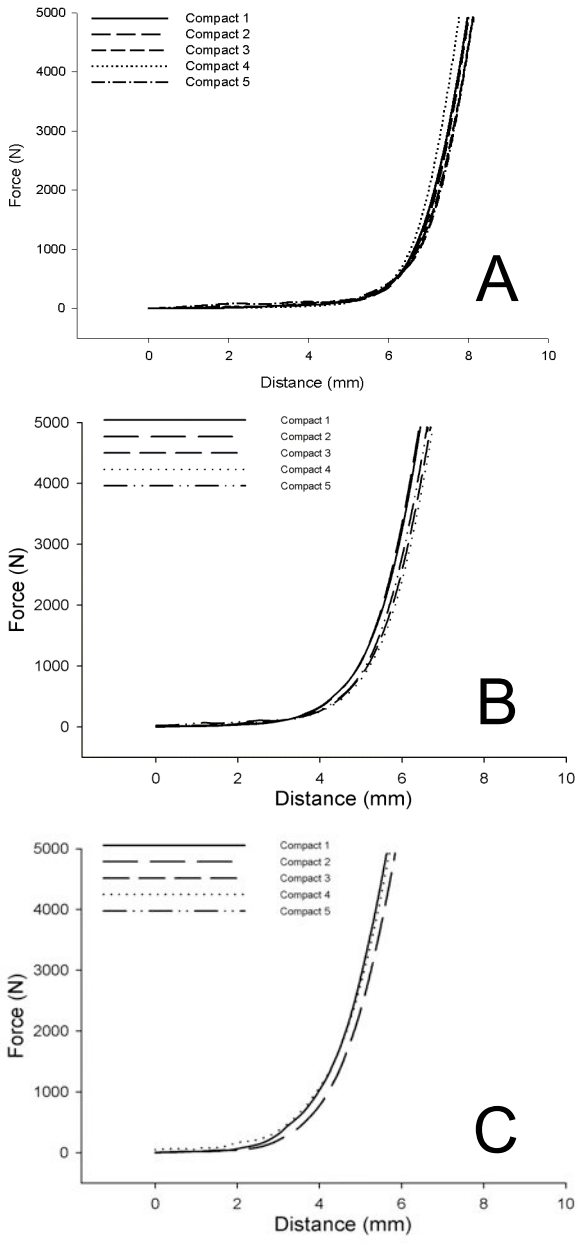

Figure 4.3.5 Compaction profiles for (a) salbutamol sulphate, (b) TAA and (c) DSCG.

However, AFM (Tapping Mode) height images of the salbutamol sulphate, TAA and DSCG model compacts shown in Figure 4.3.5 (a, b and c, respectively) suggested an irregular surface morphology.

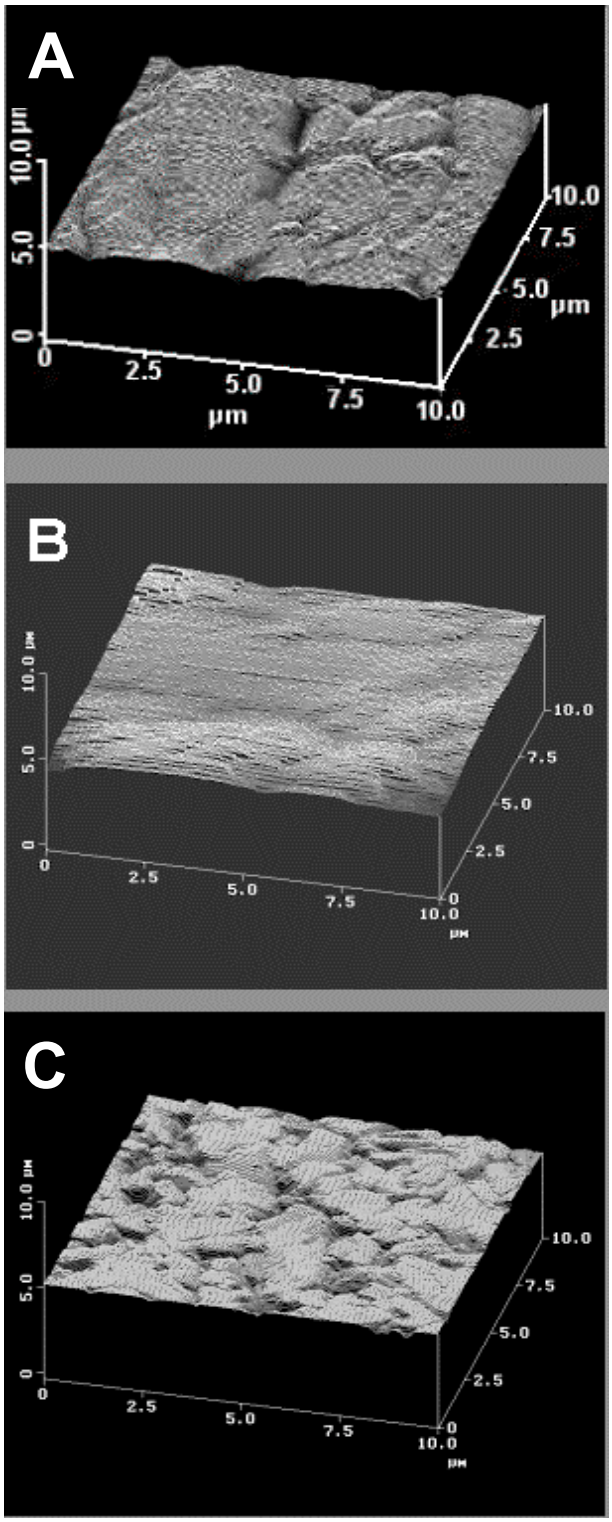

Figure 4.3.6 Representative AFM Tapping Mode 'height' images of the model drug compacts: (a) salbutamol sulphate, (b) TAA and (c) DSCG.

Root mean square roughness (R_{rms}) values for each sample were calculated from the AFM height data using Equation 4.3.1.

$$R_{rms} = \sqrt{\frac{1}{n}\sum_{i=1}^{n} y_i^{\,2}}$$

Equation 4.3.1 R_{rms} roughness calculation.

Where *n* is the number of points in topography profile and y_i is the distance of a point *i* from the centre line. Root mean square roughness values (10 μm x 10 μm areas) for salbutamol sulphate, TAA and DSCG are tabulated below (Table 4.3.1).

Drug	R_{rms}
Salbutamol sulphate	101 nm ± 16 nm
TAA	171 nm ± 10 nm
DSCG	143 nm ± 9 nm

Table 4.3.1 Root mean square roughness analysis of the model drug compacts (n=5).

All the drug model compact R_{rms} values were of similar magnitude. However, there was a statistically significant variation (ANOVA, $p<0.05$) between the compacts prepared from the different micronised drugs. This was not unexpected, however, and is most likely attributable to the variation in initial particle size (Chapter 2).

Tapping Mode AFM analysis of the three micronised drug compacts at 15, 45 and 75% RH indicated humidity to have no influence on salbutamol sulphate or TAA compact morphology. However, minor variations in the surface morphology of the DSCG compacts were observed when the humidity was ramped from 60 to 75% RH (shown in Figure 4.3.7).

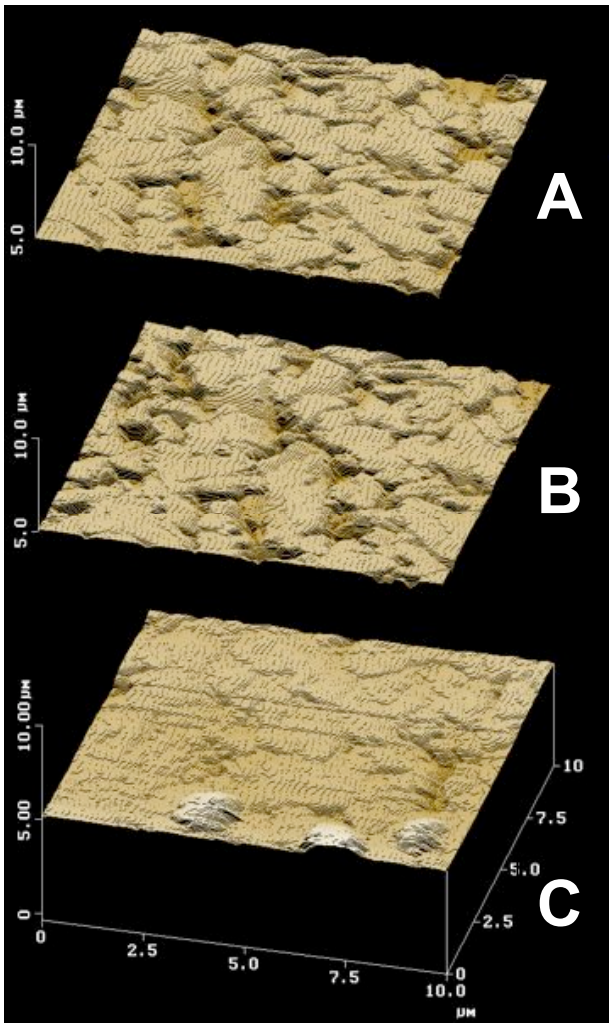

Figure 4.3.7 Representative AFM height images of the DSCG model compact taken at (a)15% RH, (b) 45% RH and (c) 75% RH.

In addition, root mean square roughness analysis of DSCG compacts showed a decrease in the mean R_{rms} as humidity was increased to 75% RH, (where R_{rms} =142 nm ± 10 nm at 15% RH to 133 nm ± 18 nm at 75% RH).

4.3.2(c) Atomically smooth drug substrates.

The solubility curve for salbutamol sulphate and TAA in mixtures of ethanol/water is expressed graphically in Figure 4.3.8 (a and b, respectively).

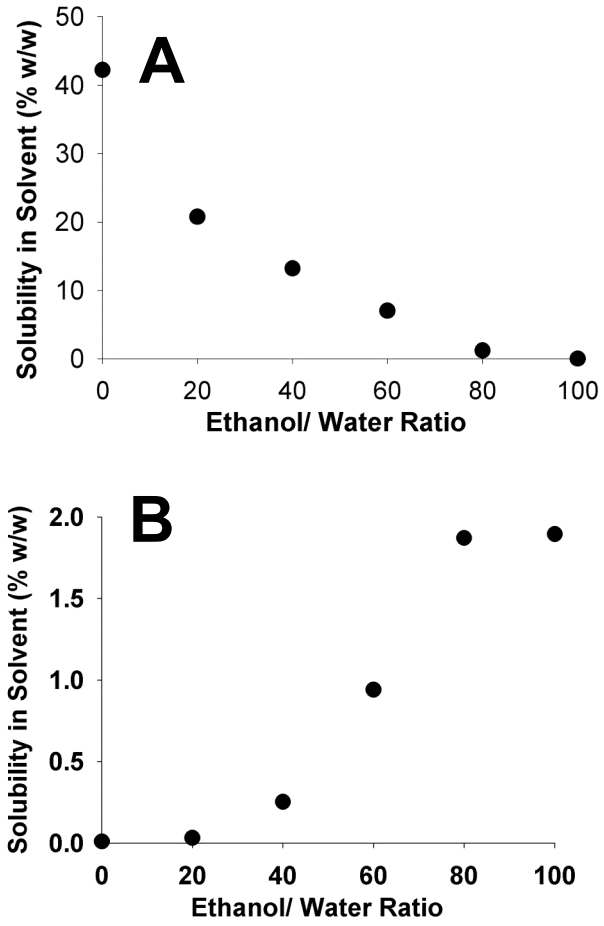

Figure 4.3.8 Solubility curves for (a) salbutamol sulphate and (b) TAA.

Re-crystallisation of salbutamol sulphate was controlled by adding ethanol as an anti-solvent. A saturated solution of salbutamol sulphate was prepared by adding 10.08 g of material to a 50/50% w/w ethanol/water mixture (calculated from the solubility curve shown in Figure 4.3.8). This should yield a theoretical recovery mass of 7 g at an 80/20 ethanol/water ratio. Recovered mass was 6.88 g indicating a recovery efficiency of 98.3%.

Re-crystallisation of TAA was controlled by adding 100 g of water (as an anti-solvent) to a saturated solution of TAA in 25 g ethanol (1.894% w/w). Solubility of TAA in a 20/80 ethanol/water mix was 0.032% w/w and therefore should produce a theoretical yield of 0.433 g. Recovered crystal mass was 0.431 g indicating a recovery efficiency of 99.5%.

Recovery of DSCG after crystallisation for over a one week period suggested a low recovery efficiency (<50%). Samples were extracted by filtration and were washed with ethanol. The low recovery efficiency is most likely due to the relative solubility of the ethanol water mixture, with a large proportion of the DSCG remaining in solution or in a liquid crystal mesophase. However the recovered crystals appeared needle like as previously reported by Cox et al (1971) and had suitable dimensions for force volume measurements.

Representative scanning electron micrographs of the re-crystallised salbutamol sulphate, TAA and DSCG are shown in Figure 4.3.9 (a, b and c, respectively).

Salbutamol sulphate SEM images (Figure 4.3.9a) had a needle like morphology with relatively smooth undamaged surfaces. In comparison TAA crystals appeared to have a tabular shape.

Scanning electron micrographs of the DSCG (Figure 4.3.9c) had a columnar needle like shape with smooth planar surfaces. However, the scanning electron microscopy process resulted in very apparent damage to the crystal surface, with the long axis of the crystal appearing to split into fragments. It is suggested that the necessary vacuum in combination with the relatively high energy electron beam (10 Kev acceleration voltage) ‘pulled’ the interstitial water molecules from the crystal structure. Such damage to the crystal structure can clearly be seen in Figure 4.3.9c. Low temperature SEM (LTSEM) may provide a means of reducing such artefacts, and clearly warrants further study. However, LTSEM was not available at the time of investigation.

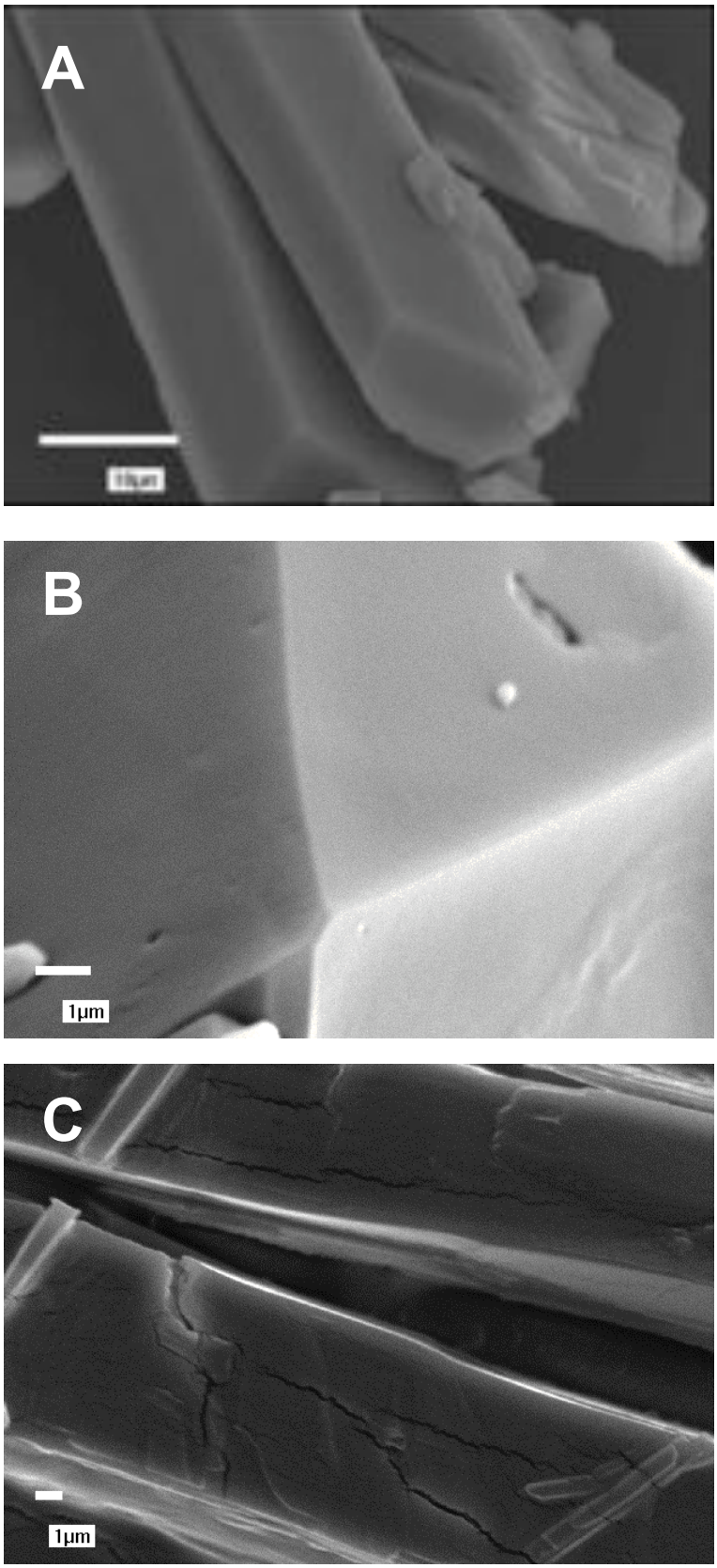

Figure 4.3.9 Representative SEM images of re-crystallised (a) salbutamol sulphate, (b) TAA and (c) DSCG.

Atomic force microscope (Tapping Mode) images of the salbutamol sulphate, TAA and DSCG model compacts (Figure 4.3.10a, b and c, respectively) suggested smooth planar crystal surfaces with minimum surface defects.

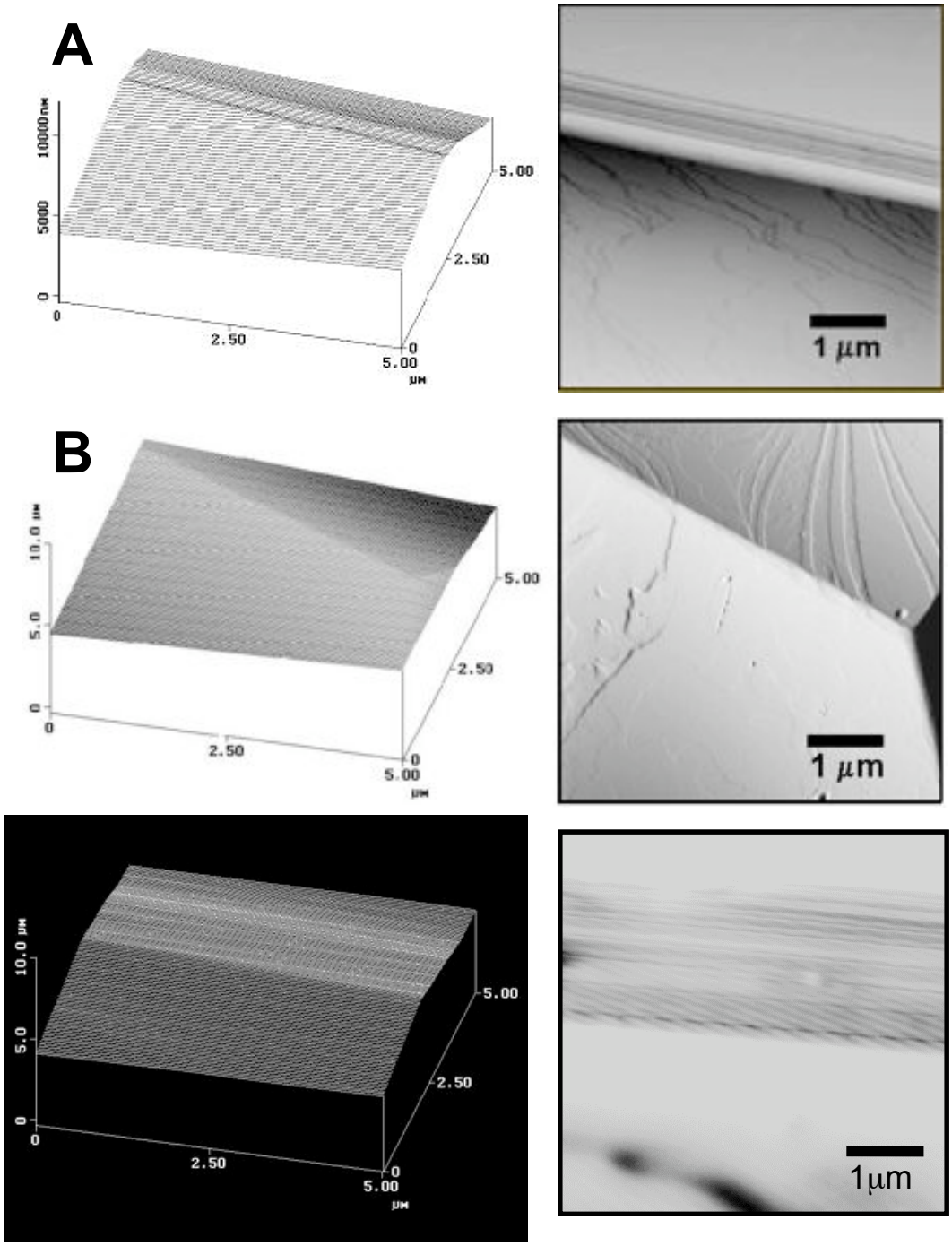

Figure 4.3.10 AFM height (with corresponding amplitude response) image of re-crystallised (a) salbutamol sulphate, (b) TAA and (c) DSCG.

Analysis of the salbutamol sulphate AFM image (Figure 4.3.10a) showed a clear distinction between two crystal faces due to the clear edge and variation in surface angles.

Literature values indicate the crystalline structure of salbutamol sulphate had a monoclinic crystal system with a β angle of 81.19° (Leger et al 1978). Cross sectional analysis of the AFM topographical data, taken perpendicular to the edge between the two faces, indicated an apparent angle of 99°. This correlated well with the consecutive angle of β (98.81°), suggesting the image was taken between the {001} and {100} crystal faces. Subsequent force volume measurements between salbutamol sulphate drug probes and the salbutamol sulphate crystal surfaces were conducted at random on the {001} and {100} crystal faces.

Again, Tapping Mode images of TAA, allowed clear distinction between crystal faces (Figure 4.2.10b), however, limited literature regarding the crystallographic structure of TAA did not allow distinction between faces. Although this clearly warrants further investigation, the production of suitable crystals for X-ray crystallographic studies is complicated and the facilities for such determinations were not readily available. Subsequently such investigations were deemed outside the scope of this research.
However, in order to maintain experimental consistency, the most dominant face was chosen as a substrate for force volume measurements.

As with salbutamol sulphate crystals, Tapping Mode images of DSCG showed a clear distinction between two distinct crystal faces (along the a axis or length of the crystal (Chen et al 1999)). Cross sectional analysis of the AFM topographical data, taken perpendicular to the two faces indicated apparent angles of around 107° - 120°. This corresponds well to previously reported values of 120° (Cox et al 1971) for the Triclinic DSCG crystal α-angle (Chen et al 1999). However variations will exist due to the number of water molecules present in the unit cell (crystal expansion). In addition, no variation in surface morphology (of the individual crystal faces) was observed

with respect to humidity. Such observations are to be expected, however, as torsional rearrangement of the DSC molecule occurs in the internal structure and therefore may not result in a directly visible surface effect. Subsequent force volume mode measurements were conducted at random on either face along the crystal length.

Atomic force microscopy R_{rms} roughness analysis of salbutamol sulphate, TAA and DSCG images are tabulated below (Table 4.3.2).

Drug	R_{rms}
Salbutamol sulphate	3.6 nm ± 2.0 nm
TAA	1.7nm ± 0.8 nm
DSCG	5.4 nm ±1.5 nm

Table 4.3.2 Root mean square roughness analysis of the re-crystallised model drug surfaces (n=5).

As expected, crystals of all three drugs exhibited roughness parameters one order of magnitude less than that for their corresponding model compacts. Essentially, the roughness values correspond to an atomic level contiguity, as the majority of variations in morphology on a particular crystal plane would be due to the unit cell crystal growth boundaries (e.g. the linear striations observed on the lower crystal plane of the AFM salbutamol sulphate amplitude image in Figure 4.3.10a).

4.3.3 Atomic Force Microscope Drug Probe Cohesion Measurements.

In order to understand the influence of humidity on particle-particle interactions a series of cohesion profiles were constructed for salbutamol sulphate, TAA and DSCG on a series of model drug substrates.

4.3.3(a) AFM on polymer mounted particulates.

The influence of humidity on drug particle cohesion was investigated by conducting FV scans (25 μm^2) between a drug probe and corresponding drug particles mounted in Tempfix polymer resin.

An example of a force volume scan, conducted between a salbutamol sulphate drug probe and salbutamol sulphate mounted particles is shown in Figure 4.3.11. The white areas on the FV 'relief' height image correspond to regions with a Z-axis height of greater than 2.5 μm. It would be reasonable to assume that such undulations in the surface could be identified as micronised drug particles, as they correspond to observations made using conventional AFM tips and imaging methods (Figure 4.3.3). Comparison of the 'relief' height image with the FV image (Figure 4.3.11) suggested the raised 'drug particle' areas have a low adhesion force in comparison to the polymer surface. A representative force curve for the salbutamol sulphate interactions is included in the FV scan with its relative position marked with a cross in the 'relief' height and FV images, respectively.

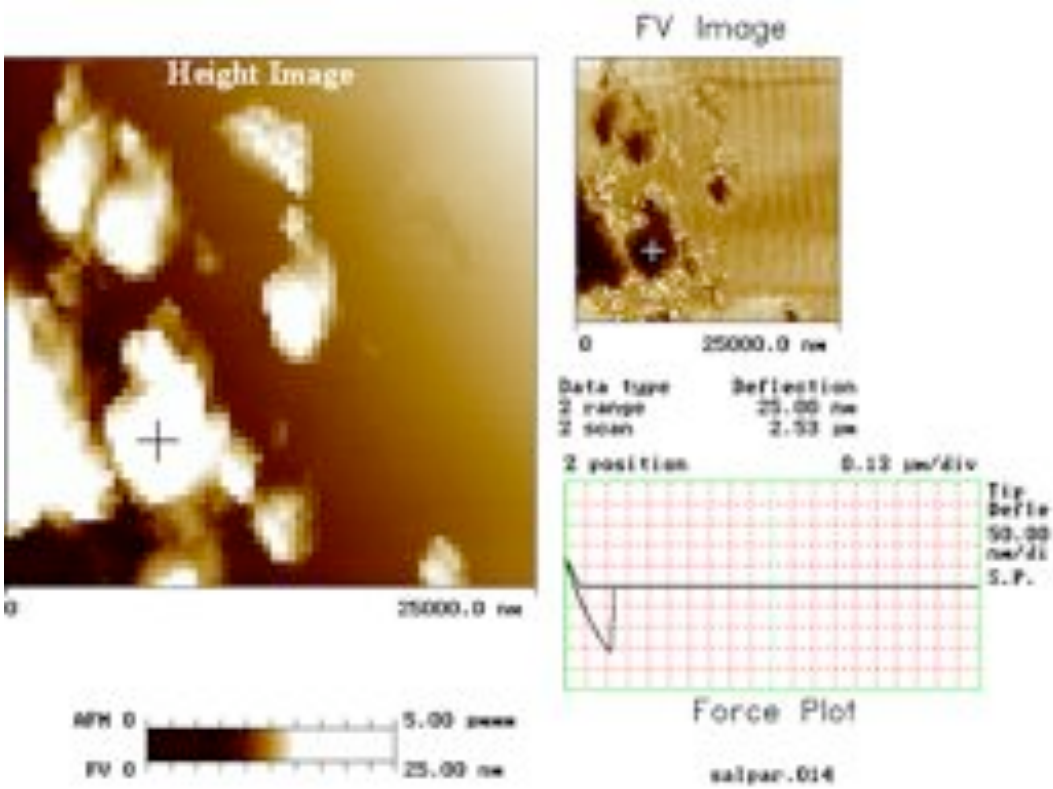

Figure 4.3.11 Force volume data for salbutamol sulphate drug probe interactions with salbutamol sulphate particles mounted in Tempfix.

In order to quantify such drug probe interactions, randomly chosen force curves taken across five distinct 'raised particle' regions were exported and manually integrated to obtain both cohesion force and separation energy values. This procedure was repeated at each humidity. Furthermore, a series of force curves taken on the Tempfix polymer resin was exported for comparison.

It is important to note that although an individual analysis approach does not allow such comprehensive statistical analysis as batch reprocessing, it was deemed necessary to ensure definition between micronised particle and drug Tempfix polymer interactions.

A summary of the salbutamol sulphate, TAA and DSCG cohesive forces are given in Appendix 4.2, while separation energies are given in Appendix 4.3.

Analysis of Cohesion Forces.

ANOVA one-way analysis of variances indicated humidity to have a significant influence ($p<0.05$) on the cohesion force of all three micronised drugs with respect to humidity. However such an observation is effectively dependent on a normal distribution. Further analysis of the cohesion force data (Appendix 4.2) suggested this not to be the case as the large standard deviations and positive skewness values indicated a non-normal distribution. Analysis of the cohesion force values indicated a lognormal distribution to best fit the data. The use of log normal distributions to describe such data is well documented and can be found in abundance in the literature. A good overview, explaining the fundamentals and treatment of such data can be found in Hinds 1999

In general, the force distance curve 'anatomy' for salbutamol sulphate agreed with previously published data using the AFM colloid probe technique (Eve et al 2002). However, values calculated for salbutamol sulphate cohesion were two orders of magnitude less than reported by Eve et al (2002). Critical review of this previously reported work indicated that the wrong cantilever spring constants were used for calculation of adhesion force. Values of ~70 $N.m^{-1}$ were used for measurements using pyramidal tipless cantilevers (clearly shown in the accompanying Figures), which usually have nominal spring constants of around 0.6 $N.m^{-1}$. As Tapping Mode tips with high aspect ratio probes are quoted as having spring constants of around 70 $N.m^{-1}$ (Correspondence with Digital Instruments, Cambridge, UK) it is envisaged that the wrong spring constants were used for calculating adhesion force. Subsequent analysis of the force curves published by Eve et al (2002) using a 'corrected' spring constant of 0.6 $N.m^{-1}$ would give equivalent cohesion values to this investigation. No such literature relating to fundamental cohesion measurements on DSCG or TAA could be found.

Analysis of lognormal probability plots of salbutamol sulphate, TAA and DSCG using Minitab statistical analysis software (Minitab Inc. PA, USA) suggested humidity to have a significant influence (CI = 0.95) on the cohesion force.

The median adhesion force ($f_{0.5}$) for salbutamol sulphate increased with respect to humidity (32.9 nN, 48.5 nN and 58.7 nN for 15, 45 and 75% RH, respectively) suggesting capillary interactions to become more dominant at higher humidities. Such observations correlate well with previous in-vitro investigations, which demonstrated a decrease in salbutamol sulphate fine particle aerosolisation as humidity was increased (Jashnani and Byron 1995, Jashnani et al 1996).

Comparison of both the mean and median salbutamol sulphate cohesion values with Tempfix adhesion measurements suggested the polymer-drug adhesion to be significantly greater than drug cohesion. All adhesion measurements conducted between the 'flat' polymer regions of the FV scan were of a higher value than that of salbutamol sulphate cohesion (142.1 nN, 152.6 nN, 164 nN at 15, 45 and 75% RH, respectively). Such observations are to be expected however, as adhesive resins have high surface energies due to the polar nature of groups present on the polymer chains (Pizzi and Mittal 1994).

In contrast to the salbutamol sulphate cohesion profile, the median separation force for TAA decreased as humidity was raised (61.2 nN, 30.6 nN and 19.9 nN for 15, 45 and 75% RH, respectively). One possible explanation for such a profile would be the presence of dominant electrostatic forces at lower humidities. Analysis of Individual TAA force-piezo distance curves taken at 15 and 75% RH are shown in Figure 4.3.12 (a and b, respectively). At low humidity (Figure 4.3.12a) a negative curve in cantilever deflection as a function of piezo displacement suggests a long-range attraction force to be acting over the Z-scan axis (2 μm). It is reasonable to assume that such a long-range attraction force would be due to electrostatic interactions.

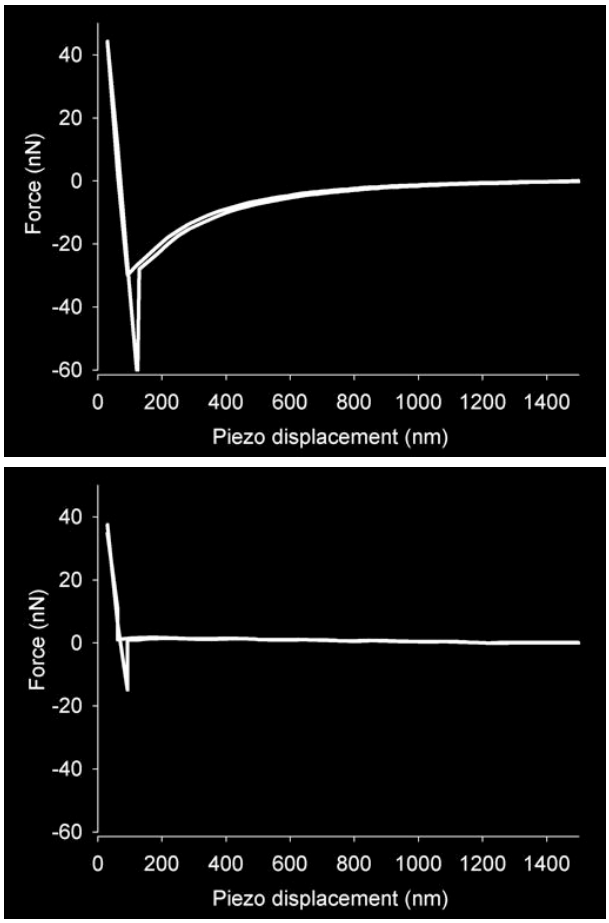

Figure 4.3.12 Influence of humidity on the force piezo-distance curve anatomy of TAA at (a) 15% RH and (b) 75% RH.

As humidity was increased to 75% RH (Figure 4.3.12b), the presence of such a long-range attraction force was not observed. Again this would be expected from an electrostaticly charged material, as progressive sorption of water at high humidities would increase surface electron mobility and hence dissipate charge.

As with salbutamol sulphate, the adhesion between TAA and Tempfix polymer resin was greater than the cohesion force in all cases (113.6nN, 349.1nN and 470.2nN at 15 45 and 75% RH). Again this was expected, however, it is interesting to note that the TAA-Tempfix adhesion increases with raised humidity, suggesting capillary interactions dominate.

The cohesion force for DSCG at 15% RH was greater than salbutamol sulphate and TAA at equivalent humidity. Furthermore, the 10th percentile values at 15% RH were greater than the median adhesion force for both salbutamol sulphate and TAA. Such observations may be due to the presence of water in the crystal structure (>5%, Chapter 3) leading to elevated capillary interactions at relatively low humidities.

Increasing the humidity from 15% RH to 45% RH resulted in an increased median cohesion force from 55.0 nN to 98.4 nN. By normalising the data, it becomes clear that the relative increase/decrease in cohesive forces for DSCG is greater than salbutamol sulphate and TAA, with a +78.8% increase between 15 and 45% RH for DSCG in comparison to +47.6% and -67.5% for salbutamol sulphate and TAA over the same humidity range. This increase can most likely be attributed to further water absorption in combination with surface morphological changes of both the drug probe and Tempfix mounted particles.

Elevation of humidity from 45 to 75% RH resulted in discontinuous FV measurements for DSCG interactions. Essentially, the force-piezo distance curves conducted between the DSCG drug probe and micronised particles became erratic, with multiple break points being observed during the retraction cycle of individual measurements. Such observations continued throughout the scan until the approach and retraction cycles were ‘separated’ lines with no observed constant compliance region. This was indicative of drug probe loss, since the tipless cantilever surface will produce a contact area far greater than the spring constant tolerance.

Subsequent observation of the DSCG drug probe tip, using optical microscopy, indicated the micronised drug to be ‘lost’. It is envisaged that such a loss may be due to morphological changes of the drug probe as water is absorbed into the crystal lattice. Furthermore, as DSCG is an interstitial solid, effectively held together by water molecules, the adhesion force between the individual drug particles may become great enough to ‘tear’ apart or fracture the crystal lattice. Consequently, the cohesion force

between DSCG particles could only be investigated by the AFM colloid probe technique at 15 and 45% RH.

As with salbutamol sulphate and TAA the median separation force for DSCG-Tempfix was greater than the cohesion force in all cases (110.1 nN and 136.8 nN for DSCG-Tempfix interactions at 15 and 45% RH, respectively).

Analysis of Cohesion (Separation) Energy.

By integration of the piezo-displacement cantilever deflection curve, the energy of separation (e_{sep}) between a drug probe and surface can be obtained. The advantage of expressing particle interactions in terms of e_{sep} is that it takes into account the variations in mechanical properties of the two contacting surfaces. Although the force of adhesion/cohesion allows us insight into the influence of physico-chemical properties, roughness and environmental conditions on the interactive mechanisms of two surfaces, it does not directly take into account the elastic moduli of the contacting surfaces. A graphical representation of the cohesion energy data values for all three drugs, as a function of humidity, is given in Figure 4.3.13.

As with the cohesion force values, a positive skew in the separation energy was observed suggesting irregular morphology to produce a lognormal separation energy distribution. Again, as with the cohesion force measurements the influence of humidity had a similar significant impact on the cohesion profile of each drug. An increase in median separation energy was observed for salbutamol sulphate (853.0 nJ, 1603.9 nJ and 2786.5 nJ at 15, 45 and 75% RH, respectively) and DSCG (2623.4 nJ and 8271.7 nJ), while a decrease was observed for TAA (2308.9 nJ, 571.5 nJ and 259.5 nJ). Comparative analysis between force and separation energy values as a function of humidity suggested good correlation. However, significant differences (ANOVA $p<0.05$) in the force-energy factors were observed (for salbutamol sulphate and TAA) suggesting, as expected, the presence of sorbed water to alter the elastic response of the separating surfaces.

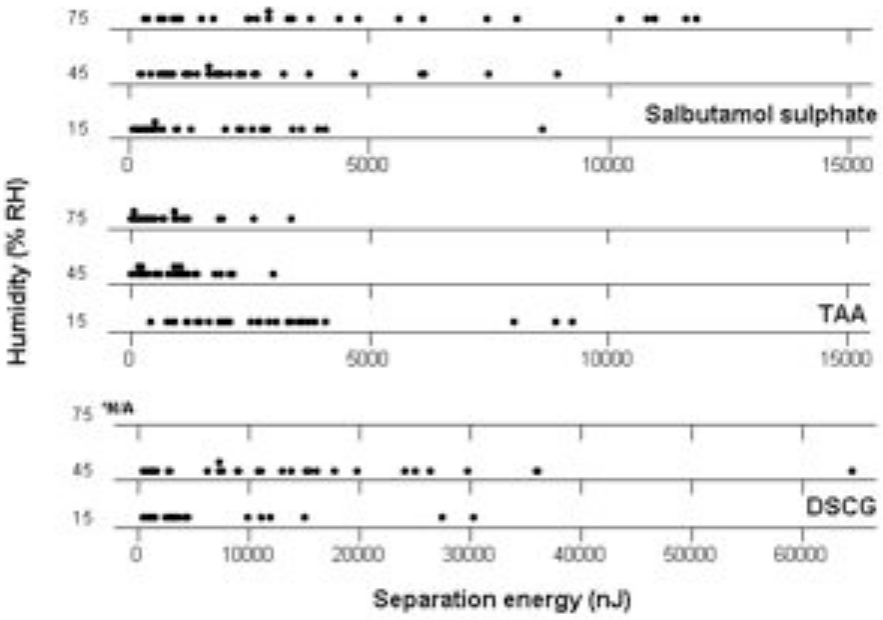

Figure 4.3.13 Distribution of separation energy values (cohesion) between individual salbutamol sulphate, TAA and DSCG particulates.

Consequently it was decided to focus primarily on separation energy values and not separation force.

4.3.3(b) AFM on model drug compacts.

The limitations of individual particle analysis were overcome by the preparation of large planar surfaces of the drug materials by direct compression. Force piezo-distance curves were conducted using the AFM in Force volume mode, over 10 μm x 10 μm areas of the model compacts and were batch reprocessed to obtain a block of 64 x 64 (4096) separation energy values corresponding to the relative position of each measurement.

Separation energy measurements between five salbutamol sulphate drug probes and salbutamol sulphate model compacts were investigated by AFM at 15, 30, 45, 60 and 75% RH and are summarised in Appendix 4.4.

As with individual particle-particle measurements, integration of the force distance curves measured over a 10 μm x 10 μm area (n=4096) produced a relatively wide distribution of separation energy values, with calculated standard deviations being of equivalent value to the mean (RSD 67 to 112% across the humidity range). Furthermore, separation energy histogram analysis showed the data spread across more than one order of magnitude in an asymmetrical, positively skewed distribution.

As expected, cumulative frequency-log distributions of the separation energy values indicated a lognormal distribution. This is demonstrated in Figure 4.3.14 as cumulative frequency log-separation energy values for salbutamol sulphate drug probe 1 (15 - 75% RH).

Cumulative frequency-log distributions for four further drug probe-compact measurements can be found in Appendix 4.5. The assumption of lognormal distribution was further justified using apparent linear regression analysis of log-probability plots (5 - 95%) where R^2 values of ≥ 0.94 were obtained (an example is given in Figure 4.3.15).

Figure 4.3.14 Separation energy distribution for salbutamol sulphate drug probe on salbutamol sulphate model surface at 15, 30, 45, 60 and 75 %RH at 25°C ± 0.2°C, (n=4096).

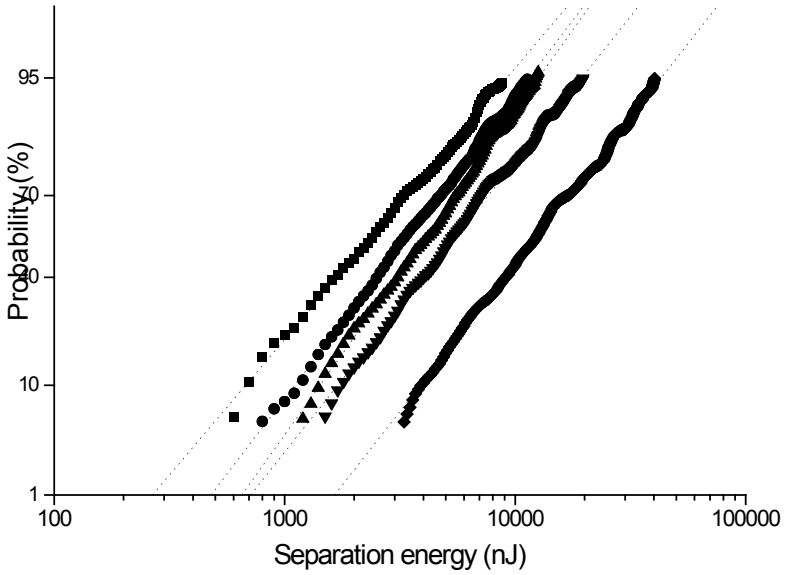

Figure 4.3.15 Example of a cumulative probability plot for salbutamol sulphate tip 1 on salbutamol sulphate model surface at ■ 15% RH, ● 30% RH, ▲ 45% RH, ▼ 60% RH and ◆ 75% RH. Dotted lines indicate apparent linear fit (5-95 % probability data).

.

As a result, a median value, or 50% cumulative undersize ($e_{0.5}$), was selected as the most appropriate descriptor for separation energy measurements between AFM drug probes and model compacts, since the large positive skew in the data may adversely affect the mean values.

Analysis of the separation energy data block (64 x 64 force curves) suggested no relationship between force curve number and separation energy value. In addition, offline analysis of individual force curves conducted at the beginning, middle and end of each run indicated no rank change in separation energy value or curve shape. Such observations would suggest that the salbutamol sulphate drug probe did not deform or appreciably tribocharge under such conditions. Furthermore, comparison of the separation energy data block values with the individual force curves, in offline analysis, indicated no surface 'hotspots' that may have been observed if contamination was present.

The influence of humidity on the $e_{0.5}$ for salbutamol sulphate-compact interactions is shown graphically in Figure 4.3.16. In all cases, change of humidity had a significant affect on the $e_{0.5}$ (CI = 0.95). Furthermore, a 6.4 ± 0.9 times increase in $e_{0.5}$ (n=5) occurred between 15 and 75% RH indicating capillary forces to become a dominating factor at higher humidities.

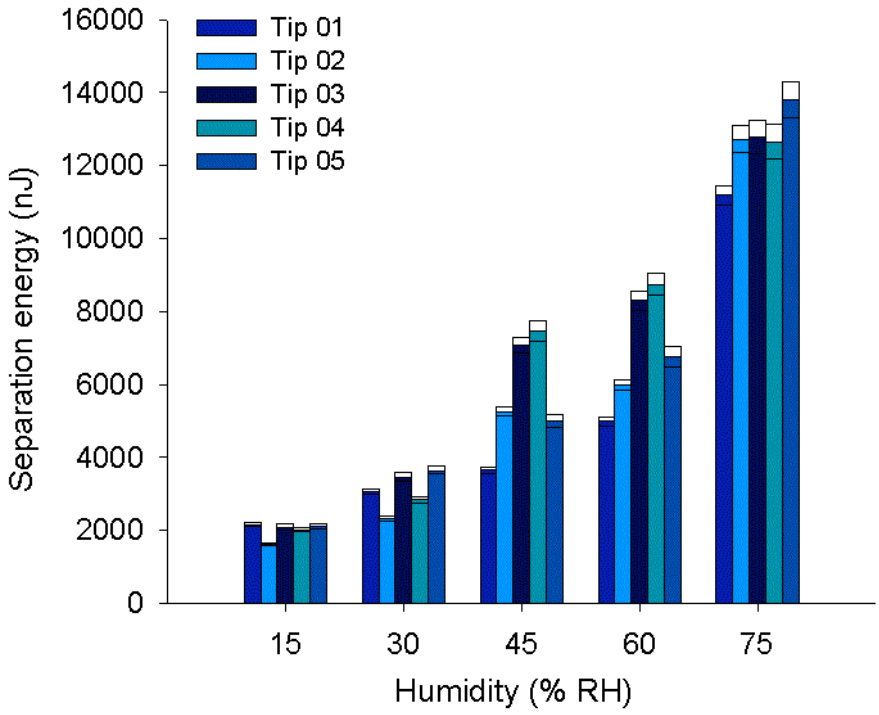

Figure 4.3.16 Influence of humidity on the median ($e_{0.5}$) separation energy values for salbutamol sulphate drug probes on model compact salbutamol sulphate surfaces. Centre line for each bar indicates median; upper and lower bars indicate upper and lower confidence intervals (CI = 0.95).

Separation energy measurements between five TAA drug probes and TAA model compacts, at 15, 30 45, 60 and 75% RH are summarized in Appendix 4.6.

Again, a large positive skew in separation energy values were observed, suggesting a lognormal distribution. Cumulative frequency log-separation energy values for TAA drug probe 1 at 15 - 75% RH is shown in Figure 4.3.17. Additionally, cumulative frequency-log distributions for the remaining four TAA drug probe-compact measurements can be found in Appendix 4.7.

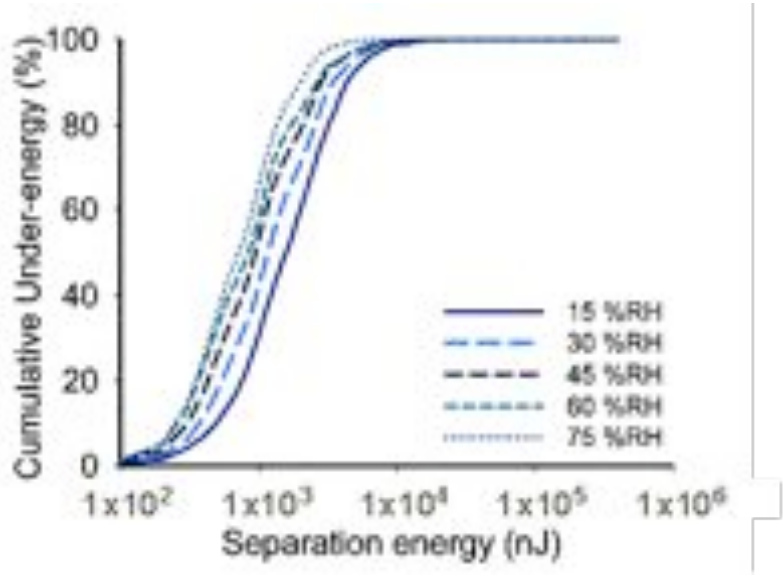

Figure 4.3.17 Separation energy distribution for TAA drug probe 1 on salbutamol sulphate model surface at 15, 30, 45, 60 and 75 %RH at 25℃ ± 0.2℃, (n=4096).

Again the assumption of lognormal distribution was justified using apparent linear regression analysis of log-probability plots (5-95%) where R^2 values of ≥ 0.96 were obtained (an example is given in Figure 4.3.18).

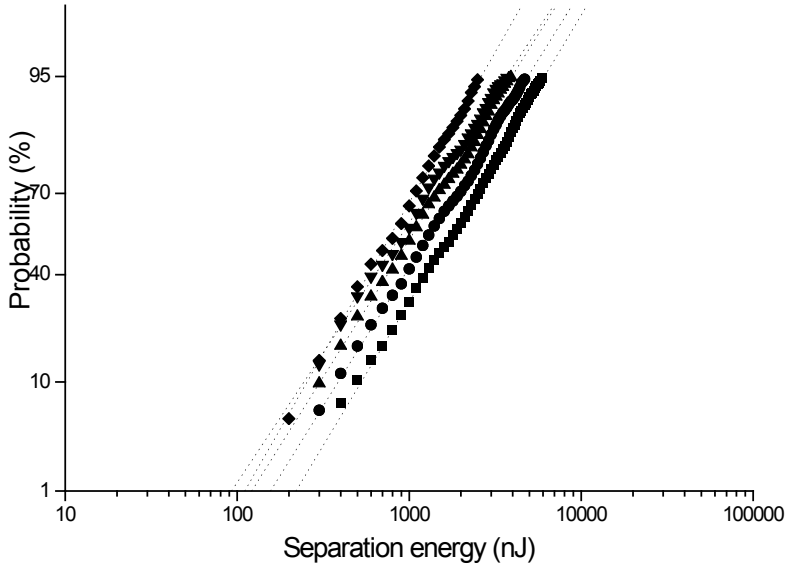

Figure 4.3.18 Example of a cumulative probability plot for TAA tip 1 on a TAA model compact surface at ■ 15% RH, ● 30% RH, ▲ 45% RH, ▼ 60% RH and ◆ 75% RH. Dotted lines indicate apparent linear fit.(5-95% probability data).

As with the salbutamol sulphate drug probe-compact interactions, offline analysis of the force-distance curves indicated no correlation between run number and separation energy value, but a clear variation in separation energy as function of humidity. As with the individual TAA particle-particle interactions (investigated in section 4.3.3a), an increase in humidity resulted in an overall decrease in separation energy. As previously discussed, this is most likely attributed to the dissipation of electrostatic forces. Again, this was qualitatively confirmed by the offline analysis of individual force-distance curves. As expected, a clear variation in force-distance curve anatomy was observed at different humidities (as was observed for TAA particle-particle interactions at low humidity show in Figure 4.3.12b). At lower humidities (ca. 15-30% RH) a clear long-range attraction force was observed between the TAA drug probes and TAA model compacts suggesting electrostatic attraction. This long-range attraction was not observed at higher humidities (ca. 45-75% RH).

The influence of humidity on the $e_{0.5}$ for TAA drug probe-compact interactions is shown graphically in Figure 4.3.19. In all cases, change of humidity had a significant affect on the $e_{0.5}$ (CI = 0.95). A 2.3 ± 0.3 times decrease in $e_{0.5}$ (n=5) occurred between 15 and 75% RH indicating electrostatic forces to be a dominating factor at lower humidities, with the presence of moisture at higher humidities potentially dissipating such interactions.

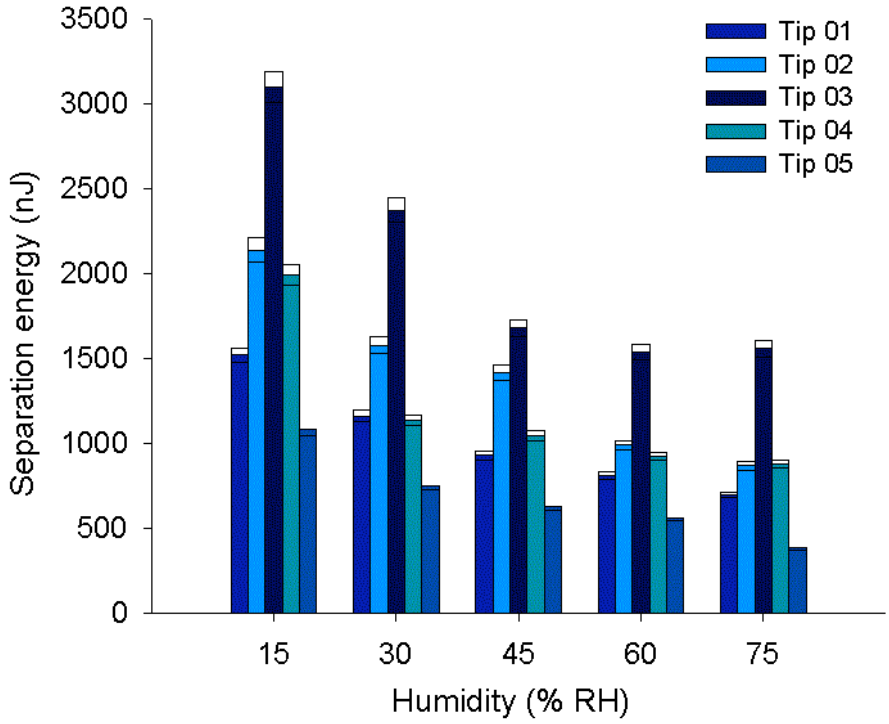

Figure4.3.19 Influence of humidity on the median ($e_{0.5}$) separation energy values for TAA drug probes on model TAA surfaces. Centre line for each bar indicates median; upper and lower bars indicate upper and lower confidence intervals (CI = 0.95).

Separation energy values obtained from DSCG drug probe measurements on DSCG model compact surface measurements are summarized in Appendix 4.8. Cumulative frequency log-separation energy values for DSCG drug probe 1 at 15 - 60% RH is shown in Figure 4.3.20. Additionally, cumulative frequency-log distributions for the remaining four DSCG drug probe-compact measurements can be found in Appendix 4.9.

Figure 4.3.20 Separation energy distribution for DSCG drug probe 1 on a DSCG model surface at 15, 30, 45,60 and 75% RH at 25°C ± 0.2°C, (n=4096).

A large statistically significant (CI = 0.95) increase in the median separation energy ($e_{0.5}$) with respect to humidity was observed for all five DSCG drug probe investigations. Furthermore, an increase in humidity from 60 to 75% RH resulted in the loss of the drug probe from the cantilever, thus making measurement impossible (confirmed by optical microscopy). Such observations are in good correlation with those made for individual particle-particle investigations, with particle loss occurring between 45 and 75% RH. As discussed, the loss of the drug probe from the cantilever at humidities in excess of 60% RH may be related to the change in particle morphology (as observed in Chapter 4.3.2, Figure 4.3.7).

As with the salbutamol sulphate and TAA model compact measurements, the model compact separation energy profile for DSCG exhibited a wide lognormal distribution. However, analysis of the 'apparent' linear fit suggested the separation energy values were not as regularly distributed. This was highlighted by the low R^2 values (0.700 to 0.968) shown in Appendix 4.8. An example of the linearity analysis is shown in Figure 4.3.21. In addition, a variation in the slope was observed for DSCG probes at various humidities, however this was not reproducible and could therefore not be statistically investigated. Again, this may be due to unpredictable variation in morphology in combination with the large water sorption.

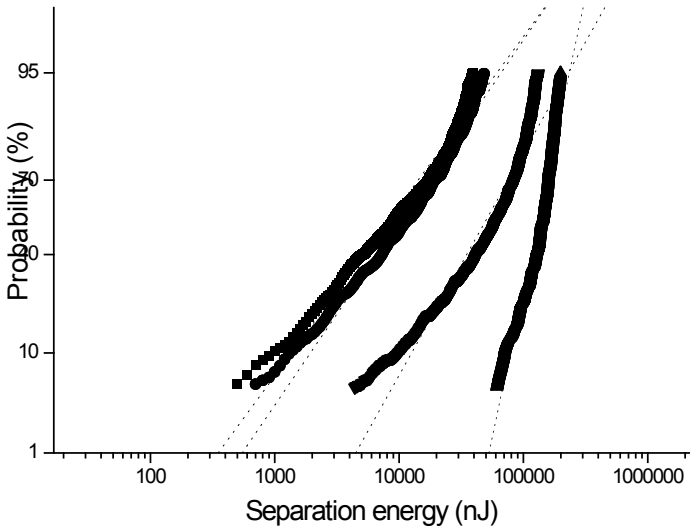

Figure 4.3.21 Example of a cumulative probability plot for DSCG tip 1 on a DSCG model compact surface at ■ 15% RH, ● 30% RH, ▲ 45% RH, ▼ 60% RH and ◆ 75% RH. Dotted lines indicate apparent linear fit.(5-95% probability data).

The influence of humidity on the $e_{0.5}$ for DSCG drug probe-compact interactions is shown graphically in Figure 4.3.22. In all cases, change of humidity had a significant affect on the $e_{0.5}$ (CI = 0.95). An 11.1 ± 6.0 times increase in mean $e_{0.5}$ (n=5) occurred between 15 and 60% RH indicating capillary forces to dominate DSCG interactions.

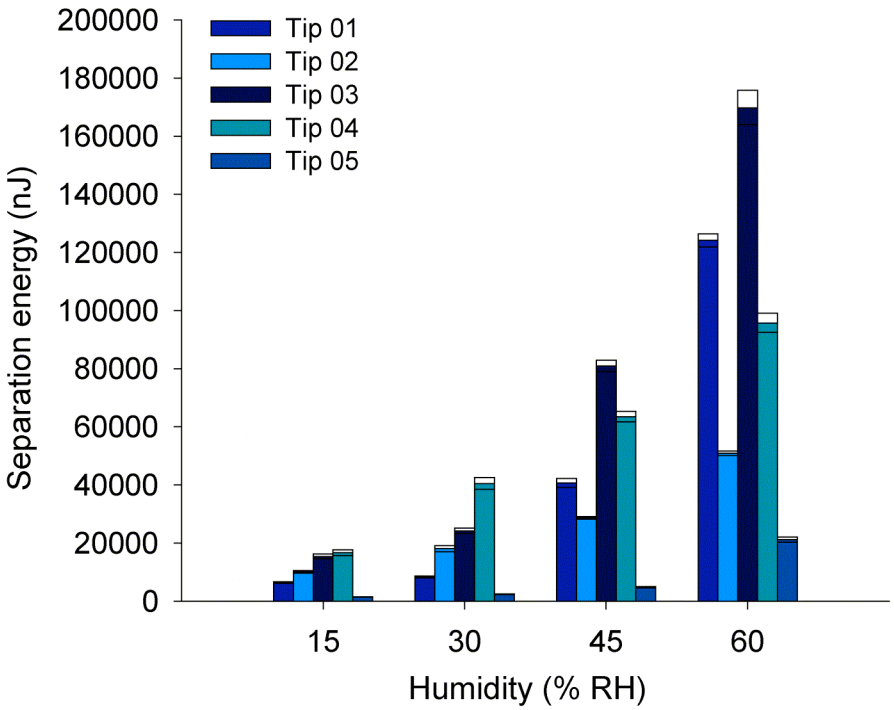

Figure 4.3.22 Influence of humidity on the median ($e_{0.5}$) separation energy values for DSCG drug probes on model DSCG surfaces. Centre line for each bar indicates median; upper and lower bars indicate upper and lower confidence intervals (CI = 0.95).

The spread in separation energy values for each of the micronised drug probe measurements can be determined from the geometric standard deviation (GSD) (Hinds, 1999).

$$GSD = \left[\frac{e_{0.84}}{e_{0.16}}\right]^{0.5} \qquad \textit{Equation 4.3.2.}$$

Where e_x are the respective percentile values for the lognormal distribution. Essentially a GSD of one would be a monomodal, monodispersed separation energy distribution (Hinds, 1999). Analyses of GSD values for each drug probe compact investigation are plotted as a function of humidity and are shown in Appendix 4.10. Statistical analysis of salbutamol sulphate and TAA drug probe-model drug compact surface interactions indicated no statistical variation (ANOVA $p<0.05$) in GSD with respect to humidity. In comparison, a statistically significant variation in GSD for DSCG interactions was observed. Again this is most likely attributed to variations in morphology with respect to humidity.

4.3.3(c) AFM on atomically flat crystalline material.

It is clear that separation energy measurements, conducted between micronised drug probes over large areas of compacted model drug substrates, allows the collection of valuable data that may be applied to bulk material properties. However, the relatively rough surfaces produced by direct compression (under these experimental conditions) resulted in large separation energy distributions. Although this may be an accurate representation of the separation energy distributions that will be observed between individual particulates (as observed previously), it would be interesting to eliminate the influence of substrate roughness on drug probe interactions.

Subsequently, a series of 'atomically smooth' surfaces were produced by controlled crystallisation. Essentially, this produced a series of model drug substrates that contained roughness parameters of a similar order to that of the crystal unit cell. It is reasonable to conclude, therefore, that such surfaces would not contain large irregularities in morphology resulting from subjection to rapid precipitation or micronisation.

Separation energy measurements, conducted at 15, 30, 45, 60 and 75% RH, between salbutamol sulphate, TAA and DSCG drug probes with their corresponding re-crystallised surfaces are summarised in Appendix 4.11, 4.12 and 4.13, respectively.

Residual low-resolution height images, produced from the 60 nm constant compliance threshold during force-volume analysis, indicated the surfaces to be smooth with clear angles relating to the change in crystal plane (similar to the high resolution Tapping Mode images shown in Figure 4.3.10). An extreme example for salbutamol sulphate drug probe measurements is shown in Figure 4.3.23a, where 3 crystal planes intersect. Separation energy values conducted over the same region was exported as a 64 X 64 block of data (relating to the X and Y positions each force-distance curve was taken) and is shown in Figure 4.3.23b. Clear variations in the separation energy

values could be directly related to the low-resolution height data, which was collected simultaneously. The majority of the separation energy values were of similar magnitude and were obtained from the two large crystal planes. A second lower set of energy values were obtained on the smaller acute angled plane. Finally a third high energy set of data points were obtained at the intersection between the two large crystal planes (Figure 4.3.23).

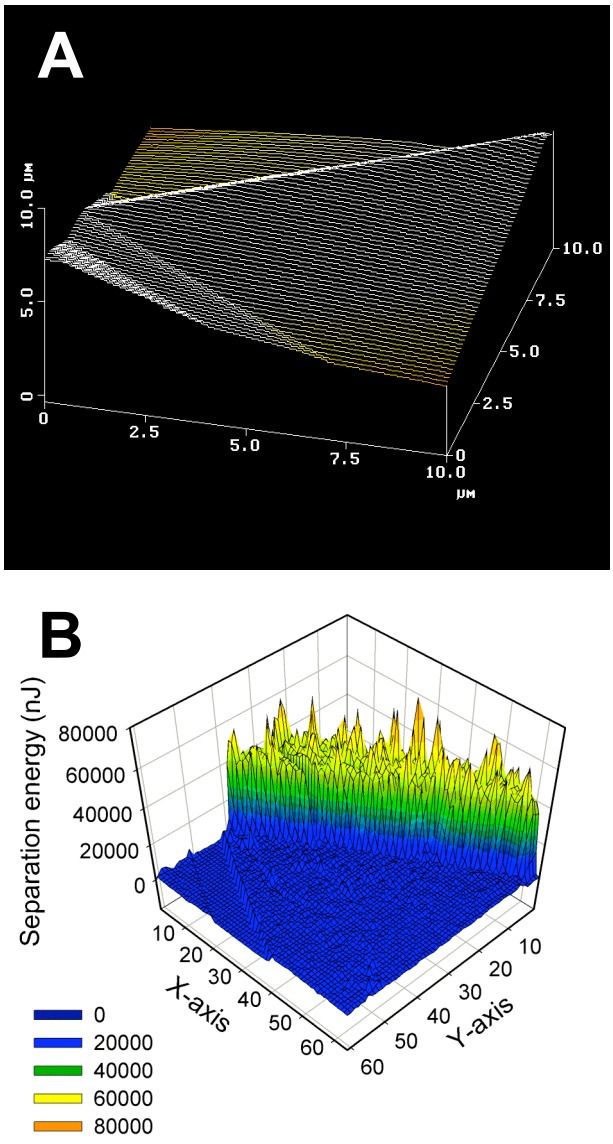

Figure 4.3.23 (a) Low resolution height image produced from force-volume measurements of salbutamol sulphate drug probe measurements on a re-crystallised salbutamol sulphate surface. (b) Separation energy distribution for as a function of colloid probe position on the same region of the re-crystallised salbutamol sulphate surface.

By comparing the separation energy values obtained over a 64 μm X 64 μm region to the corresponding height image (Figure 4.3.23) it becomes clear that the surface morphology and structure of the crystal will play an important role on the cohesion characteristics. The separation energies for salbutamol sulphate drug probe measurements obtained on the three intersecting crystal planes can be shown clearly when plotted as a frequency distribution (Figure 4.3.24).

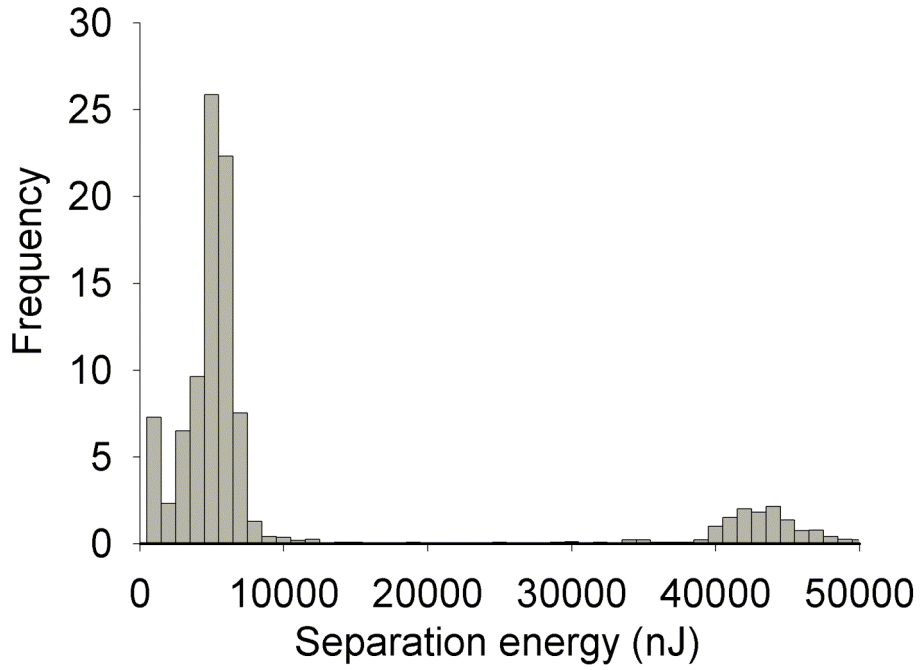

Figure 4.3.24 Frequency distribution for salbutamol sulphate drug probe measurements on the same region of the salbutamol sulphate re-crystallised surface as shown in Figure 4.3.23.

Separation energy measurements between all the drug probes and corresponding re-crystallised surfaces were conducted on large 10 μm X 10 μm areas of the apparent dominant crystal face. In general, intersections between crystal planes were not observed during this process, as the position of the drug probe in relation to the crystal could be controlled visually prior to analysis. However, regions where such intersections occurred were analysed, in a similar manner to that in Figure 4.3.23, where separation

energy values that did not correspond to the dominant plane were removed manually offline. This produced, a separation energy distribution for interactions between a drug probe and the 'apparent' dominant face of its corresponding crystal.

Representative cumulative separation energy distributions for measurements between a salbutamol sulphate, TAA and DSCG drug probe and corresponding crystal surface are shown in Figure 4.3.25 (a, b and c, respectively). In addition, two further replicate probe measurements were conducted for each drug material and are shown in Appendix 4.14.

For comparative purposes the cumulative separation energy distributions are plotted on the same scale as that for drug probe compact measurements (Figure 4.3.14, 4.3.17 and 4.3.20). Unlike the drug probe model compact measurements, narrow distributions in separation energy values were observed for each of the drug probes. This can be clearly observed by the sharp 'cut-off' in the cumulative separation energy plots (Figure 4.3.25). Furthermore, low GSD and RSD values indicated a mono-modal, normally distributed separation energy for each of the drug probe crystal interactions.

Such observations are not unexpected however, as the drug probe interactions were conducted on one face of an 'atomically flat' crystal and would therefore, theoretically produce one separation energy. The assumption of a normal separation energy distribution was further investigated by linear regression of normal probability plots (examples of which are given in Figure 4.3.26). As expected, linear regression indicated a $R^2 \geq 0.903$ across salbutamol sulphate and TAA drug probe measurements (DSCG produced lower R^2 values at high humidity), suggesting a normal distribution. Subsequently, data for drug probe-crystal interactions were analysed using conventional mean values and standard deviations.

Figure 4.3.25 Separation energy distribution for (a) salbutamol sulphate, (b) TAA and (c). DSCG drug probe interactions on their corresponding drug crystal surfaces (taken at 15, 30, 45,60 and 75% RH at 25°C).

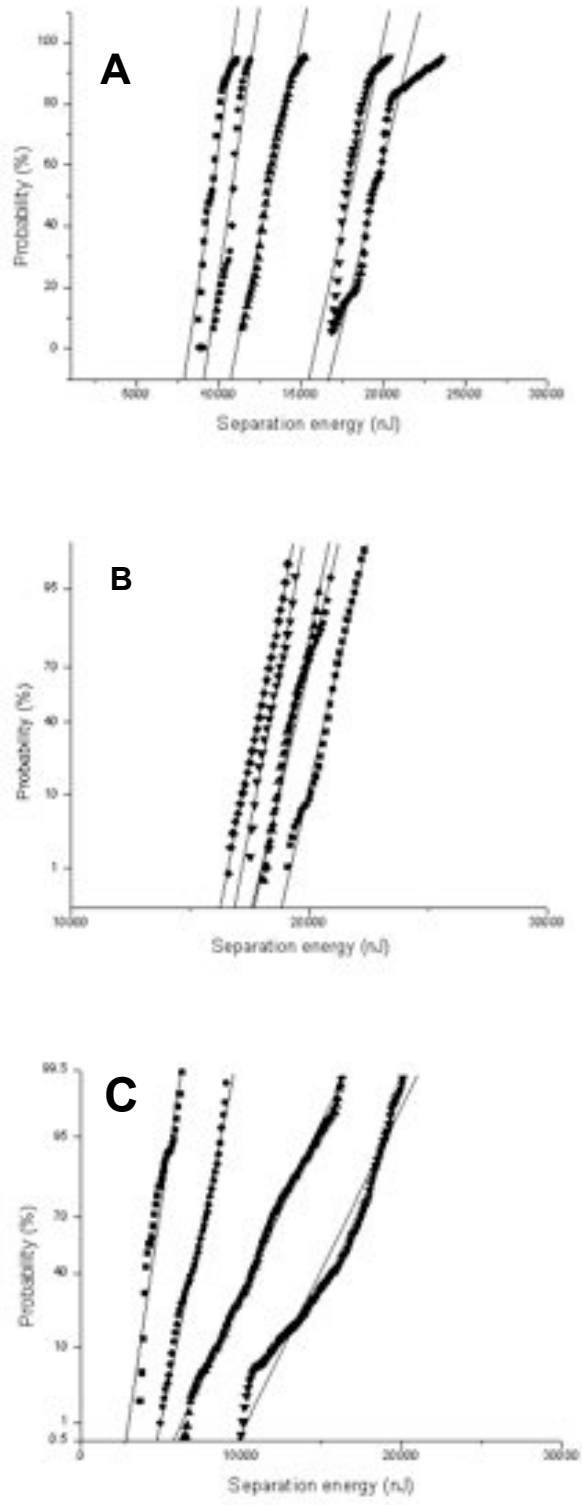

Figure 4.3.26 Examples of the normal linear fit for (a) salbutamol sulphate, (b) TAA and (c) DSCG separation energy measurements on their corresponding re-crystallised surfaces.

The influence of humidity on the separation energy profiles for salbutamol sulphate, TAA and DSCG on their corresponding re-crystallised surfaces suggested similar trends to that observed for individual particle-particle and particle-model drug compact investigations. Mean (± Std) values for salbutamol sulphate, TAA and DSCG drug probe crystal interactions are shown graphically in Figure 4.3.27.

A 3.0 ± 2.2 increase in mean separation energy for salbutamol sulphate drug probe interactions were observed between 15 and 75% RH. Statistical analysis (ANOVA, Fisher pairwise $p<0.05$) suggested this observation to be significant across all humidities for all salbutamol sulphate drug probes (n=3). As previously discussed this may be due to an increase in capillary forces at higher humidities as water is adsorbed on the drug probe and crystal surfaces.

As with the particle-particle and particle-compact measurements, TAA drug probe interactions with TAA crystalline surfaces suggested a small but statistically significant decrease (1.1 ± 0.1 times) in separation energy (ANOVA, $p<0.05$) as humidity was increased (15 - 75% RH). In addition, Fisher pair wise analysis indicated that increased humidity caused a significant ($p<0.05$) decrease in at each humidity for all drug probes with the exclusion of drug probe three (Appendix 4.12) between 30 and 45% RH. Again, long-range attractive forces were observed at low relative humidities suggesting the presence of an electrostatic attraction mechanism.

As expected analysis of the DSCG drug probe-crystal separation energy profile showed large statistically significant increase (ANOVA $p<0.05$) in separation as humidity was raised. In general, a 3.3 ± 0.3 times increase in separation energy was observed for three drug probe crystal interactions, between 15 and 60% RH, again suggesting sorption of water into DSCG to directly influence cohesion.

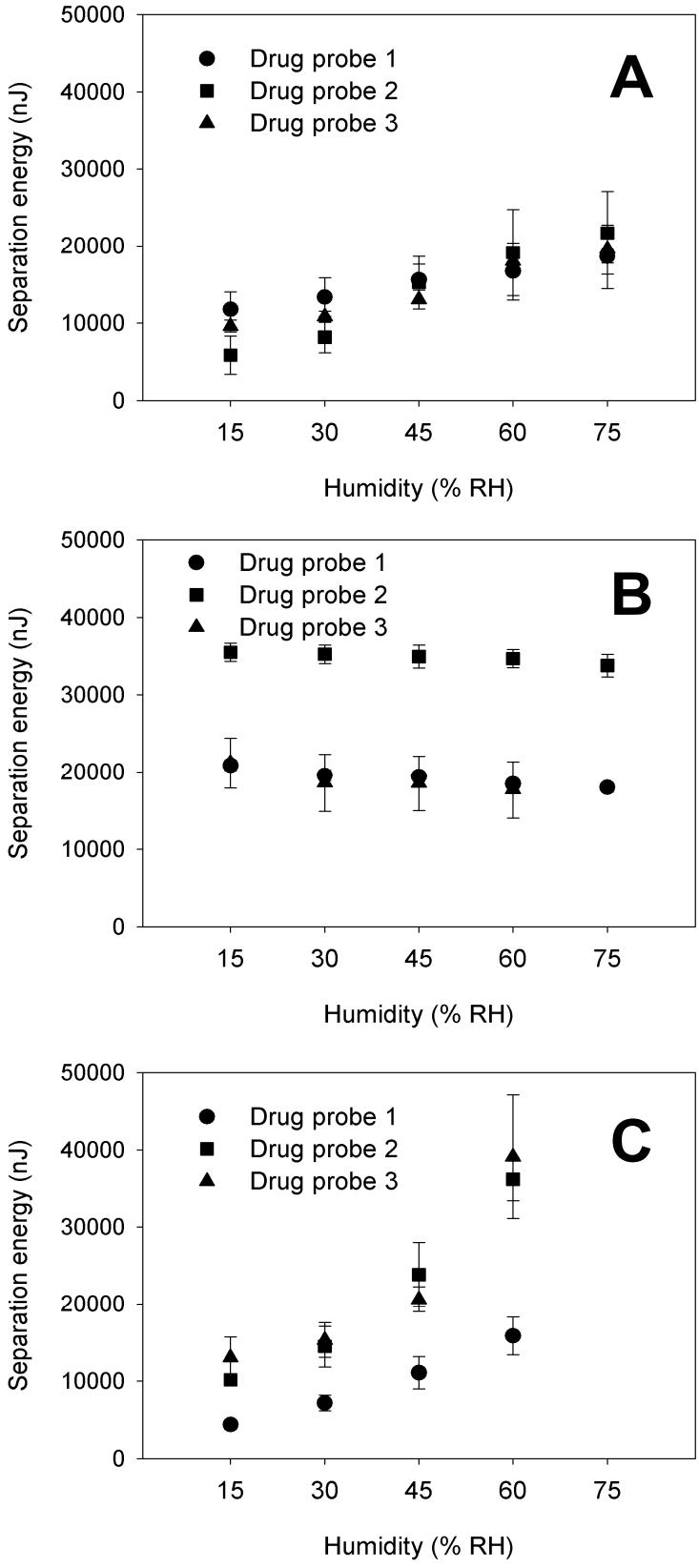

Figure 4.3.27 Mean separation energy values (± standard deviation) for (a) salbutamol sulphate, (b) TAA and (c) DSCG interactions with their corresponding re-crystallised surfaces.

4.4 CONCLUSIONS: ATOMIC FORCE MICROSCOPE COHESION MEASUREMENTS.

The AFM colloid probe technique has been successfully developed to measure separation energies for three micronised drugs as a function of humidity. Clear variations in 'cohesion profiles' for salbutamol sulphate, TAA and DSCG were observed. In general, the energy to separate salbutamol sulphate and DSCG increased with respect to humidity, while TAA decreased. It is suggested that the separation energy 'cohesion profiles' can be attributed to the physico-chemical and physico-mechanical properties of each specific drug. These factors will be discussed in more detail in Chapter 6.

In addition, a clear relationship between separation energy distribution and surface roughness was observed. This was not unexpected, however as large variations in contact area between the micronised drugs and/or compacted surfaces exist, which potentially influences cohesion. Conducting separation energy measurements on 'atomically smooth' crystals of the respective drugs subsequently proved this hypothesis.

It is important to note, however, that such measurements are undertaken between individual drug probes and model drug surfaces and therefore can not be directly related to the complex dynamics that exist during the aerosolisation process. Although such observations are fundamentally interesting, they require perspective. For dry powder inhaler formulations, such large variations in cohesion profile may directly influence aerosolisation performance, and subsequently have direct impact on the patient. Since environmental conditions in the 'real world' are not kept constant, and factors such as humidity cannot be controlled, it would be interesting to corroborate the AFM cohesion profiles with aerosolisation performance from a DPI.

5 IN-VITRO MEASUREMENT OF THE MICRONISED DRUG AEROSOLISATION EFFICIENCY.

5.1 INTRODUCTION.

It has become clear, through bulk and AFM measurements, that the influence of humidity will play an important role in the particle-particle interactions in a dry powder inhaler. However, It is important to note that such measurements are generally taken out of context and can therefore not be directly related to the complex dynamics that exist during the aerosolisation process. As a function of this, an investigation was undertaken to correlate the bulk (Chapter 3) and individual drug particle measurements (Chapter 4) with the in-vitro aerosolisation performance from a dry powder inhaler.

Studies investigating the influence of humidity on drug aerosolisation performance have been conducted in the past, but have generally focused on drug-carrier interactions or short exposure times. In addition, these previous studies have been conducted by a series of research establishments and therefore were not standardised to allow direct comparison. However, a brief description of the most relevant investigations is given below.

Recent investigations (Jashnani et al 1995, Jashnani and Byron 1996) have shown that storage of a variety of micronised salbutamol salts in relatively high humidities for short periods (3-60 mins) resulted in an apparent decrease in the relative amount of fine particle fraction (<6.4 μm). Additionally, studies describing the relationship between drug aerosolisation and humidity reported similar effects for DSCG, (Hindle and Makinen 1996, Braun et al 1996). However, these investigations concentrated on the aerosolisation of DSCG from larger carrier materials and therefore were not specific to the drug-drug interactions. No published reports for TAA could be found.

The in-vitro aerosolisation investigations of each pure micronised drug was conducted during storage inside an environmental humidity test chamber. In contrast to previously reported studies (Jashnani et al 1995, Jashnani and Byron 1996, Hindle and Makinen 1996, Braun et al 1996), this study focused on the investigation of pure drug-drug interactions after relatively long storage times (12 hours) at a variety of specific humidities.

Aerosolisation efficiency of each drug at each specific humidity was measured using a twin stage impinger (TSI) that separates the drug by effective mass median aerodynamic diameter (6.4 μm at a flow rate of 60 $L.min^{-1}$ being equivalent to the fine particle fraction). Drug recovered from each stage of the TSI and inhaler components was determined by high performance liquid chromatography (HPLC).

5.2 QUANTIFICATION OF DRUG CONTENT BY HPLC.

5.2.1 Materials and Methods.

The drug concentrations collected from the various components and TSI sampling stages during the in-vitro studies were analysed by reverse phase HPLC. In simple terms the HPLC operates by separating organic compounds by their relative affinity for the solid phase. Chemicals used for the HPLC determination of drug content, collected from the TSI sampling stages, are given in Table 5.2.1.

The HPLC used was a Waters Alliance unit (Waters, UK). Briefly, the system comprised of a 2690 separations module, (containing a temperature-controlled autosampler, variable injection sample syringe, four-channel gradient pump and column oven) and a 486 tunable absorbance UV spectrophotometer. Data were recorded and integrated using waters millennium software. Details of the experimental set-up for each of the five micronised drugs is summarised in Table 5.2.2.

Material	**Manufacturer**
Acetonitrile (HiPerSolv Far UV grade for HPLC)	BDH, Poole, UK
Ammonium acetate (HiPerSolv for HPLC)	BDH, Poole, UK
di-sodium hydrogen orthophosphate anhydrous - (analytical grade)	Fisher scientific, Leicestershire, UK
orthophosphoric acid (analytical grade)	Fisher scientific, Leicestershire, UK
Potassium dihydrogen orthophosphate – (HiPerSolv for HPLC)	BDH, Poole, UK
Water (purified through Millipore RiO_5 and $milliQ_{plus}$ – at 18.5)	Millipore, Watford, UK

Table 5.2.1 Materials used for the in-vitro *study and HPLC analysis.*

Drug Substance	**Salbutamol -** sulphate	**DSCG**	**TAA**
HPLC Column	*Sphereclone ODS, 5 μm packing, 25 cm x 0.32 cm id	*Hypersil 5ODS, 5 μm packing, 10 cm x 0.5 cm id	*Hypersil 5ODS-2 5 μm packing, 10 cm x 0.46 cm id
Column Oven Temperature (°C)	40°C	45°C	40°C
Column Flow Rate (ml/min)	0.75 $ml.min^{-1}$	1.5 $ml.min^{-1}$	1.5 $ml.min^{-1}$
Sample Tray Temperature (°C)	25°C	25°C	25°C
Injection Volume (μl)	100 μl	100 μl	100 μl
Detector Wavelength (nm)	223 nm	254 nm	239 nm
Retention Time (minutes)	4.5 ~ mins	2.5 ~ mins	4 ~ mins

*Phenomenex, Cheshire, UK

Table 5.2.2. HPLC experimental set-up and instrument settings for the micronised drug substances.

Drug was recovered or diluted in a suitable wash solution and analysed using a drug specific mobile phase. Details of the specific wash solutions and mobile phase are given below.

5.2.1(a) Preparation of reagents.

Salbutamol sulphate dilution solvent - 0.05 M potassium phosphate buffer.
Potassium dihydrogen orthophosphate (6.8 g) was added to 950 ml of milliQ water. The solution was adjusted to pH 4.5 by drop wise addition of orthophosphoric acid and made up to 1000 ml with milliQ water.

Salbutamol sulphate mobile phase - 8:92% $^{w}/_{w}$ acetonitrile: potassium phosphate buffer.
Salbutamol sulphate dilution solvent (920 ml) was added to 80 ml acetonitrile.

TAA mobile phase and dilution solution – 37:63% $^{w}/_{w}$ acetonitrile: potassium phosphate buffer.
Potasium dihydrogen orthophosphate (3.4 g) (BDH, Poole, UK) was added to 950 ml of milliQ water. The solution was adjusted to pH 3.0 by drop wise addition of orthophosphoric acid and made up to the mark with milliQ water. 370 ml of acetonitrile was added to 630 ml of the 0.05 M phosphate buffer.

DSCG dilution solvent - 0.05 M sodium phosphate buffer.
Anhydrous disodium hydrogen orthophosphate (7.01 g) was added to 950 ml of milliQ water. The solution was adjusted to pH 7.4 by drop wise addition of orthophosphoric acid and made up 1000 ml with milliQ water.

DSCG mobile phase – 21% $^{w}/_{v}$ 0.015 M sodium phosphate buffer, 0.015 M potassium dihydrogen phosphate buffer solution.
Anhydrous disodium hydrogen orthophosphate (2.13 g) and potassium dihydrogen orthophosphate (2.04 g) were added to 700 ml of milliQ water. 210 ml of methanol was added and the solution made up to 1000 ml.

5.2.1(b) Preparation of standards.

Standards for each of the micronised drugs were prepared as follows; Duplicate stock standard solutions were prepared by accurately weighing approximately 25 mg aliquots of material into two 100 ml volumetric flasks. Drug in each flask was dissolved in specific dilution solution. Solutions were ultrasonicated for not more than 10 minutes to ensure dissolution, left to cool to room temperature, and made up to the mark with dilution solvent.

Working standard solutions were prepared by serial dilution of the stock standard solutions using calibrated (class A) laboratory pipettes and same dilution solution. A series of working standard with concentrations between 0.1 $\mu g.ml^{-1}$ and 10 $\mu g.ml^{-1}$ were prepared for each drug substance.

Duplicate injections of each working standard were analysed by HPLC with a blank, containing dilution solution, being sampled before the first injection and after the highest standard. System repeatability was investigated by conducting six replicate injections of the lowest working standard. The accuracy (*A*) between the two standard solutions was investigated by Equation 5.1.1.

$$A = \frac{A_1}{A_2} x \frac{W_2}{W_1} \qquad \textit{Equation 5.1.1} \qquad \textit{Accuracy stock solution weighings.}$$

Where A_1 is the mean peak area for the lower working standard 1, A_2 is the mean peak area for the working standard 2 of same dilution, W_1 is weight of drug added in stock solution 1 and W_2 the weight of drug added in stock solution 2. A value of between 0.99 and 1.01 was considered accurate.

5.2.2 Results and Discussion.

Sample chromatographs for each of the three drugs (low and high concentrations) are given in Appendix 5.1. All drugs exhibited single peaks at the approximate retention times given in Table 5.2.2. The concentration-absorbance linear response for salbutamol sulphate, TAA and DSCG was investigated through linear regression analysis and is shown in Figure 5.2.1.

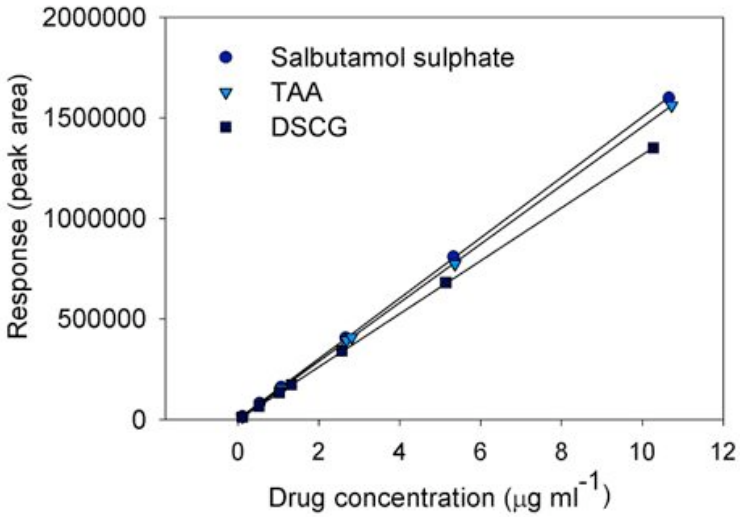

Figure 5.2.1. Linear peak area to concentration response for salbutamol sulphate, TAA and DSCG micronised drugs. Linear regression analysis was forced through zero. R^2 values of 0.9999, 1.0000 and 1.0000 were recorded for salbutamol sulphate, TAA and DSCG, respectively.

Linear regression analysis for each of the five drugs showed R^2 values were equal to or greater than 0.9999 inferring a direct linear response between peak area and concentration over the range ~ 0.1 $\mu g.ml^{-1}$ to 10 $\mu g.ml^{-1}$. Relative standard deviations between six replicate injections for all five drugs were less than 0.5% and accuracy (*A*), between the weight of stock solution 1 and stock solution 2, for each of the drugs was within the established parameters (0.99-1.01). In addition, no interfering peaks were observed in any of the initial blanks, and no sample carryover was observed in blanks injected after the higher standards.

5.3 OPERATION AND SAMPLING OF TWIN STAGE IMPINGER AT SPECIFIC HUMIDITIES.

5.3.1 Materials and Methods.

The influence of humidity on the aerosolisation of the micronised drug materials was investigated using apparatus A (see Figure 5.3.1), the twin stage glass impinger (Copley Scientific, Nottingham, UK). All experiments were conducted inside an environmental test chamber (type KBP 6395 F Copley Scientific, Nottingham, UK) capable of maintaining an environment of 10 – 95% RH (± 0.2% RH) at 25°C.

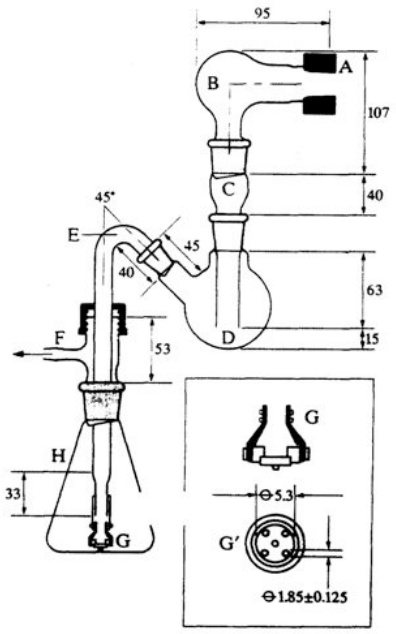

Figure 5.3.1. Schematic of the twin stage impinger (adapted from the British Pharmacopoeia, 2001, Volume II).

The TSI was assembled as represented diagrammatically in Figure 5.3.1 and contained 7 ml of dilution solution in stage one and 30 ml dilution solution in stage two. A pump (Model 1423-101Q-Q626X, GAST, Buckinghamshire, UK) generated a flow rate through the TSI of 60 $L.min^{-1}$ (± 2 $L.min^{-1}$), which was calibrated using a micromanometer (model FC012, Furness controls, Bexhill, UK) by adjustment of a needle valve flow regulator. Flow rate was set

using a dummy DPI, (Turbohaler®, Astra-Draco AB, Lund, Sweden) containing no drug, excipients or desiccant, assembled inside a sealed flow chamber.

The micronised drugs were stored in open pans in the environmental test chamber at the required humidity for 12 hours prior to analysis. Approximately 1500 μg of equilibrated drug material was accurately weighed into the plastic metering chamber of a modified DPI (Turbohaler®, Astra-Draco AB, Lund, Sweden) containing no desiccant. The DPI and assembled TSI were equilibrated, at the humidity under investigation, in the environmental chamber for 30 minutes prior to analysis. The loaded DPI was inserted into a specially constructed mouthpiece and tested at 60 $L.min^{-1}$ for five seconds using the solenoid valve timer. A three second delay in activating the timer, after the pump was engaged, was invigilated to allow equilibrium of the pump.

A photograph and diagrammatic representation of the sampling apparatus assembled inside the humidity test chamber is shown in Figure 5.3.2.

The DPI, mouthpiece adaptor: throat assembly, stage one and stage two were thoroughly rinsed into suitable volumetric flask with dilution solvent and made up to the mark. Drug content remaining in the DPI device was collected by carefully deconstructing the device components and washing separately with solvent. The device components were then rinsed with distilled water followed by methanol, and dried at 40°C in an oven. The DPI components were left to cool, reassembled and re-used. No apparent degradation in component parts or device integrity was observed by conducting this procedure. A similar water-methanol rinsing procedure was used for the TSI.

All samples were analysed by HPLC using a bracketing standard protocol described in Appendix 5.2. For each humidity and drug, TSI investigations were carried out in triplicate.

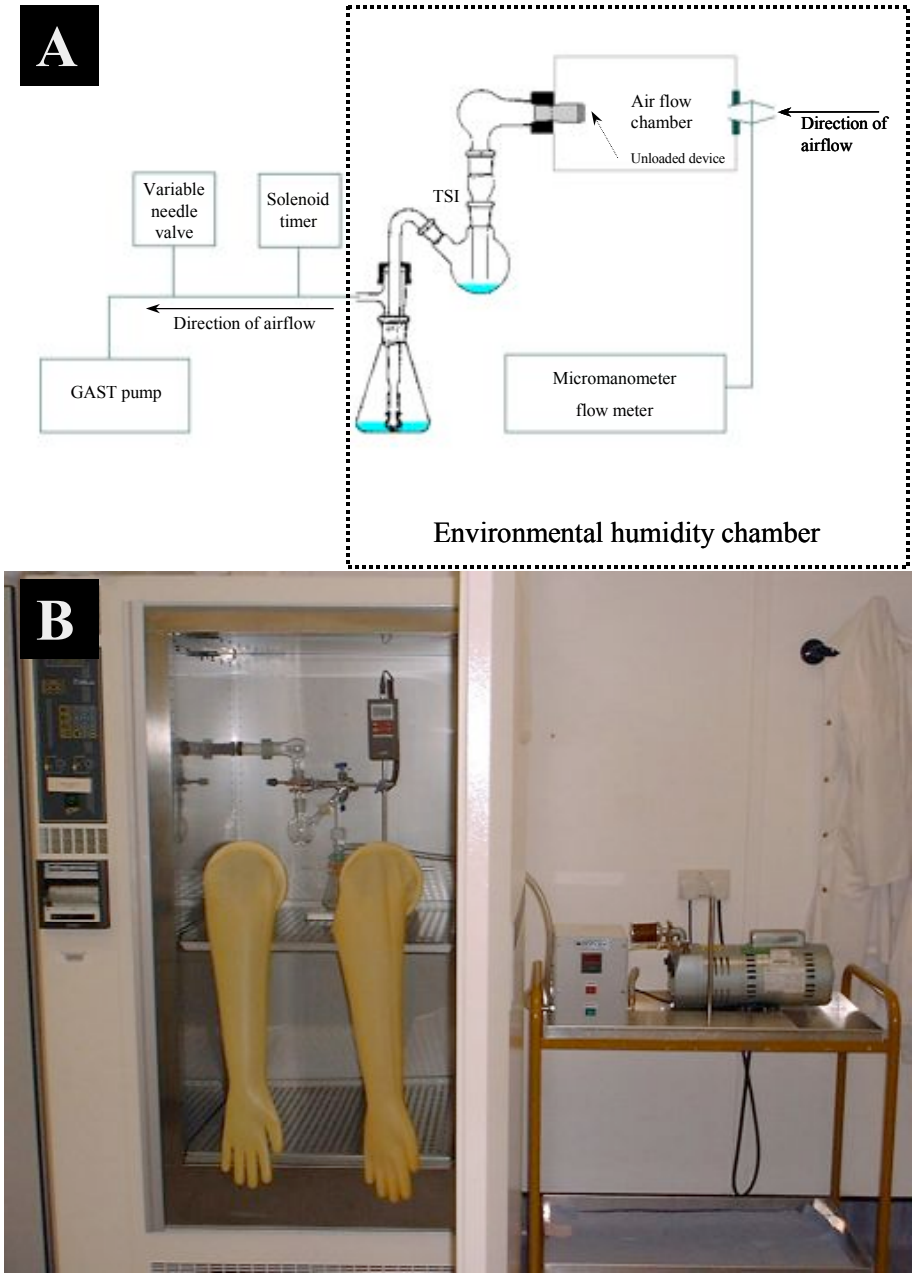

Figure 5.3.2 (a) Diagrammatic representation of TSI set-up with calibration flow meter and chamber. (b) Photograph of TSI set-up inside environmental test chamber.

5.3.2 Results and Discussion.

The in-vitro characterisation for aerosolisation of salbutamol sulphate, TAA and DSCG was conducted at 15, 30, 45, 60 and 75% RH at 25°C using a TSI. The results obtained from the in-vitro investigations are shown in Table 5.3.1, and are represented as percent remaining in device, percent in TSI throat and mouthpiece adaptor, percent in stage one and percent in stage two (Hallworth and Westmoreland 1987).

	Humidity	Loaded dose (µg)	% in DPI	% in Throat	% in Stage 1	*% in Stage 2
Salbutamol sul.	15	1782 (219)	14.8 (5.5)	10.7 (3.2)	62.0 (10.3)	12.5 (3.4)
	30	1777 (86)	17.9 (3.6)	10.4 (1.1)	57.3 (6.8)	14.4 (2.7)
	45	1365 (102)	26.9 (3.5)	11.8 (1.5)	47.9 (9.3)	13.3 (1.5)
	60	1465 (86)	37.4 (8.5)	7.5 (1.3)	44.0 (10.0)	10.8 (2.8)
	75	1637 (438)	87.4 (10.9)	2.0 (2.5)	7.9 (9.9)	2.7 (3.7)
TAA	15	1446 (82)	31.5 (3.3)	30.2 (3.2)	32.3 (1.1)	6.0 (1.9)
	30	1630 (155)	23.2 (5.0)	34.2 (7.1)	34.6 (4.9)	7.9 (0.6)
	45	1585 (161)	21.5 (5.6)	25.1(1.0)	45.1 (3.7)	8.3 (0.9)
	60	1624 (126)	25.8 (4.7)	22.7 (4.0)	42.0 (7.6)	9.5 (3.5)
	75	1444 (256)	21.8 (6.2)	23.9 (6.8)	41.9 (14.9)	12.3 (3.5)
DSCG	15	1274 (251)	16.3 (0.4)	34.8 (6.0)	18.9 (7.1)	29.2 (9.0)
	30	1517 (249)	36.2 (11.1)	17.0 (9.6)	21.8 (18.4)	23.0 (5.7)
	45	1445 (203)	39.7 (11.5)	19.9 (12.9)	20.0 (6.5)	17.3 (7.4)
	60	1632 (337)	74.4 (39.1)	4.2 (3.9)	16.6 (14.3)	1.2 (1.0)
	75	1662 (137)	92.1 (10.2)	1.1 (1.8)	2.1 (1.8)	0.1 (0.0)

Table 5.3a. Influence of humidity on the aerosolisation performance of salbutamol sulphate, TAA and DSCG. Where stage 2 represents a MMAD <6.4µm.*

It was considered that the most relevant descriptors for drug aerosolisation were the percentage delivered dose (total dose emitted from the DPI as a percentage of the loaded dose) and the fine particle fraction (stage 2 of the TSI, <6.4 µm) of the loaded dose (FPF_{LD}). It is important to note, however, that the fine particle fraction is commonly determined as the dose collected from stage 2 as a percentage of the delivered dose and not of the loaded dose. However, in cases where large deviations in delivered dose occur (i.e.

where the delivered dose becomes very small), this standard method of determination may lead to exaggerated FPF values.

The aerosolisation of all three micronised drugs was significantly affected by variations in humidity (ANOVA, $p<0.05$), and can be seen graphically in Figure 5.3.3.

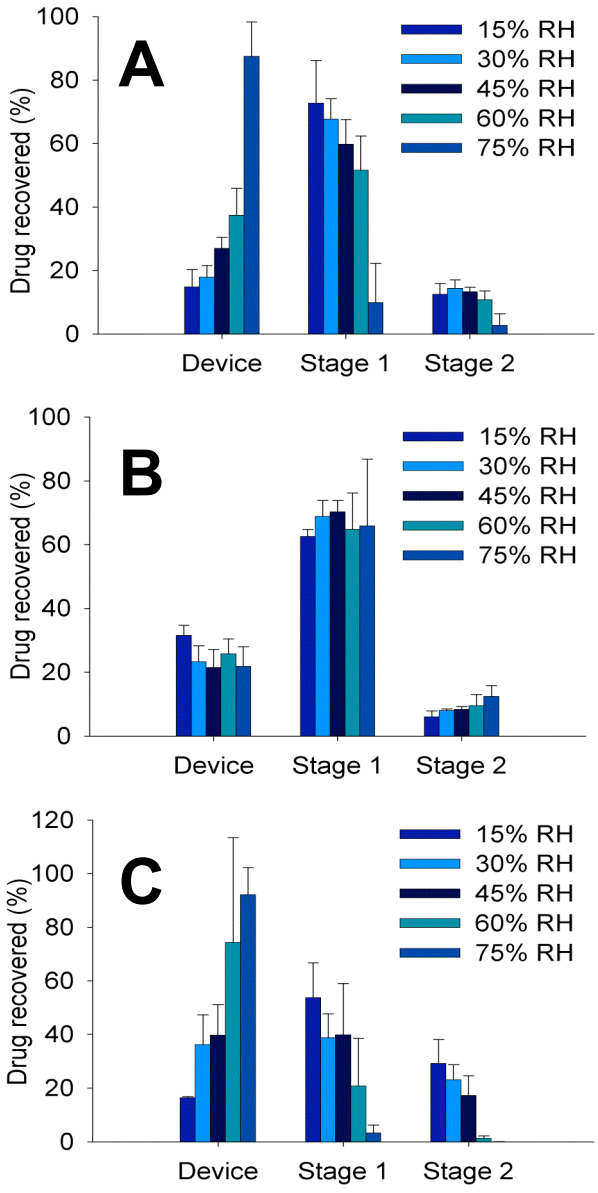

Figure 5.3.3 Drug distribution of aerosolised (a) salbutamol sulphate, (b) TAA and (c) DSCG as a function of humidity. Stage 1 includes throat and mouthpiece adaptor concentrations.

Large standard deviations in the stage recoveries of the TSI can be attributed to a non-optimised formulation containing 'as supplied' micronised drug particles only.

Increased humidity had the greatest impact on the aerosolisation efficiency of DSCG, with the mean delivered dose falling from 82% at 15% RH to 3% at 75% RH. The data in Table 5.3.1 suggest that there is a significant decrease (ANOVA, $p<0.05$) in both the delivered dose and the stage two recoveries at higher humidity levels. In order to compare the significance of this observation a Fisher pair wise analysis ($p<0.05$) was performed for stage two recoveries at paired humidities. No significant differences were observed at paired humidities 15 - 3 0, 30 - 45, and 60 - 75% RH, however, a significant difference between 45 - 60% RH and all remaining unpaired combinations was observed, suggesting a change over the whole humidity range with the greatest impact on fine particle aerosolisation (<6.4 μm) acting between the humidities 45 and 60% RH.

A plot of FPF_{LD} against humidity, presented in Figure 5.3.4 suggests a decrease in mean FPF_{LD} of DSCG, between 15 and 45% RH. This may be attributed to the relative uptake (1.6% $^{w}/_{w}$) in water across the same range (Chapter 3). It is also important to note that the FPF_{LD} of DSCG across the range 15 to 45% RH was greater than that of both salbutamol sulphate and TAA in all cases. This may be due to a higher density (1.604 $g.cm^{-3}$) and particle size (5.44 μm) of DSCG (Chapter 2), as the forces acting in a turbulent airstream to break up agglomerates will be directly related to particle mass.

An increase in humidity from 45 to 60% RH resulted in a large statistically significant decrease in FPF_{LD} to such an extent that only 1.2% (±1.0) of the loaded dose was deposited in stage two of the TSI. Again, this large decrease in aerosolisation performance could possibly be attributed to a large increase (3.7% $^{w}/_{w}$) in moisture uptake at 60% RH (Chapter 3). An increase in the humidity from 60 to 75% RH resulted in a further increase (3% $^{w}/_{w}$) in moisture sorption, of similar magnitude as for the transition from

45 to 60% RH, this was coupled with a decrease in deposition to all stages of the TSI, with 92.1% (±10.2) of the loaded dose remaining in the DPI, effectively terminating powder aerosolisation.

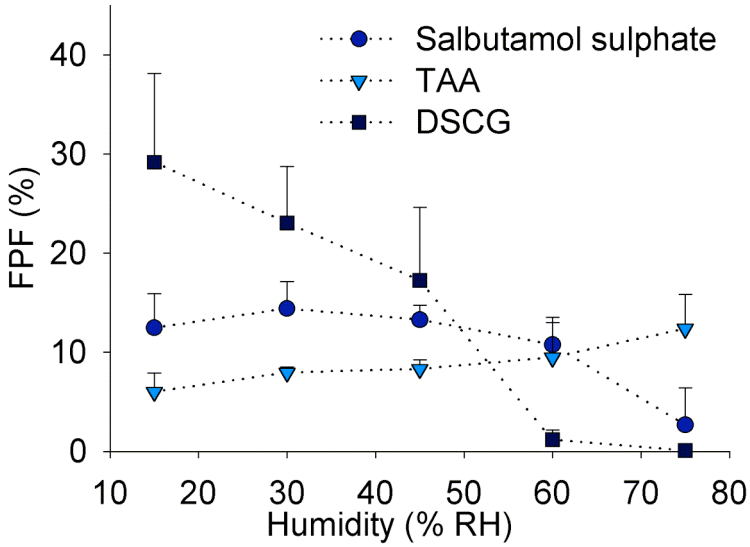

Figure 5.3.4 Influence of humidity on the fine particle fraction (MMAD < 6.4 μm) of salbutamol sulphate, TAA and DSCG. Error bars indicate standard deviations. Lines between points are for clarification purposes only.

The relationship between increased humidity and decreased aerosolisation performance of DSCG is most likely attributed to the hygroscopic nature of the powder, as water is rapidly absorbed into the crystal lattice at a specific humidity until it forms an equilibrium with the surrounding environment (Cox et al 1971). The presence of such a dynamic equilibrium can only promote the condensation of water between the capillaries of the powder particulates, thus increasing the interparticulate forces whilst decreasing the aerosolisation efficiency.

A significant decrease in the aerosolisation efficiency of salbutamol sulphate at higher humidities was also observed (ANOVA, $p<0.05$), However, Fisher pair wise analysis ($p<0.05$) of both the delivered and stage two deposition showed this to be significant between 60 and 75% RH only. Moisture sorption profiles (Chapter 3), of the salbutamol sulphate showed little increase in

water across the range 15 to 75% RH with a total water content of 0.2% $^{w}/_{w}$, at 75% RH in comparison to 15.8% $^{w}/_{w}$ (±0.4) moisture for the DSCG over the same range. These observations suggest that water is being appreciably adsorbed onto the crystal surface of salbutamol sulphate making the rapid condensation of water between capillaries only likely when the humidity approaches saturation (Schubert 1984).

The FPF_{LD} of TAA collected at each humidity shown in Figure 5.3.4. In contrast to DSCG and salbutamol sulphate, TAA exhibited a small but statistically significant (ANOVA, $p<0.05$) increase in FPF across the humidity range 15 to 75% RH. Statistical analysis of the mean percentage delivered dose showed no significant difference across the humidity range, therefore, suggesting that the variation in aerosolisation efficiency was related to particle-particle interactions. The improved aerosolisation efficiency of TAA at higher humidities may be attributed to the dissipation of triboelectrification induced surface charges. Such charges may be a consequence of the irregular plate-like structure of TAA (Chapter 2), facilitating increased particle-particle contact area. A 1% $^{w}/_{w}$ increase in moisture content of TAA between 11 and 75% RH, would almost certainly allow the mobilisation of electrons on the particulate surfaces leading to possible charge dissipation. This possibly indicates electrostatic forces as a dominating factor between micronised TAA particulates.

5.4 GENERAL DISCUSSION AND CONCLUSIONS: IN-VITRO STUDIES.

The in-vitro investigation has shown the three micronised drug materials to have significantly different aerosolisation profiles when exposed to, and aerosolised in different environmental humidities. The relationship between humidity and aerosolisation of micronised material can be attributed to the balance of forces acting between the individual particulates, the proportion of each being related to the physical and chemical properties of the material.

In general terms, the fine particle fraction profiles for salbutamol sulphate TAA and DSCG correlated well with the particle-particle 'cohesion' separation energy measurements conducted by AFM (Chapter 4). For example, an increase in humidity resulted in a decreased fine FPF_{LD} for salbutamol sulphate and DSCG. While in comparison; the AFM separation values increased suggesting increased cohesion between micronised particles at higher humidity. Furthermore, the small but significant increase in FPF_{LD} for TAA at increased humidities correlated well with decrease in AFM measured separation energies, suggesting the micronised material to be more cohesive at low humidity.

It is important to note however, that such in-vitro measurements are dependent on a plethora of factors that would not be measurable using fundamental studies such as AFM. For example, the airflow used to disperse the micronised material is turbulent, and therefore would induce unpredictable angular velocities on the drug (resulting in frictional and angular forces), whereas AFM particle interactions were conducted perpendicular to the adhesion plane. Additionally the micronised material in the in-vitro investigation may only be partially agglomerated and will have unpredictable particle-particle and particle-device component contact areas.

Consequently, such constant variables may lead to disparities between the observed in-vitro performance and AFM measurements.

6 SUMMARY, CONCLUSIONS AND FURTHER WORK.

6.1 INTRODUCTION.

The degree to which particle-particle interactions dominate in a pharmaceutical system will be dependent on both the particulate size and the solid dosage form used. When considering DPI systems (which target delivery of <5 μm particulates to the respiratory tract), the magnitude of the adhesion or cohesion forces will be critical for both the interactive mechanism and drug liberation during aerosolisation.

Of particular interest was drug cohesion in DPI systems; as such interactions will be critical during the aerosolisation process. Three micronised drugs were chosen as models for investigation (salbutamol sulphate, TAA and DSCG), as they had similar surface area, size and were directly applicable to inhalation therapy.

One of the initial goals of the study was to develop the AFM colloid probe technique for the fundamental measurement of interactive mechanisms between micronised drug particles. Of particular interest was the influence of humidity on particle cohesion, since such a variable environmental factor can have direct influence on the balance of interparticulate forces. In addition, the AFM investigations were conducted along side a series of bulk techniques that allowed prediction of the drug cohesion profile. Finally, a series of in vitro studies were conducted to allow comparison of the AFM colloid probe investigations with aersolisation efficiency.

6.2 COMPARATIVE ANALYSIS OF THE THREE MICRONISED DRUGS.

Atomic force microscopy studies of three micronised drugs indicated significant differences in the cohesion properties, particularly with respect to humidity. In general, the cohesive force (and energy) of salbutamol sulphate and DSCG increased with respect to humidity (15-75% RH), while a decrease was observed for TAA. In order to conduct such cohesion measurements, fixed substrates were required. Three techniques were employed for the production of immobilised drug substrates: polymer mounting, direct compression and crystallisation. As expected, the drug substrates had very different physical characteristics and thus allowed some insight into the influence of roughness on separation energy distributions. It is important to note however, the rank consistency in cohesion profile with respect to relative humidity, remained consistent.

Normalised data for all the cohesion separation measurements (conducted by AFM) plotted with the aerosolisation efficiency (FPF_{LD}, determined from in vitro investigation) are shown in Figure 6.2.1. In general, the increase or decrease in cohesion separation energy as a function of relative humidity, between the different substrates showed good correlation. However, significant differences did exist (ANOVA $p<0.05$). For example, in all cases the compacted surfaces had a greater impact on separation energy at higher humidities (60-75% RH) than the re-crystallised substrates. This may be attributed to the variation in surface roughness of each substrate. For example, compact and individual polymer mounted particulates had irregular surface morphologies, which would promote condensation of water at higher humidities. Subsequently, capillary forces and or electrostatic dissipation would be more likely to occur for irregular surfaces.

Another issue to consider is the variation in crystal structure. The compacted surfaces and individual polymer mounted drug particles will have, to some extent, a random orientation of molecules present on the surface due to the micronisation process. Although comminution or compressive forces will cause fractures along specific planes of a crystal, it is still envisaged that there would be a significant number of randomly oriented molecules present. Indeed, it has been well documented that micronisation can induce large quantities of amorphous material in such systems (Ward and Schultz 1995). However, analysis of the water sorption isotherms of each micronised drug indicated no characteristic mass loss that would indicate such amorphous nature. This observation may be attributed to the storage history of the materials used (approximately 40-60% RH for a two years prior to study). However, it is important to note that techniques such as DVS are limited to around 1% amorphous content determination, and therefore amorphous content in such systems cannot be ruled out.

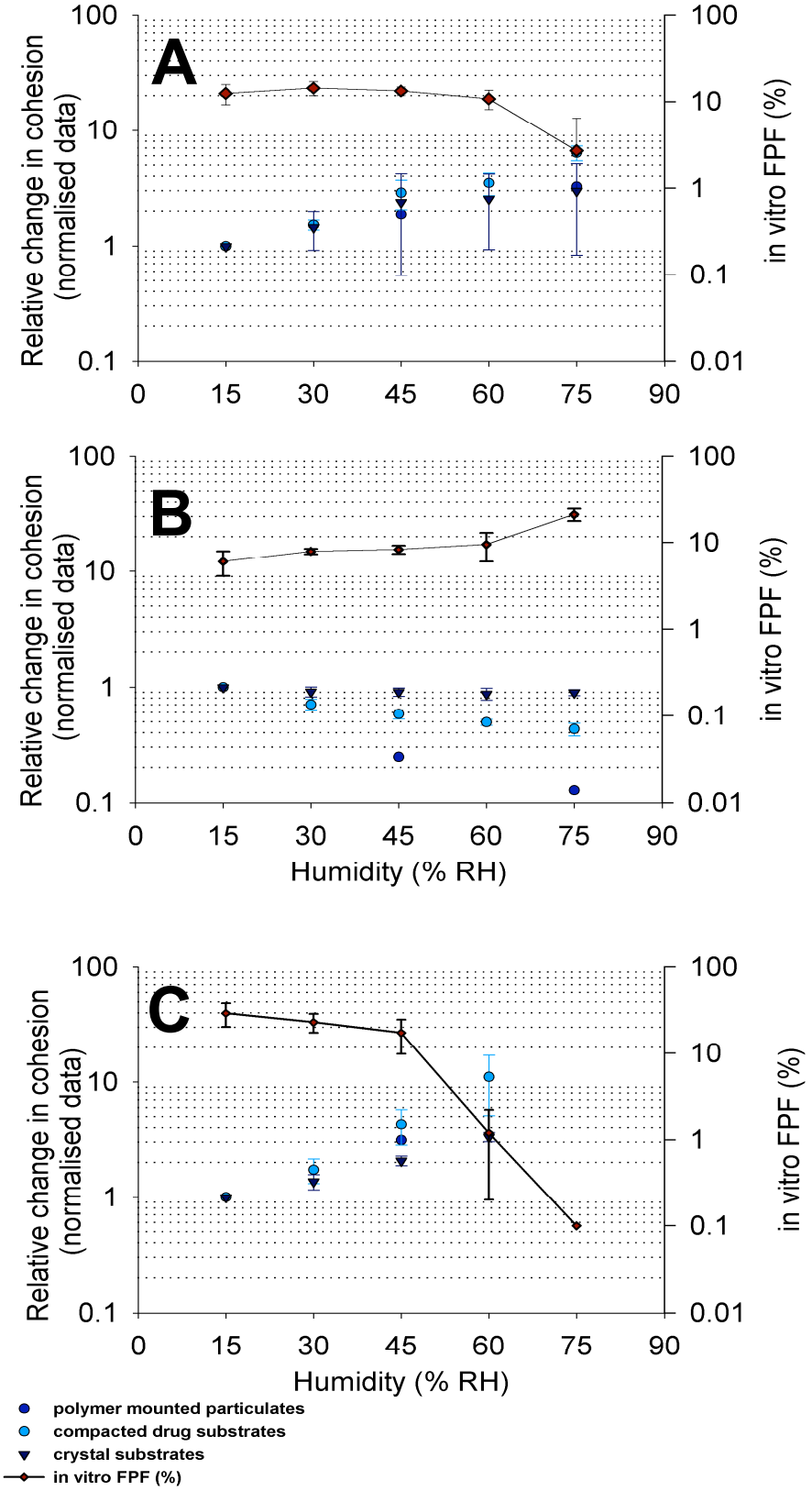

Figure 6.2.1 Normalised AFM colloid probe data plotted with in vitro aerosolisation efficiency for (a) salbutamol sulphate, (b) TAA and (c) DSCG.

Essentially, the chemical structure of a specific drug will underpin the cohesion properties of a DPI system, and when combined with knowledge of the crystal structure, may provide a means of explaining why such large variations in cohesion profile exist between similarly sized drug particulates.

For example, consider the chemical structure of the model drugs investigated here (Figure 2.1.1). Salbutamol sulphate contains two salbutamol groups for each sulphate group and thus forms a relatively neutral charged system. In comparison, the chemical structure for TAA will result in a polar distribution across the molecule (Figure 6.2.2), with the ketone group on the first ring being particularly susceptible to protonation.

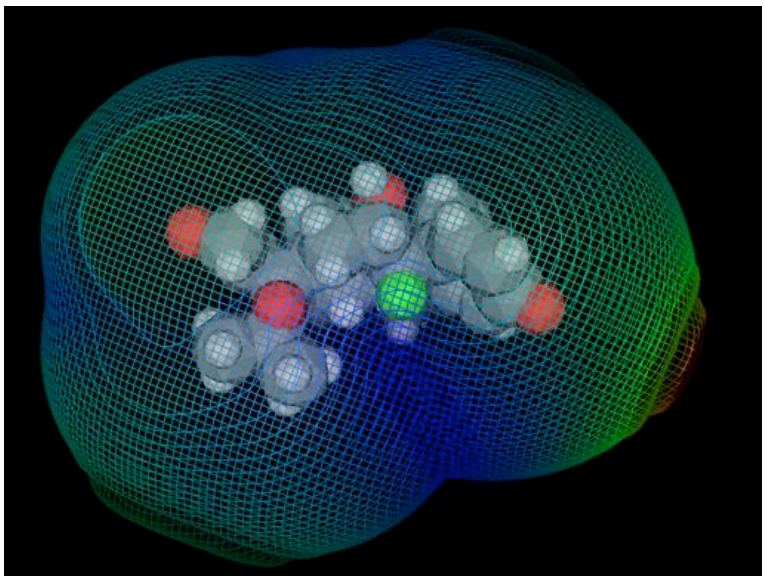

Figure 6.2.2 computer simulation of the electrostatic potential across a TAA molecule. Where red, green and red areas correspond to negative, neutral and positive polarities.

Although the crystal structure of TAA has not been documented, it would be reasonable to assume the molecule would align, in a linear fashion, to minimise such polarity. Subsequently it is envisaged that a polarity would exist across the crystalline material.

If this were the case, it may explain the long-range electrostatic forces and subsequent high cohesion at low humidity (as observed by AFM). Furthermore, the presence of such groups on the surface of the micronised material may explain both the relatively high moisture sorption values. For example, if polar groups were present across the TAA crystal surface, water molecules present in the gas phase would align on the surface due to their respective dipoles. Consequently the projected surface area for the water molecule would decrease, allowing greater sights at equivalent humidity. In addition, the assumption of such polar interactions may explain the increased basic contribution to surface free energy measured by IGC (in comparison to salbutamol sulphate).

There is no doubt that DSCG is a polar molecule, however, long-range electrostatic forces were not observed. Again such observations were expected. As previously discussed, DSCG is an interstitial solid held together by water molecules. Even at relatively low humidities (15% RH), a large percentage of water molecules will still be present, thus making the build up of charge unlikely (due to dissipation).

Clearly, the relationship between such physico-chemical properties and the aerosolisation behaviour of micronised drugs warrants further study. The computation of both chemical and crystal structure information would provide invaluable when combined with fundamental measurements as conducted here.

However, of primary interest here was the prediction of aersolisation performance through direct and fundamental measurement. Indeed, by comparison of the normalised AFM separation energy data with the in vitro FPF_{LD} a clear correlation can be observed (Figure 6.2.1). Effectively, the FPF_{LD} mirrors the separation energy values as a function of humidity. This is to be expected, as increased separation energy would result in increased cohesion forces during aeroslisation, and thus reduced performance.

6.3 SUMMARY.

Variations in the cohesion properties of micronised drugs may be attributed to the balance of interparticulate forces that exist within the respective systems. Clearly, such a balance will be dependent upon a multitude of factors including, chemistry, crystal structure and surface morphology. For dry powder inhalation systems the balance of such forces are critical as particulates of micron size (<5 μm) must be aerosolised and delivered to the respiratory tract. Subsequently, the understanding and measurement of such interactions is of great interest.

Although such studies can be undertaken using conventional in vitro techniques, they often prove time consuming. In comparison the AFM, if used in the early stages of development, may provide as an invaluable tool for the rapid screening of formulation components.

6.4 RECOMMENDED FURTHER WORK.

Although the techniques used within this study have proven useful in predicting the aerosolisation behaviour of micronised drug particulates, many avenues of investigation could be the subject of further work.

It has been shown that the controlled crystallisation of model substrates is a useful technique for determining fundamental separation energy measurements. The natural progression of this methodology would be to model the specific groups present on the surface and apply this knowledge to particle-particle adhesion. Furthermore, knowledge of the drug probe geometry and surface chemistry would prove invaluable when modelling adhesion forces. This could be achieved by controlled crystallisation of the drug probes, or the application of novel characterisation techniques to existing micronised drug probes.

Finally, it would be interesting to apply such techniques to the entire DPI system. Investigation into the physico-mechanical and physico-chemical properties of device components, carrier systems and ternary agents would provide invaluable information that may predict the performance and stability of DPI systems.

APPENDICES FOR CHAPTER 1.

A 1.1 Determination of Salbutamol Sulphate Adhesion on Model Surfaces Using the Centrifugal Particle Detachment (CPD) Method*.

Introduction

The centrifugal particle detachment method (CPD) was assessed as a possible tool for the determination of individual particle interactions. A standardised method, developed by Clarke et al (2002), was utilized to deposit uniform quantities of drug, of a specific size range, onto model substrates prior to study. In this case, the resolution of the technique was determined by the quantity of remaining drug on the substrates post centrifugation.

Materials and Methods.

The CPD method, developed by Clarke et al (2002) was utilized for the determination of drug detachment forces. A brief overview of the methodology is given below.

Samples of salbutamol sulphate (approximately 5 mg) were aerosolised from a DPI (Spiros, Dura Pharmaceuticals, California, USA) into an Anderson cascade impactor (ACI, Apparatus 2, British Pharmacopoeia) at 28.3 $L.min^{-1}$ flow rate. Samples were collected from stage 2 (particle size range 4.7 - 5.8 μm), on aluminium discs (that had been placed around the rim of the upturned stage plate, as to maintain an equivalent plate to jet distance).

* Work conducted during an invitation to the School of Pharmacy (2000), Virginia Commonwealth University, Richmond, USA).

The aluminium sample disks, containing drug deposits, were placed in a centrifuge tube assembly, with the drug-substrate surface facing the direction of angular velocity. The ultracentrifuge used throughout was a Fullerton L8-60M (Fullerton, California, USA), with a swinging basket rotor (SW 41 Ti Fullerton, California, USA). This allowed the centrifugal force to act at right angles to the substrate, and thus eliminated frictional considerations.

The aluminium discs, containing drug deposits, were exposed to rotational speeds of 10,000, 20,000 30,000, 35,000 and 40,000 rev.min^{-1}. Considering a substrate-pivot radius of 0.0674 m the relative centrifugal force (RCF) can be calculated (Equation A.1).

$$RCF = \frac{\omega^2 r_{cent}}{g}$$ *Equation A1.1 RCF calculation.*

Where ω is the angular velocity (rads.s^{-1}), r the radius (m) and g gravity. This gave relative accelerations of 7542 to 120673 X g.

After centrifugation at a specific velocity, the substrate discs and sample chamber were washed into separate volumetrics with HPLC mobile phase (0.1% ammonium acetate solution in 30:70 $^{v}/_{v}$ methanol water). Samples were analysed by HPLC using the following parameters: ODS C-18 spherisorb column (Alltech Associates, Illinois, USA), flow rate - 0.8 ml.min^{-1}, RF 551 Flouresence detector (Shimadzu Corp., Japan), excitation and emission wavelengths 276 nm and 609 nm, respectively.

Results and Discussion.

Salbutamol sulphate, aerosolised using the Spiros DPI, formed discrete deposits on the aluminium sample discs (between 8 and 10 deposits per disc). Analysis of the total recovered drug (substrate disc plus sample chamber) indicated a mean deposit mass of 1490.4 ng ± 258.6 ng across all experiments and centrifuge velocities. In addition, ANOVA one way and

Fisher pair wise analysis indicated no significant difference ($p<0.05$) between the deposits used at different centrifuge velocities.

Analysis of the percentage drug remaining on the aluminium substrates was calculated as a function of the total recovered drug concentration. and is shown graphically in Figure A.1.

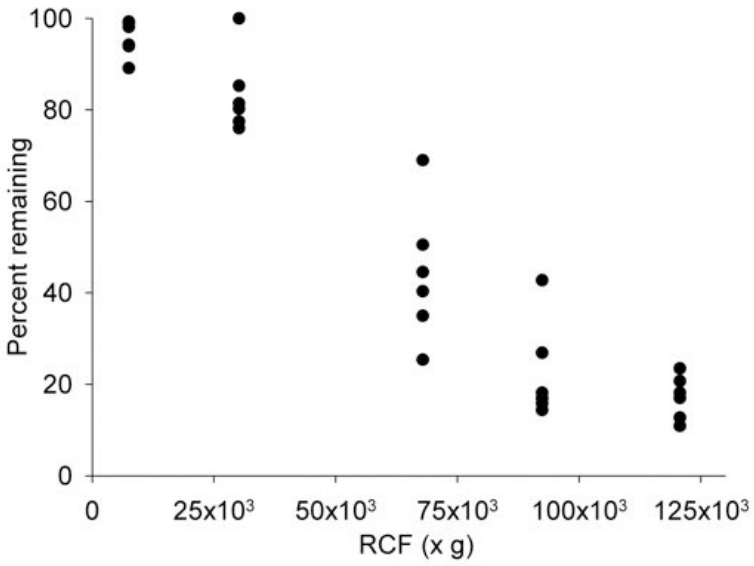

Figure A 1. Percentage drug remaining on aluminium substrate as a function of relative centrifugal acceleration.

At a maximum centrifugal acceleration of 120673 g (40,000 rev.min^{-1}), 17.2% ± 4.7% of the drug remained on the aluminium substrate. Subsequent observation of the substrate indicated this to be a layer of micronised particles, with the majority of particles being removed as a mound. It is therefore purposed (in this case), the drug cohesion forces to be weaker than the drug-substrate forces.

Since, the measurement of cohesion forces would prove difficult using the CPD method (a primary goal of this research) it was consequently decided not to pursue the technique.

A 1.2 Determination of Salbutamol Sulphate Adhesion Using the Re-Entrainment Tube Method.

Materials and Methods.

Figure A 1.2 shows a schematic of the custom-built entrainment apparatus, consisting of a 0.005 m x 0.005 m square glass duct 1.5 m in length. A sample test section was positioned 1 m downstream from the air inlet duct, and consisted of a removable substrate holder and viewing screen, that when positioned, were flush with the duct as not to affect flow. In addition, a calibrated glass flow meter (0-200 $L.min^{-1}$) was used to measure the airflow, generated by two rotary vein pumps (connected in parallel to the entrainment tube). Samples of salbutamol sulphate, were deposited on either aluminium, or glass substrates by sieving through a 45 μm aperture sieve (found to remove large agglomerates).

Drug particle removal was recorded by a CCD video reflection microscope (Digital Instruments, Cambridge, UK), with a 500 X long working distance lens, connected to a PC with associated software (Optimas 5.2, Media Cybernetics, Rochester, New York, USA).

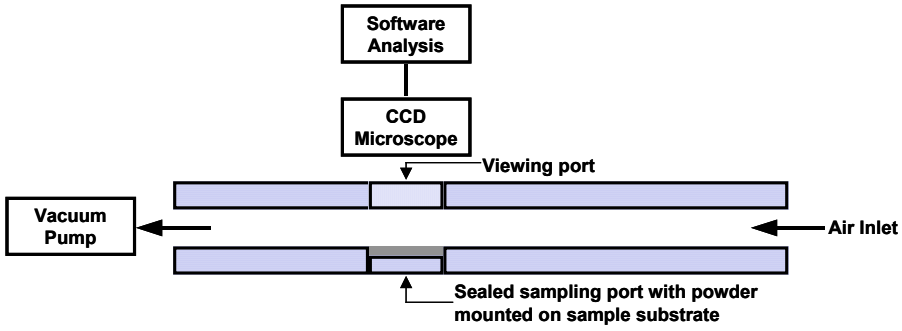

A 1.2(I) Entrainment tube schematic.

Results and Discussion.

Using two pumps in parallel, linear flow velocities of up to 133 $m.s^{-1}$ could be achieved (calculated from Bernoullis theorem; V = Q/A, where V is velocity, Q is flow rate and A the duct cross sectional area).

In general, only agglomerated material was removed (>10 μm). Such an observation was expected as the relative linear acceleration acting on the individual particles resulted in an applied force less than the force of adhesion (three orders of magnitude). However, it is interesting to note, many small agglomerates (with diameters that would result in removal forces less than the adhesion force (~$1x10^{-3}$ m)) were removed.

An explanation for the removal of small agglomerates is most likely due to a series of factors. For example, the agglomerates will have a relatively small particulate substrate contact area and therefore low adhesion force. In addition, at relatively high flow rates, the turbulence produced would result in a complicated and difficult array of forces. Turbulence can be described by the dimensionless Reynolds number (Equation A 1.2).

$$\mathrm{Re} = \frac{\rho \bar{u} h_c}{\mu}$$

Equation A 1.2 Reynolds number.

Where h_c is the channel diameter, ρ the gas density, and μ the gas viscosity By plotting the Reynolds number against flow rate, the degree of turbulence can be assessed.

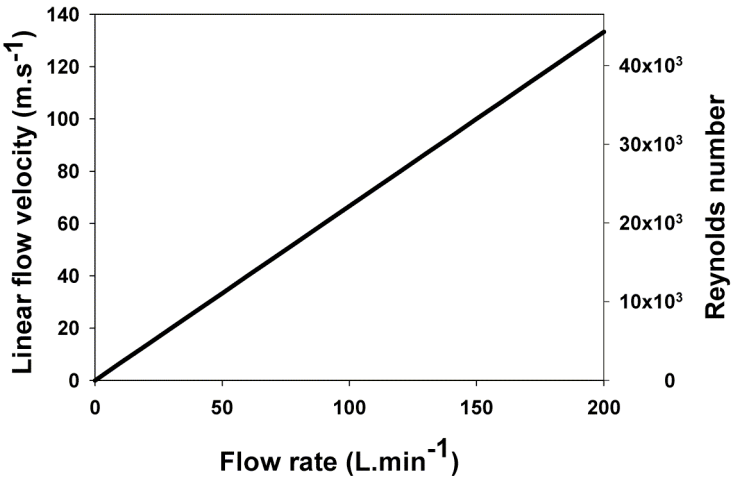

A 1.2(II) influence of flow rate and velocity on Reynolds number (for a air duct with 0.005 m diameter).

For airflow through pipes, a Reynolds number less than 2000 is considered laminar, while a Reynolds number greater than 4000 is considered turbulent (Hinds 1999). Thus, for an entrainment tube with a diameter of 0.005 m a flow velocity greater than approximately 13 $m.s^{-1}$ (20 $L.min^{-1}$) would result in turbulent flow.

Since a turbulent flow would result in many angular forces acting on adhered particles, the fundamental measurement of removal forces would be difficult. Furthermore, as the majority of micronised particles were not removed at the maximum flow rate it was consequently decided not to pursue the technique.

APPENDICES FOR CHAPTER 2.

A 2.1 Optimum De-aggregation Time for Particle Size Measurement.

Approximately 100 mg of powder was suspended in a 0.1% w/w lecithin cyclohexane solution and measured for mode diameter (μm) (Malvern Mastersizer X, Malvern Instruments, Worcs, UK) using a small volume sample dispersion cell (MSX1, Malvern Instruments, Worcs, UK). Samples were ultra-sonicated (FS 300B ultra-sonicator, Decon Laboratories Ltd, Sussex, UK) for cumulative periods between measurements. All measurements were determined in triplicate.

Time (Seconds)	Salbutamol sulphate	TAA	DSCG
0	24.3 ± 14.33	6.6 ± 0.50	2.4 ± 0.34
20	5.3 ± 0.03	3.8 ± 0.01	1.7 ± 0.05
40	4.7 ± 0.16	3.4 ± 0.03	1.5 ± 0.01
60	4.4 ± 0.11	3.4 ± 0.02	1.5 ± 0.04
80	4.2 ± 0.07	3.2 ± 0.03	1.5 ± 0.02
100	4.0 ± 0.04	3.2 ± 0.07	1.4 ± 0.03
120	3.8 ± 0.05	3.1 ± 0.08	1.4 ± 0.01
180	3.6 ± 0.07	3.1 ± 0.02	1.4 ± 0.05
240	3.5 ± 0.06	2.9 ± 0.05	1.4 ± 0.01
300	3.1 ± 0.07	2.7 ± 0.03	1.4 ± 0.10
600	2.8 ± 0.17	2.5 ± 0.13	1.4 ± 0.02
1200	2.9 ± 0.04	2.5 ± 0.03	1.4 ± 0.02

A 2.1 (I) Influence of sonication time on particulate mode diameter (μm), at 25°C.

An ultra-sonication time of 5 minutes was determined sufficient to de-agglomerate the micronised drugs prior to particulate distribution analysis.

A 2.2 Particle Size Distributions for the Micronised Drugs.

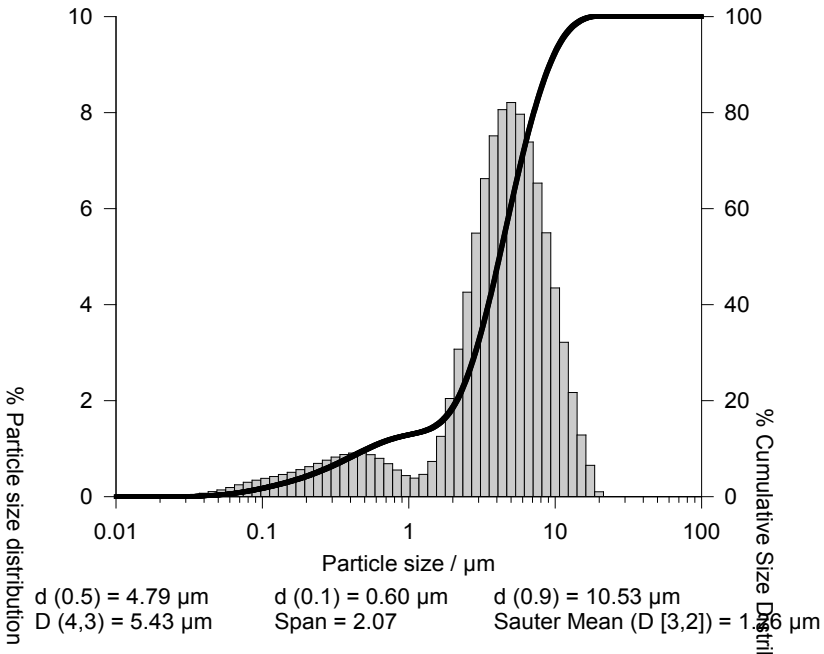

A 2.2 (I) Particle size distribution for salbutamol sulphate.

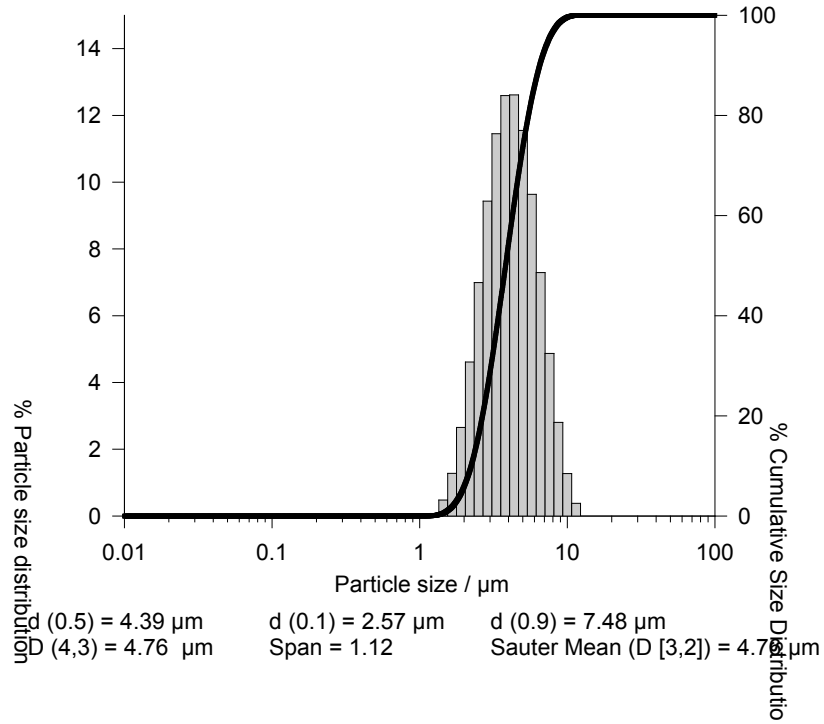

A 2.2 (II) Particle size distribution for TAA.

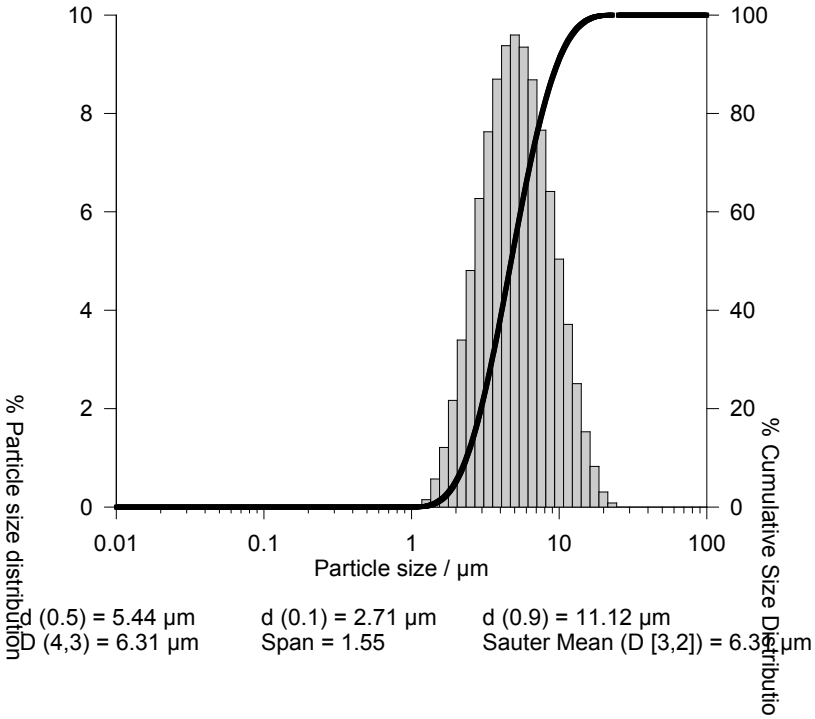

A 2.2 (III) Particle size distribution for DSCG.

APPENDICES FOR CHAPTER 3.

A 3.1 Salts for the Control of Relative Humidity.

Static relative humidities were maintained by storing saturated salt solutions in tightly sealed containers. In addition, the desiccant, phosphorous pentoxide was used to produce a humidity free environment. A summary of the saturated salts used is given in table A 3.1(I).

Saturated salt solution.	**Percent relative humidity (% RH).**
Phosphorous pentoxide.	0
Lithium chloride.	11
Calcium chloride.	29
Potassium carbonate.	43
Sodium permanganate.	63
Sodium chloride.	75
Potassium chloride.	84

A 3.1(I) Salts used for the preparation of relative humidities. Taken from Richarson and Malthus (1955).

A 3.2 Karl Fischer Equilibrium Moisture Content Determination for the Three Micronised Materials after Storage at Various Humidities.

	Equilibrium moisture content (% w/w)		
Humidity (% RH)	Salbutamol - sulphate	TAA	DSCG
0	0.11 ± 0.01	0.63 ± 0.06	3.17 ± 0.55
11	0.12 ±0.01	0.93 ± 0.06	7.40 ± 0.17
29	0.16 ± 0.01	1.33 ± 0.06	7.90 ± 0.10
43	0.16 ± 0.01	1.50 ± 0.00	9.13 ± 0.12
62	0.16 ± 0.02	1.70 ± 0.00	12.83 ± 0.06
75	0.18 ± 0.01	1.87 ± 0.06	15.80 ± 0.36
84	0.19 ± 0.03	1.97 ± 0.06	17.17 ± 0.31

A 3.2(I) Equilibrium moisture content for salbutamol sulphate, TAA and DSCG measured by Karl Fischer water titration. (Mean ± standard deviation).

APPENDICES FOR CHAPTER 4.

A 4.1 Validation of AFM Drug Probe Force Curve Parameters.

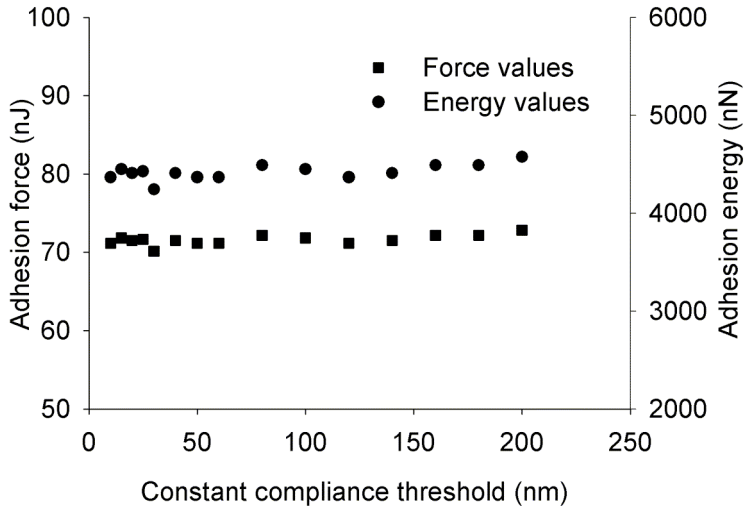

A 4.1 (I) Influence of compressive loading (constant compliance region) on the separation force and energy to separate a salbutamol sulphate drug probe from a mica surface.

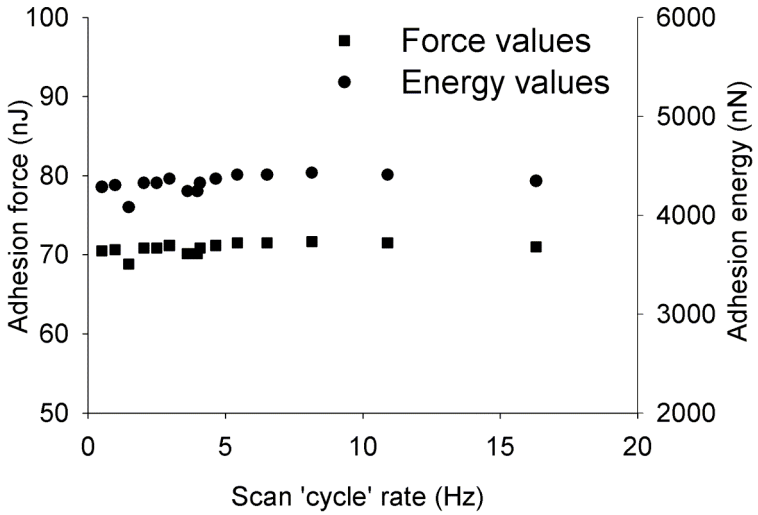

A 4.1 (II) Influence of scan rate (cycle time) on the separation force and energy to separate a salbutamol sulphate drug probe from a mica surface.

Drug	Humidity (% RH)	Mean	StDev	Medien ($f_{0.5}$)	10th Percentile ($f_{0.1}$)	90th Percentile ($f_{0.9}$)	GSD	Skewness
Salbutamol sulphate	15	39.941	24.155	32.887	14.198	76.174	1.924	0.748
	45	54.795	28.144	48.531	25.767	91.405	1.638	1.021
	75	65.731	30.910	58.747	31.417	109.853	1.629	0.725
TAA	15	65.088	21.421	61.154	37.923	100.818	1.451	1.100
	45	36.491	18.297	30.599	12.821	73.027	1.961	0.756
	75	27.339	19.871	19.903	6.090	65.045	2.516	1.066
DSCG	15	66.292	45.269	55.041	25.749	117.656	1.808	1.604
	45	116.491	60.086	98.431	43.662	221.901	1.884	0.221
	75*	-	-	-	-	-	-	-

Appendix 4.2 *Separation force (nN) for interaction between an individual SS, TAA an DSCG drug probes and 5 corresponding micronised drug particles (n=30). * DSCG drug probe was 'lost' during measurements at 75 %RH.*

Drug	Humidity (% RH)	Mean	StDev	Medien ($e_{0.5}$)	10th Percentile ($e_{0.1}$)	90th Percentile ($e_{0.9}$)	GSD	Skewness
Salbutamol sulphate	15	1605.49	1838.02	853.0	108.8	4023.6	3.330	2.124
	45	2376.04	2213.17	1603.9	495.3	5193.9	2.500	1.613
	75	4342.79	3693.94	2786.5	736.3	10545.3	2.820	0.877
TAA	15	2935.63	2155.23	2308.9	935.3	5699.8	2.022	1.781
	45	909.82	719.88	571.5	122.3	2670.4	3.322	1.010
	75	675.59	804.45	295.9	36.3	2410.2	5.127	1.929
DSCG	15	5270.94	7389.25	2632.4	598.7	11575.6	3.171	2.455
	45	14492.10	13978.80	8271.7	1688	40530.1	3.450	1.803
	75*	-	-	-	-	-	-	-

Appendix 4.3 *Separation energy (nJ) for interaction between an individual drug probes and 5 corresponding micronised drug particles (n=30). * DSCG drug probe was 'lost' during measurements at 75 %RH.*

Tip id.	Humidity (% RH)	$e_{0.1}$	$e_{0.5}$	$e_{0.9}$	GSD	$^{*}R^2$	$^{**}R^2$
Tip 01	15	725	2154	6399	2.34	0.982	0.997
	30	1124	3065	8356	2.19	0.967	0.999
	45	1361	3651	9793	2.16	0.941	0.998
	60	1879	4990	13253	2.14	0.960	0.997
	75	424	11188	29507	2.13	0.952	0.998
Tip 02	15	520	1628	5099	2.43	0.962	0.994
	30	729	2325	7419	2.47	0.961	0.973
	45	1973	5262	14035	2.15	0.950	0.980
	60	2334	5981	15328	2.08	0.950	0.997
	75	5269	12726	30733	1.99	0.915	0.994
Tip 03	15	355	2091	12321	3.98	0.873	0.976
	30	795	3451	14984	3.14	0.945	0.977
	45	2013	7067	24806	2.66	0.940	0.972
	60	2139	8294	32167	2.88	0.927	0.980
	75	2898	12779	56356	3.18	0.865	0.975
Tip 04	15	743	2023	5507	2.18	0.957	0.993
	30	793	2837	10150	2.70	0.951	0.992
	45	1604	7465	34753	3.31	0.989	0.998
	60	1987	8742	38470	3.17	0.980	0.997
	75	2688	12663	59655	3.35	0.952	0.996
Tip 05	15	626	2112	7127	2.58	0.983	0.989
	30	1027	3662	13061	2.69	0.986	0.993
	45	1306	5011	19224	2.85	0.938	0.981
	60	1241	6756	36783	3.74	0.899	0.942
	75	3179	13803	59936	3.14	0.947	0.965

Appendix 4.4 *Separation energy values (nJ) (obtained from log-normal fit) for salbutamol sulphate drug probes on salbutamol sulphate model compact surfaces at specific humidities.* $^{*}R^2$ *indicate apparent linear regression analysis across full data set,* ** R^2 *indicate apparent linear regression analysis between 5 and 95% probabilities.*

Appendix 4.5

Influence of humidity on the cumulative separation energy values for salbutamol sulphate drug probes 2-5 on model compact salbutamol sulphate surfaces.

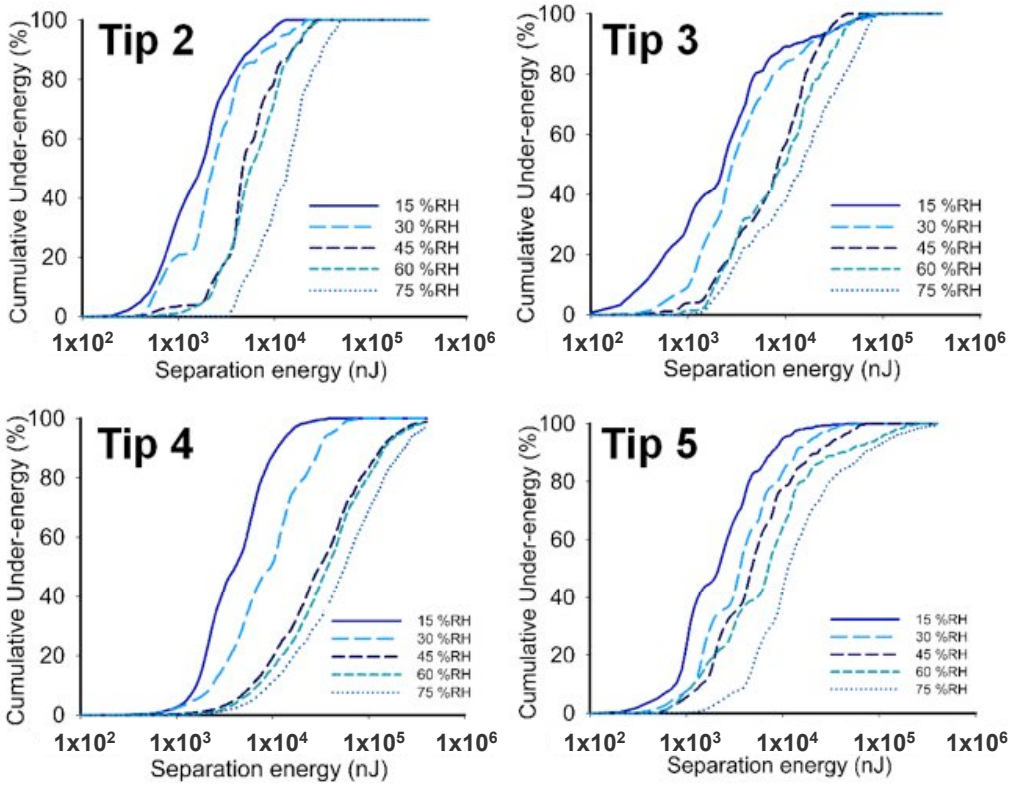

Tip id.	Humidity (% RH)	$e_{0.1}$	$e_{0.5}$	$e_{0.9}$	GSD	$^{*}R^2$	$^{**}R^2$
Tip 01	15	481	1520	4802	2.45	0.998	0.997
	30	365	1163	3702	2.50	0.980	0.998
	45	290	930	2987	2.48	0.987	0.997
	60	245	808	2672	2.54	0.992	0.998
	75	244	697	1988	2.26	0.991	0.998
Tip 02	15	560	2139	8167	2.84	0.993	0.997
	30	419	1579	5942	2.81	0.980	0.999
	45	506	1414	4928	2.65	0.978	0.998
	60	325	990	3016	2.38	0.995	0.998
	75	275	869	2743	2.45	0.993	0.998
Tip 03	15	899	3099	10685	2.62	0.996	0.993
	30	672	2374	8390	2.67	0.972	0.995
	45	492	1679	5729	2.60	0.985	0.998
	60	441	1540	5374	2.65	0.988	0.996
	75	437	1557	5539	2.69	0.990	0.998
Tip 04	15	539	1990	7353	2.77	0.993	0.994
	30	350	1135	3681	2.50	0.975	0.971
	45	347	1048	3166	2.37	0.990	0.990
	60	313	924	2727	2.32	0.961	0.963
	75	285	879	2710	2.40	0.990	0.989
Tip 05	15	235	1086	5020	3.30	0.973	0.981
	30	210	746	2652	2.69	0.995	0.996
	45	175	627	2242	2.70	0.988	0.997
	60	268	562	1879	2.56	0.986	0.998
	75	101	385	1460	2.83	0.960	0.996

Appendix 4.6 *Separation energy values (nJ) (obtained from log-normal fit) for TAA drug probes on model compact TAA surfaces at specific humidities.* $^{*}R^2$ *indicate apparent linear regression analysis across full data set,* $^{**}R^2$ *indicate apparent linear regression analysis between 5 and 95% probabilities.*

Appendix 4.7

Influence of humidity on the cumulative separation energy values for TAA drug probes 2-5 on model compact TAA surfaces.

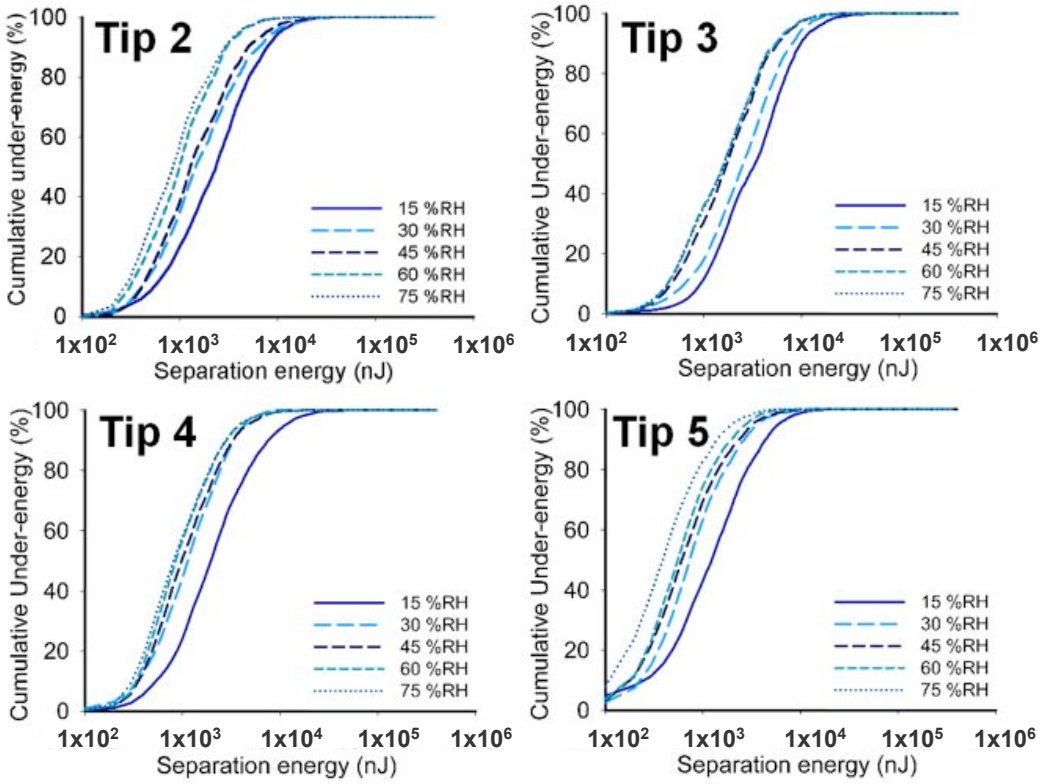

Tip id.	Humidity (% RH)	$e_{0.1}$	$e_{0.5}$	$e_{0.9}$	GSD	$^{*}R^2$	$^{**}R^2$
Tip 01	15	1052	6429	39308	4.1	0.874	0.958
	30	1550	8378	45279	3.7	0.954	0.972
	45	9392	40693	176317	3.1	0.742	0.942
	60	70461	124130	218677	1.6	0.785	0.922
	75	-	-	-	-	-	-
Tip 02	15	1826	10098	55836	3.8	0.893	0.950
	30	1579	18086	207155	6.7	0.864	0.908
	45	14639	28740	56425	1.7	0.968	0.983
	60	26230	50900	98772	1.7	0.963	0.980
	75	-	-	-		-	-
Tip 03	15	1628	15402	145756	5.8	0.703	0.861
	30	4494	24252	130886	3.7	0.881	0.981
	45	37589	80926	174229	1.8	0.935	0.970
	60	49997	169735	576235	2.6	0.872	0.875
	75	-	-	-	-	-	-
Tip 04	15	3472	16705	80380	3.4	0.883	0.973
	30	5109	40468	320556	5.0	0.938	0.962
	45	19156	63440	210092	2.5	0.841	0.910
	60	23105	95716	396521	3.0	0.700	0.786
	75	-	-	-	-	-	-
Tip 05	15	307	1477	7101	3.4	0.879	0.996
	30	407	2368	13759	3.9	0.938	0.941
	45	828	4812	27636	3.9	0.968	0.941
	60	4359	21223	103330	3.4	0.850	0.942
	75	-	-	-	-	-	-

Appendix 4.8 *Separation energy values (nJ) (obtained from log-normal fit) for DSCG drug probes on model compact DSCG surfaces at specific humidities.* $^{*}R^2$ *indicate apparent linear regression analysis across full data set,* $^{**}R^2$ *indicate apparent linear regression analysis between 5 and 95% probabilities.*

Appendix 4.9

Influence of humidity on the cumulative separation energy values for DSCG drug probes 2-5 on model compact DSCG surfaces.

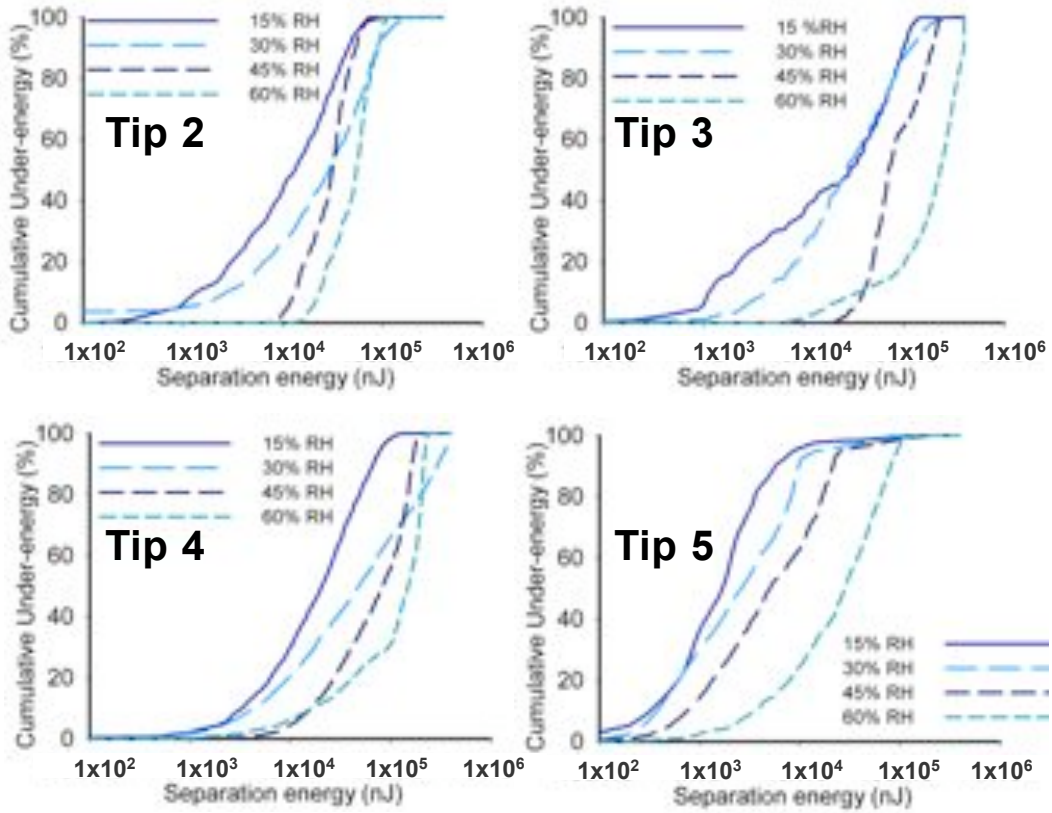

Appendix 4.10

Influence of humidity on the GSD for (a) salbutamol sulphate drug probes on model compact salbutamol sulphate surfaces (b) TAA drug probes on TAA compact model surfaces and (c) DSCG drug probes on DSCG compact model surfaces .

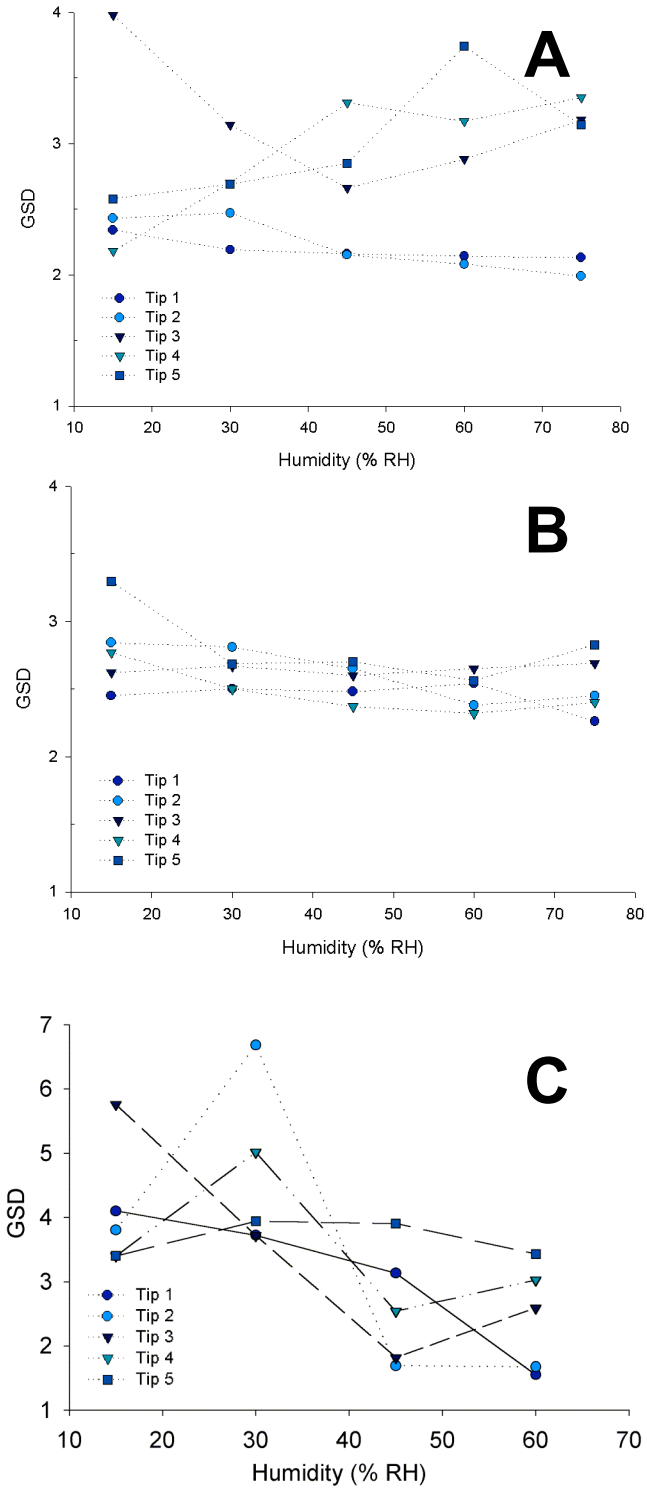

Appendix 4.11

Influence of humidity on the cumulative separation energy values for (a) salbutamol sulphate drug probes two and three interactions with re-crystallised salbutamol sulphate surfaces, (b) TAA drug probe two and three interactions with re-crystallised TAA surfaces and (c) DSCG drug probe two and three interactions with re-crystallised DSCG surfaces (taken at 15, 30, 45, 60 and 75% RH).

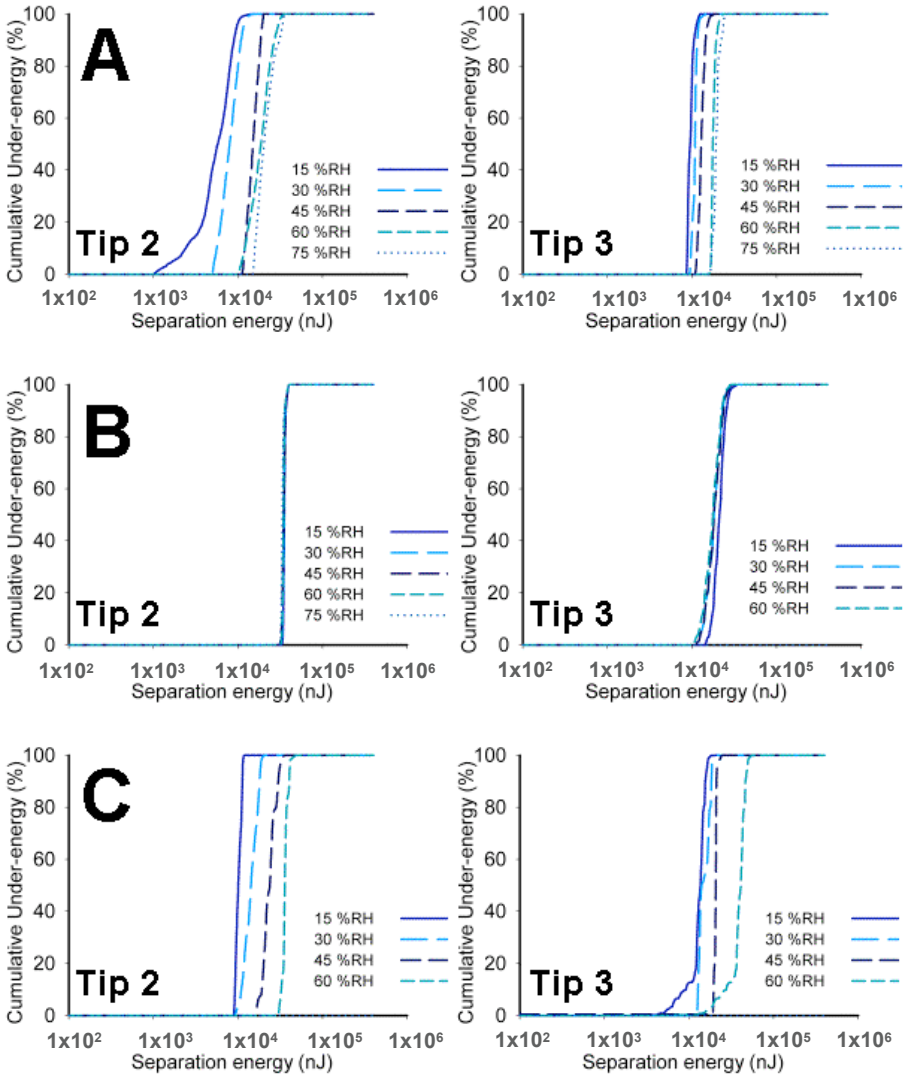

Tip id.	Humidity (% RH)	Mean (± StDev)	$e_{0.1}$	$e_{0.5}$	$e_{0.9}$	GSD	R^2
Tip 01	15	11751 ± 2262	8851	11751	14650	1.215	0.993
	30	13362 ± 2503	10154	13362	16570	1.208	0.992
	45	15594 ± 3034	11705	15594	19482	3.850	0.972
	60	16694 ± 3706	11944	16694	21443	1.253	0.983
	75	18613 ± 4130	13321	18613	23906	1.253	0.931
Tip 02	15	5863 ± 2454	2718	5863	9008	1.561	0.982
	30	8200 ± 2000	5637	8200	10764	1.282	0.960
	45	15250 ± 2380	12199	15250	18300	1.170	0.978
	60	19157 ± 5605	11974	19157	26340	1.351	0.991
	75	21721 ± 5379	14827	21720	28614	1.287	0.987
Tip 03	15	9609 ± 765	8628	9609	10590	1.083	0.902
	30	10832 ± 726	9902	10832	11762	1.069	0.912
	45	13044 ± 1195	11513	13044	14237	1.096	0.938
	60	18023 ± 1165	16531	18023	19516	1.067	0.903
	75	19579 ± 1798	17274	19579	21883	1.096	0.937

Appendix 4.12 *Separation energy values (nJ) (normal fit) for salbutamol sulphate drug probes on re-crystallised salbutamol sulphate surfaces at specific humidities. Data sets were constructed from force volume measurements conducted on the apparent dominant crystal face. Data was manually adjusted to neglect values obtained on other faces and crystal plane edges (corrected through comparison corresponding force-volume height image.*

Tip id.	Humidity (% RH)	Mean (± StDev)	$e_{0.1}$	$e_{0.5}$	$e_{0.9}$	GSD	R^2
Tip 01	15	20870 ± 659	20025	20870	20025	1.032	0.982
	30	19550 ± 715	18633	19550	18633	1.037	0.973
	45	19405 ± 611	18623	19405	18623	1.032	0.986
	60	18456 ± 544	17758	18456	17758	1.030	0.980
	75	17985 ± 593	17226	17985	17226	1.033	0.991
Tip 02	15	35502 ± 1151	34027	35502	34027	1.033	0.937
	30	35258 ± 1190	33732	35258	33732	1.034	0.945
	45	34945 ± 1490	33036	34945	33036	1.044	0.979
	60	34684 ± 1176	33176	34684	33176	1.034	0.915
	75	33809 ± 1464	31933	33809	31933	1.044	0.881
Tip 03	15	21171 ± 3269	16981	21171	16981	1.168	0.981
	30	18594 ± 3720	13827	18594	13827	1.224	0.993
	45	18527 ± 3536	13996	18527	13996	1.213	0.992
	60	17713 ± 3660	13022	17713	13022	1.233	0.993
	-	-	-	-	-	-	-

Appendix 4.13 *Separation energy values (nJ) (normal fit) for TAA drug probes on re-crystallised TAA surfaces at specific humidities. Data sets were constructed from force volume measurements conducted on the apparent dominant crystal face. Data was manually adjusted to neglect values obtained on other faces and crystal plane edges (corrected through comparison corresponding force-volume height image.*

Tip id.	Humidity (% RH)	Mean (± StDev)	$e_{0.1}$	$e_{0.5}$	$e_{0.9}$	GSD	R^2
Tip 01	15	4413 ± 602	3642	4413	5184	1.147	0.966
	30	7171 ± 1027	5855	7171	8486	1.155	0.992
	45	11067 ± 2079	8403	11067	13731	1.216	0.977
	60	15843 ± 2419	12743	15843	18943	1.166	0.917
	-	-	-	-	-	-	-
Tip 02	15	10189 ± 770	9202	10189	11175	1.079	0.918
	30	14467 ± 2636	11089	14467	17845	1.202	0.974
	45	23843 ± 4172	18497	23843	29189	1.193	0.981
	60	36204 ± 2789	32630	36204	39779	1.080	0.963
	-	-	-	-	-	-	-
Tip 03	15	13039 ± 2663	9627	13039	16452	1.230	0.881
	30	15326 ± 2263	12426	15326	18227	1.160	0.880
	45	20629 ± 1624	18547	20629	22711	1.082	0.924
	60	39118 ± 7989	28880	39118	49356	1.230	0.877
	-	-	-	-	-	-	-

Appendix 4.14 *Separation energy values (nJ) (normal fit) for DSCG drug probes on re-crystallised DSCG surfaces at specific humidities. Data sets were constructed from force volume measurements conducted on the apparent dominant crystal face. Data was manually adjusted to neglect values obtained on other faces and crystal plane edges (corrected through comparison corresponding force-volume height image.*

APPENDICES FOR CHAPTER 5.

Appendix 5.1 Sample Chromatographs of Salbutamol Sulphate, TAA and DSCG.

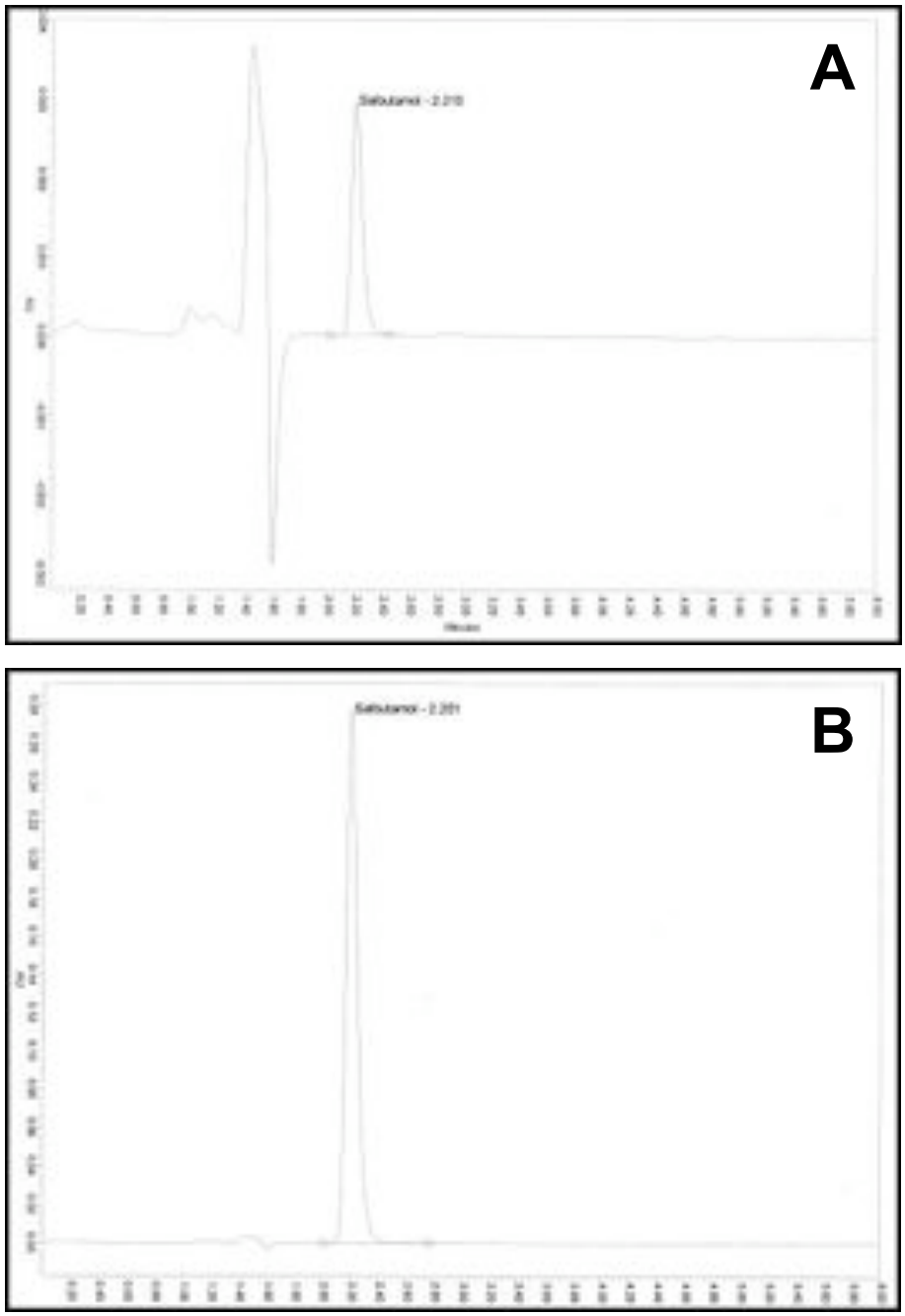

A 5.1 (I) HPLC chromatogram for salbutamol sulphate (a) low working standard and (b) high working standard.

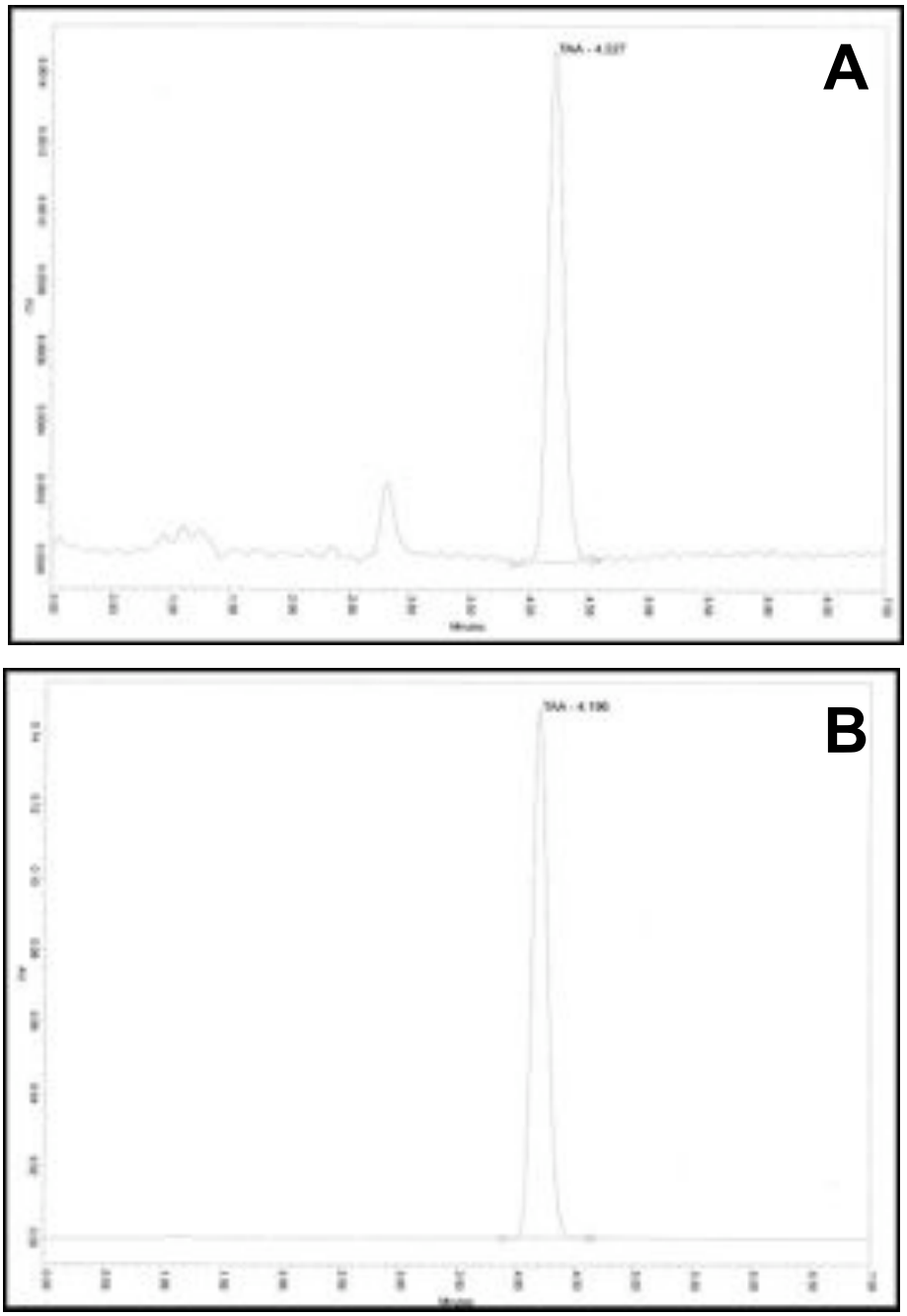

A 5.1 (II) HPLC chromatogram for TAA (a) low working standard and (b) high working standard.

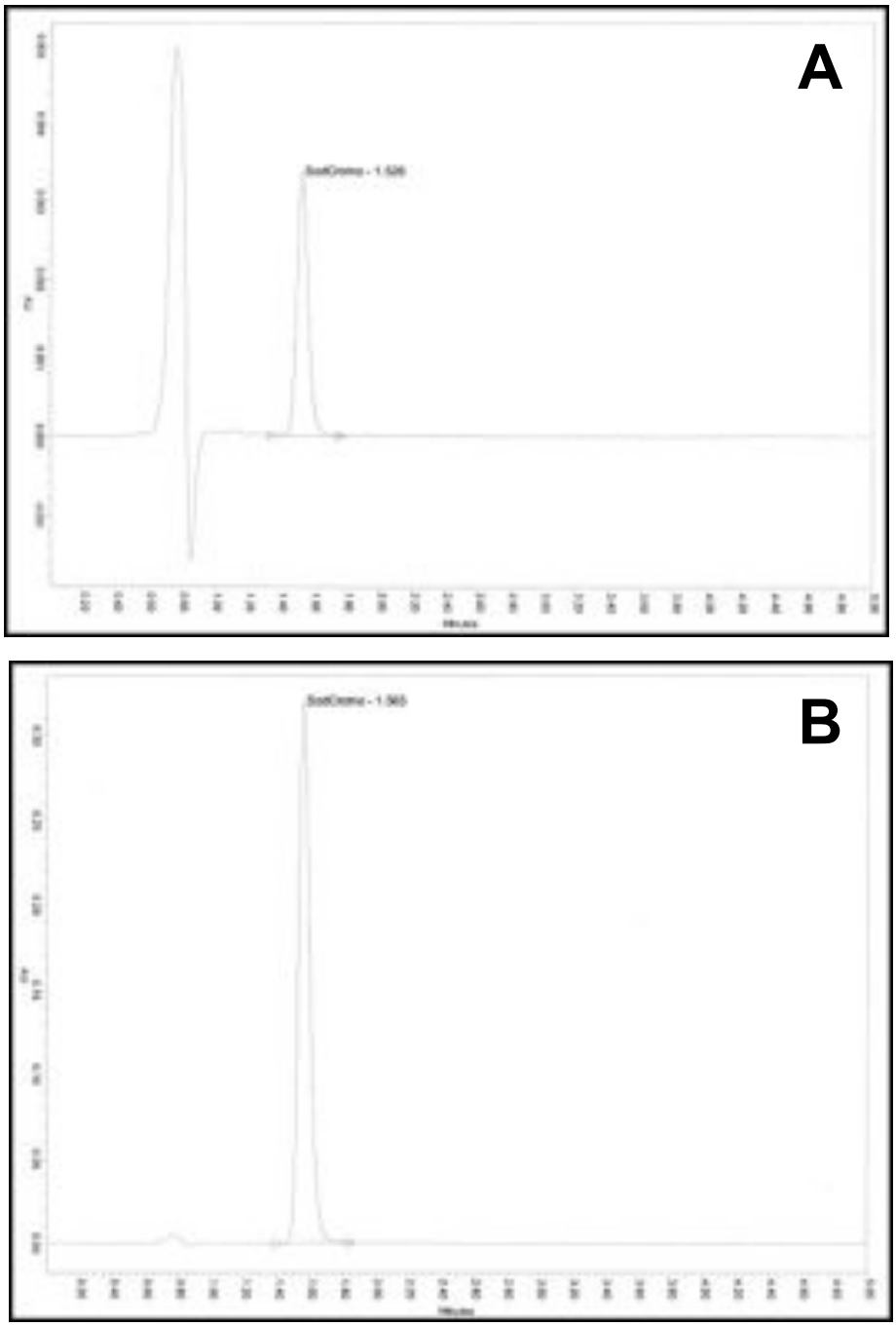

A 5.1 (III) HPLC chromatogram for DSCG (a) low working standard and (b) high working standard.

Appendix 5.2 Calculation of Bracketing Standards for HPLC.

Calculation of sample concentration in HPLC samples using the bracketing standards method.

Two stock standard solutions were prepared from separate weighings, and were subsequently diluted to give standard concentrations either side of the expected sample concentrations. Both standard and sample concentrations were prepared/diluted to fit within the validated linearity region (Chapter 5).

Samples (SAMP) were run bracketed between two standards (std) i.e.

STD1, SAMP, SAMP, STD2, SAMP, SAMP, STD1, SAMP……..

Each sample and standard was run twice and the mean peak area calculated. Sample concentration was calculated using response factors obtained from the adjoining standards.

$$C_{samp} = A_{samp} D_{samp} \overline{R_f}$$

Where C_s is sample concentration A_{samp} is sample absorbance D_{samp} dilution factor and R_f response factor

The independent response factors for each of the bracketing standards was calculated.

$$R_f = \frac{C_{std}}{A_{std}}$$

Percentage variance between R_f from bracketing standards must be less than 3%

REFERENCES.

Ahn, J-S., Choi, H-K., Chun, M-K., Ryu, J-M., Jung, J-H., Kim Y-U., Cho,C-S. (2002) Release of triamcinolone acetonide from mucoadhesive polymers composed of chitosan and poly(acrylic acid) in vitro. *Biomaterials* **23:** 1411-1416.

Akiyama, T., Tanijiri, Y. (1989) Criterion for re-entrainment of particles. *Powder Technol.* **57:** 21-26.

Anon. (2002) Data taken from internet site: http://www.Wunderground.com, which utilises the U.S National Weather Service (NWS).

Bailey, A.G. (1984) Electrostatic phenomena during powder handling. *Powder Technol.* **37:** 71-85.

Berard, V., Lesniewska, E., Andres, C., Pertuy, D., Laroche, C., Pourcelot, Y. (2002) Dry powder inhaler: influence of humidity on topology and adhesion studied by AFM. *Int. J. Pharm.* **232:** 213-224.

Biggs, S., Spinks, G. (1998) Atomic force microscopy investigation of the adhesion between a single polymer sphere and a flat surface. *J. Adh. Sci. Tech.* **12**: 461-478.

Binnig, G., Quate, C.F., Gerber, C. (1986) Atomic force microscope. *Phys. Rev. Lett.* **56:** 930-933.

Böhme, G., Krupp, H., Rabenhorst, H., Sandstede, G. (1962) Adhesion measurements involving small particles. *Trans. Inst. Chem. Engs.* **40:** 252-259.

Booth, S.W., Newton, J.M. (1987) Experimental investigation of adhesion between powders and surfaces. *Int. J. Pharm.* **39:** 679-684.

Braun, M.A., Oschmann, R., Schmidt, P.T. (1996) Influence of excipents and storage humidity on the deposition of disodium cromoglycate (DSCG) in the twin Impinger. *Int. J. Pharm.* **135**: 53-62.

Broadhead, J., Rouan, S.K.E., Rhodes, C.T. (1992) The spray drying of pharmaceuticals. *Drug Dev. Ind. Pharm.* **18:** 1169-1206.

BSI, British standard Institute (1999) Particle size analysis laser diffraction methods, Part 1: general principles. BS ISO number 13320-1:1999.

Byron, P.R., Peart, J., Staniforth, J.N. (1997) Aerosol electrostatics 1: Properties of fine powders before and after aerosolization by dry powder inhalers. *Pharm. Res.* **14:** 698-705.

Charsley, E.L., Warrington, S.B., *eds.* (1992) Thermal analysis – techniques and applications. Royal society of chemistry, Cambridge, UK.

Chen, R.L., Young, V.G., Lechuga-Ballesteros, D., Grant, D.J.W. (1999) Solid-state behaviour of cromolyn sodium hydrates. *J. Pharm. Sci.* **88:** 1191-1200.

Clarke, M.J., Peart, J., Cagnani, S., Byron, P.R. (2002) Adhesion of powders for inhalation: an evaluation of drug detachment from surfaces following deposition from aerosol streams. *Pharm. Res.* **19:** 322-329.

Clarke, M.J., Potter, U.J., Gilpin, C., Tobyn, M.J., Staniforth, J.N. (1998) Imaging of hygroscopic ultrafine pharmaceutical powders using low temperature and environmental scanning electron microscopy. *Pharm. Pharmacol. Commun.* **4:** 419-425.

Connors, K.A. (1988) The Karl Fischer titration of water. *Drug. Dev. Ind. Pharm.* **14:** 1891-1903.

Corn, M. (1961) The adhesion of small particles to surfaces II. *J. Air. Pol. Control. Assoc.* **11:** 566-584.

Corn, M., Stein, F. (1965) Re-entrainment of particles from a plane surface. *Am. Ind. Hyg. Assoc. J.* **26:** 325-336.

Cox, J.S.G., Woodard, G.D., McRone, W.C. (1971) Solid-state chemistry of cromolyn sodium (disodium cromoglycate). *J. Pharm. Sci.* **60:** 1458-1465.

Desai, T.R., Wong, J.P., Finlay, W.H. (2002) Use of capillary penetration technique to determine the surface free energy of dry powder liposome formulations. *Proc. Respiratory Drug Delivery VIII.* Davis Harwood International Publishing, Ltd. Raleigh, North Carolina, USA.

DI (Digital Instruments). Applications of force volume imaging with the NanoScope® atomic force microscope. *Application Note.* DI, Cambridge UK (web address, http://www.di.com).

Ducker, W.A., Senden, T.J., Pashley, R.M. (1991) Direct measurement of colloidal forces using an atomic force microscope. *Nature.* **253:** 239-241.

Eklund, E.A., Wayman, W.H., Brillson, L.J., Hays, D.A. (1995) Toner adhesion: The effect of neighbouring particles. *Electrostatics.* **143:** 85-92.

Eve, J.K., Patel, N., Luk, S.Y., Ebbens, S.J., Roberts, C.J. (2002) A study of single drug particle adhesion interactions using atomic force microscopy. *Int. J. Pharm*. **238:** 17-27.

Florence, A.T., Attwood, D. (1998) Physicochemical principles of pharmacy. 3rd edition, Macmillan, UK.

Florey, K. (1972) Analytical profiles of drug substances. Academic Press, London, UK.

Führer, C. (1996) In: Pharmaceutical powder compaction technology. eds. Alderborn, G., Nystrom, C. Marcel Decker Inc, New York, USA.

Gady, B., Reifenberger, R., Rimai, D.S. (1998) Contact electrification studies using atomic force microscope techniques. *J. Appl. Phys.* **84:** 319-322.

Ganderton, D. & Kassem, N.M. (1992). Advances in pharmaceutical sciences. Academic Press, London, UK.

Giles, C.H., MacEwan, T.H., Nakhwa, S.N., Smith, D. (1960) Studies in adsorption. Part XI.* A system for classification of solution adsorption isotherms, and its use in diagnosis of adsorption mechanisms and in measurement of specific surface areas of solids. *J. Chem. Soc.* 3973-3993.

Gomez, A., Bingham, D., Juan, L.d., Tang, K. (1998) Production of protein nanoparticles by electrospray drying. *J. Aerosol. Sci.* **29:** 561-574.

Good, R.J. (1992) Contact angle, wetting and adhesion: a critical review. *J. Adhesion Sci. Technol.* **6:** 1269-1302.

Guinier, A. (1994) X-ray powder diffraction: In crystals, imperfect crystals and amorphous bodies. Dover Publications, New York, USA.

Gutmann, V. (1978) The donor-acceptor approach to molecular interactions. Plenum press, London, UK .

Hallworth, G.W., Westmoreland, D.G. (1987) The twin impinger: a simple device for assessing the delivery of drugs from metered dose pressurized aerosol inhalers. *J. Pharm. Pharmacol.* **39**: 966-972.

Hartshorne, N.H., Woodard, G.D. (1973) Mesomorphism in the system disodium cromoglycate - water. *Mol. Cryst. Liquid. Cryst.* **23:** 343-368.

Heinz, W. F., Hoh, J. H. (1999) Spatially resolved force microscopy of biological surfaces using the atomic force microscope. *Tri. Biotec*. **17:** 143-150.

Hersey, J.A. (1975) Ordered mixing, a new concept in powder mixing practice. *Powder Technol.* **11:** 41-44.

Hindle, M., Makinen, G.M. (1996) Effects of humidity on the in-vitro aerosol performance and aerodynamic size distribution of cromolyn sodium for inhalation. *Eur. J. Pharm. Sci*. **4**: S142.

Hinds, W.C. (1999) Aerosol technology. John Wiley & Sons, New York, USA.

Hutter, J.L., Bechhoefer, J. (1993) Calibration of atomic-force microscope tips. *Rev. Sci. Instrum.* **64:**1868-873.

Ibrahim, T.H., Burk, T.R., Etzler, F.M., Neuman, R.D. (2000) Direct adhesion measurements of pharmaceutical particles to gelatin capsule surfaces. *J. Adhes. Sci. Technol.* **14:** 1225 –1242.

Ikegami, K., Kawashima, Y., Takeuchi, H., Yamamoto, H., Momose, D.I., Saito, N., Isshiki, N. (2000) In vitro inhalation behaviour of spherically agglomerated steroid particles with carrier lactose. *Adv. Powder. Tech.* **11:** 323-332.

Jashnani, R.N., Byron, P.R. (1996) Dry powder aerosol generation in different environments: performance comparisons of albuterol, albuterol sulphate, albuterol adipate and albuterol stearate. *Int. J. Pharm.* **130**: 13-24.

Jashnani, R.N., Byron, P.R., Dalby, R.N. (1995) Testing of dry powder aerosol formulations in different environmental conditions. *Int. J. Pharm.* **113**: 123-130.

Kontny, M.J. (1988) Distribution of water in solid pharmaceutical systems. *Drug Dev. Ind. Pharm*. **14:** 1991-2027.

Kulvanich, P., Stewart, P.J. (1988) Influence of relative humidity on the adhesive properties of a model interactive system. *J. Pharm. Pharmacol.* **40:** 453-458.

Langbein, D. (1969). Van der Waals attraction between macroscopic bodies. *J. Adhes.* **1:** 237.

Leger, P. J-M., Goursolle, M., Gadret, M. (1978) Structure cristalline du sulfate de salbutamol [*tert*-Buttylamino-2 (hydroxy-4 hydroxyméthyl-3 phényl)-1 ethanol. ½ H_2SO_4]. *Acta. Cryst.* **B34:** 1203-1208.

Lord, J.D. (1993) Particle interactions in dry powder inhalations. (*PhD Thesis),* University of Bath, Bath, UK.

Louey, M.D., Mulvaney, P., Stewart, P.J. (2001) Characterisation of adhesional properties of lactose carriers using atomic force microscopy. *J. Pharm. Anal*. **25:** 559-567.

Mizes, H., Ott, M., Eklund, E., Hays, D. (2000) Small particle adhesion: measurement and control. *Col. Surfaces. A*. **165**: 11-23.

Packham, D.E. (1996) Work of adhesion: contact angles and contact mechanics. *Int. J. Adh.* **16:** 121-128.

Patton, J.S. (1996). Mechanisms of macromolecule absorption by the lungs. *Adv. Drug Del. Rev.* **19:** 3-36.

Peart, J., Staniforth, J.N., Meakin, B.J. (1995). Electrostatic charge interactions in pharmaceutical dry powder aerosols. *Inst. Phys. Conf. Ser.* **143:** 271-274.

Pizzi, A., Mittal, K.L. (1994) Handbook of adhesive technology. Marcel Decker, USA.

Podczeck, F., Newton. J.M, James, M.B. (1996) Influence of constant and changing relative humidity of the air on the autoadhesion force between pharmaceutical powder particles. *Int. J. Pharm.* **145:** 221-229.

Podczeck, F., Newton, J.M., James, M.B. (1997a) Variations in the adhesion force between a drug and carrier particles as a result of changes in the relative humidity of the air. *Int. J. Pharm.* **149:** 151-160.

Podczeck, F., Newton, J.M., James, M.B. (1997b) Influence of relative humidity of storage air on the adhesion and autoadhesion of micronized particles to particulate and compacted powder surfaces**.** *J. Col. Int. Sci.* **187:** 484-491.

Podczeck, F. (1998a) Adhesion forces in interactive powder mixtures of a micronised drug and carrier particles of various particle size distributions. *J. Adh. Sci. Technol.* **12:** 1323-1339.

Podczeck, F. (1998b) Particle-particle adhesion in pharmaceutical powder handling. Imperial College Press, London, UK.

Preuss, M., Butt, H-J. (1998) Direct measurement of particle-bubble interactions in aqueous electrolyte: dependence on surfactant. *Langmuir*. **14:** 3164-3174.

Pritchard J.N. (2001) The influence of lung deposition on clinical response. *J Aerosol Med.* **14:** S19-S26.

Richardson, G.M., Malthus, R.S. (1955) Salts for static control of humidity at relatively low levels. *J. Appl. Cem.* **5:** 557-567.

Riddle, F.L., Fowkes, F.M. (1990) Spectral shifts in acid-base chemistry 1: Van der Waals contributions to acceptor numbers. *J. Am. Chem. Soc.* **112:** 3259–3264.

Safatov, A.S., Yashin, V.A., Kulkin, S.N., Frolov, V.G., Shishkin, A.V., Buryak, G.A. (1998) Variations in disperse composition of dry powders according to energy of their dispersion. *Powder Technol.* **97:** 227-232.

Schubert, H. (1984) Capillary forces - modelling and application in particulate technology. *Powder Technol.* **37**: 105-116.

Sedin, D.L., Rowden, K.L. (2000) Adhesion forces measured by atomic force microscopy in humid air. *Anal. Chem*. **72:** 2183-2189.

Shekunov, B.Y., York, P**.** (2000) Crystallization processes in pharmaceutical technology and drug delivery design. *J. Crystal Growth.* **211:** 122-136.

Sindel, U., Zimmermann, I. (2001) Measurement of interaction forces between individual powder particles using an atomic force microscope. *Powder Technol.* **117:** 247-254.

Staniforth, JN. (1980) Ordered mixing of drugs with particulate excipients. *(PhD Thesis),* University of Aston, Birmingham, UK.

Staniforth,J.N. (1995) Performance modifying influences in dry powder inhalation systems. *Aerosol Sci. Technol.* **22:** 346-353.

Staniforth, J.N. (1996) Pre-formulation aspects of dry powder aerosols. *Proc. from Respiratory Drug Delivery V.* Davis Harwood International Publishing, Ltd. Raleigh, North Carolina, USA.

Staniforth, J.N. (1997) Improvements in dry powder inhaler performance: surface passivation techniques. *Proc. Drug Delivery to the Lung 8* pp. 85-86. Aerosol Society, London, UK.

Staniforth, J.N. (2000) Particle size reduction. In: Pharmaceutics: The science of solid dosage form design. Livingstone, London, UK.

Ticehurst, M.D., Rowe, R.C., York, P. (1994) Determination of the surface properties of two batches of salbutamol sulphate by inverse gas chromatography. *Int. J. Pharm.* **111:** 241-249.

Timsina, M.P., Martin, G.P., Marriot, C., Ganderton, D., Yianneskis, M. (1994) Drug delivery to the respiratory tract using dry powder Inhalers. *Int. J. Pharm.* **101:** 1-13.

Visser, J. (1989) Van der waals and other cohesive forces affecting powder fluidization. *Powder Technol.* **58:** 1-10.

Ward, G.H., Schultz, R.K. (1995) Process-induced crystallinity changes in albuterol sulphate and its effect on powder physical stability. *Pharm Res.* **12:** 773-779.

Webb, P.A. Orr, C. (1997) Analytical methods in fine particle technology. Micromeritics Instruments Corp. Norcross, GA. USA.

Webster, C.E., Drago, R.S., Zerner, M.C. (1998). Molecular dimensions for adsorptives. *J Am Chem Soc*. **120:** 5509-5516.

Yalamanchilli, M.R., Veeramasuneni, S., Azevedo, M.A.D., Miller, J.D. (1998) Use of the atomic force microscope in particle science technology research. *Coll. Surfaces A.* **133:** 77-88.

Zimmon, A. D. (1982) Adhesion of dust and powder. (2nd edition), Consultants Bureau New York, USA.